

Lawrence Berkeley National Laboratory

Recent Work

Title

THE STATE OF SURFACE STRUCTURAL CHEMISTRY: THEORY, EXPERIMENT, AND RESULTS

Permalink

<https://escholarship.org/uc/item/9rd7d17r>

Authors

Hove, M.A. Van

Wang, S.W.

Ogltree, D.F.

Publication Date

1988-05-01

Center for Advanced Materials

CAM

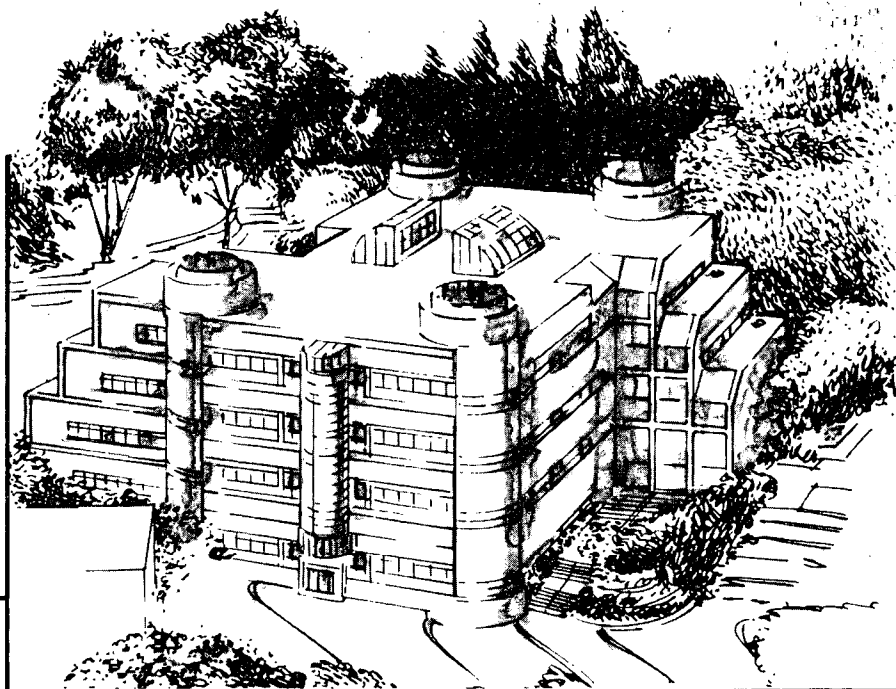
Submitted to Advances in Quantum Chemistry

The State of Surface Structural Chemistry: Theory, Experiment, and Results

M.A. Van Hove, S.-W. Wang, D.F. Ogletree,
and G.A. Somorjai

May 1988

RECEIVED
LAWRENCE
BERKELEY LABORATORY
JUN 1 4 1988
LIBRARY AND
DOCUMENTS SECTION



Materials and Chemical Sciences Division
Lawrence Berkeley Laboratory • University of California
ONE CYCLOTRON ROAD, BERKELEY, CA 94720 • (415) 486-4755

LBL-24464

e.2

DISCLAIMER

This document was prepared as an account of work sponsored by the United States Government. While this document is believed to contain correct information, neither the United States Government nor any agency thereof, nor the Regents of the University of California, nor any of their employees, makes any warranty, express or implied, or assumes any legal responsibility for the accuracy, completeness, or usefulness of any information, apparatus, product, or process disclosed, or represents that its use would not infringe privately owned rights. Reference herein to any specific commercial product, process, or service by its trade name, trademark, manufacturer, or otherwise, does not necessarily constitute or imply its endorsement, recommendation, or favoring by the United States Government or any agency thereof, or the Regents of the University of California. The views and opinions of authors expressed herein do not necessarily state or reflect those of the United States Government or any agency thereof or the Regents of the University of California.

**The State of Surface Structural Chemistry:
Theory, Experiment, and Results**

M.A. Van Hove, S.-W. Wang, D.F. Ogletree,
and G.A. Somorjai

Center for Advanced Materials
Materials and Chemical Sciences Division
Lawrence Berkeley Laboratory
1 Cyclotron Road
Berkeley, California 94720

May 1988

THE STATE OF SURFACE STRUCTURAL CHEMISTRY
THEORY, EXPERIMENT AND RESULTS

M. A. Van Hove

S.-W. Wang

D. F. Ogletree

G. A. Somorjai

Materials and Chemical Sciences Division
Lawrence Berkeley Laboratory
University of California at Berkeley
Berkeley, California 94720

1. INTRODUCTION
2. EXPERIMENTAL TECHNIQUES FOR SURFACE
STRUCTURE DETERMINATION
 - 2.1. Electron Diffraction Techniques
 - 2.2. Fine Structure Techniques
 - 2.3. Surface Topography Techniques
 - 2.4. Ion Scattering
 - 2.5. Complementary Techniques
3. THE THEORY OF MODERN TECHNIQUES FOR
SURFACE STRUCTURE ANALYSIS.

- 3.1. General Four-Step Description of Electron-Diffraction Techniques
 - 3.2. Structural Information
 - 3.3. Theoretical Aspects of Individual Techniques
 - 3.4. Formalism for Individual Processes
 - 3.5. Unifying and Distinguishing Features
 4. THE THEORY OF SURFACE CHEMISTRY AND BONDING
 - 4.1. The Extended Hückel Theory and Applications
 - 4.2. The SCF $X\alpha$ Scattered Wave Method
 - 4.3. SCF- $X\alpha$ -SW Calculations
 - 4.4. Results of the $X\alpha$ -Method
 - 4.5. The Hartree-Fock-Slater Method and Its Applications
 - 4.6. The *ab initio* Quantum Chemical Calculation
 - 4.7. Conclusion
 5. RESULTS OF SURFACE CRYSTALLOGRAPHY
 - 5.1. Ordering Principles
 - 5.2. Notation for surface lattices
 - 5.3. Numbers and types of solved surface structures
 - 5.4. Major trends among surface structures
 6. FUTURE NEEDS AND DIRECTIONS OF SURFACE STUDIES
-
1. INTRODUCTION

The atomic and molecular structures of clean solid surfaces and of monolayers of adsorbed molecules are at the heart of most problems in surface science. The surface chemical bond can be investigated by determining the bond distances and bond angles of surface atoms with respect to their neighbors. Changes of surface structure with temperature, adsorbate coverage and surface composition are important ingredients of surface phenomena, including catalysis, corrosion, surface phase transformations (reconstruction, sintering, crystal growth and evaporation) and lubrication.

During the last ten years profound changes have occurred in surface science that resulted in the rapid improvement of our understanding of surface structure. Electron, atom and ion scattering techniques proved to be very sensitive to the surface monolayer structure and composition. High intensity photon fluxes can also be employed in ways to obtain high surface structure sensitivity.

Low energy electron diffraction (LEED) has produced most of the information on surface structure, while other techniques increasingly contribute to the data base. From these studies we learned that clean and flat solid surfaces often restructure; atoms often "relax" to shorten the first interlayer distance or seek new equilibrium positions that alter the long range order of the surface (reconstruction). Atoms of more open, rough surfaces relax more readily and often exhibit periodic steps of one atom in height. The surface composition of polyatomic solids (alloys, oxides, sulfides, etc.) can be very different from that in the bulk, resulting in altered atomic surface structures. Adsorbed atoms and molecules often form ordered two-dimensional layers. The structure and bonding in these layers changes with coverage and temperature.

The two-dimensional world of surface structural chemistry is rich, diverse, and full of surprises that reflect our incomplete knowledge of bonding and chemical interactions in the surface phase. This review attempts to summarize much of the knowledge that was gained in recent years.

We first discuss the various experimental methods of surface structure determination. Next we discuss the theoretical questions that arise when experimental data are analyzed to obtain surface chemical bond distances and angles, in particular the problem of electron propagation in solids, and the progress that has been made in answering these questions. A number of important techniques in addition to LEED rely on a proper understanding of electron propagation in solids to enable surface structure determination. This is followed by a discussion of the application of theoretical quantum chemistry to the calculation of the structure and bonding of chemisorbed atoms and molecules. Various calculational methods are reviewed, along with the results that have been obtained. The last section of this review surveys the surface structural results that have become available, ranging from clean surfaces to reconstructed

surfaces, multi-component systems and chemisorbed atoms and molecules. In conclusion we indicate the needs and possible directions for future studies of surface structural chemistry.

2. EXPERIMENTAL TECHNIQUES FOR SURFACE STRUCTURE DETERMINATION

Most quantitative information on surface structure and chemical bonding comes from studies of the solid-vacuum interface. In large part this is because the most powerful probes of surface structure rely on the propagation of electron, ion or atom beams. New developments such as the scanning tunneling microscope (STM), which can also investigate the solid-gas and solid-liquid interface, and new optical techniques, which can potentially investigate all types of surfaces and interfaces, may greatly extend our understanding of surface structural chemistry in the future. At this time, however, the solid-vacuum interface is the focus of most active investigations in surface structural chemistry. In this chapter we review the major experimental methods used in the study of surface structure and their application, along with recent experimental developments.

The majority of the known surface structures have been solved by comparing experimental data with theoretical predictions based on models of the surface. A theoretical description of the interaction of the probe with the surface is used to calculate spectra for a given model geometry (see part 3). Different geometries are tried, and structural parameters within a given model are varied, until a good fit is obtained between the experimental data and the theoretically calculated spectra. This basic approach has been used to interpret results from low-energy electron diffraction (LEED) and other electron diffraction techniques, as well as from helium diffraction and ion scattering.

Structural information has also been obtained by matching the observed frequencies of surface vibrational and electronic excitations with spectra calculated from structural models (see part 4). This approach has been applied

to the frequencies of electronic states as measured by angle-resolved ultra-violet photo-emission (ARUPS) and to the frequencies of vibrational excitations as measured by high-resolution electron energy-loss spectroscopy (HREELS).

There has been an ongoing search for a way to "image" surface structure directly from experimental results without fitting experimental data to theoretical calculations for model systems. So far this search has not been successful, although certain techniques yield more direct information for some special cases. Structure sensitive techniques such as scanning tunneling microscopy (STM) and field ionization microscopy (FIM) do give results that can be interpreted directly, but these results do not provide complete information on atomic coordinates in the near-surface region. Extended fine-structure techniques provide direct information on bond-lengths in many cases, but this is sometimes insufficient to fully determine the surface structure.

Most surface structural studies combine results from several different surface science techniques applied to the same system. For an approach based on model calculations to be successful, it is necessary to construct reasonable structural models of surfaces. The application of techniques which cannot give explicit information on the arrangement of atoms in the near-surface region is often necessary to develop good surface structural models.

A wide range of techniques have been developed to study surfaces in vacuum, and many techniques are commonly referred to by acronyms. Table I lists acronyms and brief descriptions of most common techniques used in surface science.

2.1. Electron Diffraction Techniques

The majority of known surface structures have been solved with electron diffraction techniques. Low energy electrons (below ~ 400 eV) interact strongly with atoms through both elastic and inelastic processes. Inelastic scattering in solids limits electrons with energies below a few hundred eV to a mean free path of $\sim 2\text{-}20$ Å. Elastic interactions are strong enough that multiple scattering is important in this energy range, so elastically scattered electrons are sensitive to

TABLE I. Surface Science Techniques

Acronym	Name	Description
AD	Atom or Helium Diffraction	Monoenergetic beams of thermal energy neutral atoms are elastically scattered off of ordered surfaces and detected as a function of scattering angle. This gives structural information on the outermost layer of the surface. Atom diffraction is extremely sensitive to surface ordering and defects.
AEAPS	Auger Electron Appearance Potential Spectroscopy	The EAPFS cross-section is monitored by Auger electron intensity. Also known as APAES.
AES	Auger Electron Spectroscopy	Core-hole excitations are created, usually by 1-10 KeV incident electrons, and Auger electrons of characteristic energies are emitted through a two-electron process as excited atoms decay to their ground state. AES gives information on the near-surface chemical composition.
AFM	Atomic Force Microscopy	Similar to STM. An extremely delicate mechanical probe is used to scan the topography of a surface, and a STM-type tunneling-current probe is used to measure the deflection of the mechanical surface probe. This is designed to provide STM-type images of insulating surfaces.

TABLE I (continued)

Acronym	Name	Description
APAES	Appearance Potential Auger Electron Spectroscopy	See AEAPS.
APXPS	Appearance Potential X-ray Photoemission Spectroscopy	The EAPFS excitation cross-section is monitored by fluorescence from core-hole decay (also known as SXAPS).
ARAES	Angle-Resolved Auger Electron Spectroscopy	Auger electrons are detected as a function of angle to provide information on the spatial distribution or environment of the excited atoms (see AES).
ARPEFS	Angle-Resolved Photo-Emission Fine Structure	Electrons are detected at given angles after being photoemitted by polarized synchrotron radiation. The interference in the detected photoemission intensity as a function of electron energy ~ 100 -500 eV above the excitation threshold gives structural information.

(continued)

TABLE I (continued)

Acronym	Name	Description
ARPES	Angle-Resolved Photo-Emission Spectroscopy	A general term for structure sensitive photoemission techniques, including ARPEFS, ARXPS, ARUPS, and ARXPD.
ARUPS	Angle-Resolved Ultraviolet Photoemission Spectroscopy	Electrons photoemitted from the valence and conduction bands of a surface are detected as a function of angle. This gives information on the dispersion of these bands (which is related to surface structure), and also structural information from the diffraction of the emitted electrons.
ARXPD	Angle-Resolved X-ray Photoemission Diffraction	Similar to ARXPS and ARPEFS. The angular variation in the photoemission intensity is measured at a fixed energy above the excitation threshold to provide structural information.
ARXPS	Angle-Resolved X-ray Photoemission Spectroscopy	The diffraction of electrons photoemitted from core-levels gives structural information on the surface.

(continued)

TABLE I (continued)

Acronym	Name	Description
CEMS	Conversion-Electron Mössbauer Spectroscopy	A surface-sensitive version of Mössbauer spectroscopy. Like Mössbauer Spectroscopy, this technique is limited to some isotopes of certain metals. After a nucleus is excited by ray absorption, it can undergo inverse β -decay, creating a core-hole. The decay of core-holes by Auger processes within an electron mean free path of the surface produces a signal. Detecting emitted electrons as a function of energy gives some depth-profile information, because of the changing electron mean free path.
DAPS	Dis-Appearance Potential Spectroscopy	The EAPFS cross-section is monitored by variations in the intensity of electrons elastically back-scattered from the surface.

(continued)

TABLE I (continued)

Acronym	Name	Description
EAPFS	Electron Appearance Potential Fine-Structure	A fine-structure technique (see EXAFS). Core-holes are excited by monoenergetic electrons at ~ 1 KeV. The modulation in the excitation cross section may be monitored through adsorption, fluorescence, or Auger emission.
ELNES	Electron energy-Loss Near-Edge Structure	Similar to NEXAFS, except monoenergetic high-energy electrons ~ 60 -300 KeV excite core-holes.
ELS	Electron Energy Loss Spectroscopy	Monoenergetic electrons ~ 5 -50 eV are scattered off a surface the energy losses are measured. This gives information on the electronic excitations of the surface and adsorbed molecules (see HREELS). Sometimes called EELS.
ESCA	Electron Spectroscopy for Chemical Analysis	Now generally called XPS.

(continued)

TABLE I (continued)

Acronym	Name	Description
ESDIAD	Electron Stimulated Desorption Ion Angular Distribution	Electrons break chemical bonds in adsorbed atoms or molecules, causing ionized atoms or radicals to be ejected from the surface along the axis of the broken bond by Coulomb repulsion. The angular distribution of these ions gives information on the bonding geometry of adsorbed molecules.
EXAFS	Extended X-ray Adsorption Fine-Structure	Monoenergetic photons excite a core-hole. The modulation of the adsorption cross-section with energy \sim 100-500 eV above the excitation threshold yields information on the radial distances to neighboring atoms. The cross-section can be monitored by fluorescence as core-holes decay or by the attenuation of the transmitted photon beam. EXAFS is one of many "fine-structure" techniques. This is not intrinsically surface sensitive (see SEXAFS).

(continued)

TABLE I (continued)

Acronym	Name	Description
EXELFS	Extended X-ray Energy Loss Fine Structure	A fine-structure technique similar to EXAFS, except that 60-300 KeV electrons rather than photons excite core-holes. Like EXAFS, this techniques is not explicitly surface sensitive.
FIM	Field-Ionization Microscopy	A strong electric field \sim volts/angstrom is created at the tip of a sharp, single crystal wire. Gas atoms, usually He, are polarized and attracted to the tip by the strong electrostatic field, and then ionized by electrons tunneling from the gas atoms into the tip. These ions, accelerated along radial trajectories by Coulomb repulsion, map out the variations in the electric-field strength across the surface with atomic resolution, showing the surface topography.

(continued)

TABLE I (continued)

Acronym	Name	Description
FTIR	Fourier-Transform Infra-Red spectroscopy	Broad-band IRAS experiments are performed, and the IR adsorption spectrum is deconvoluted by using a doppler-shifted source and Fourier analysis of the data. This technique is not restricted to surfaces.
HEIS	High-Energy Ion Scattering	High-energy ions, above ~ 500 KeV, are scattered off of a single crystal surface. The "channeling" and "blocking" of scattered ions within the crystal can be used to triangulate deviations from the bulk structure. HEIS has been used in particular to study surface reconstructions and the thermal vibrations of surface atoms (see also MEIS, ISS)
HREELS	High-Resolution Electron Energy Loss Spectroscopy	A monoenergetic electron beam, usually $\sim 2-10$ eV, is scattered off a surface and energy losses below ~ 0.5 eV to bulk and surface phonons and vibrational excitations of adsorbates are measured as a function of angle and energy (also called EELS).

(continued)

TABLE I (continued)

Acronym	Name	Description
INS	Ion Neutralization Spectroscopy	Slow ionized atoms, typically He^+ , are incident on a surface where they are neutralized in a two-electron process which can eject a surface electron, a process similar to Auger emission from the valence band. The ejected electrons are detected as a function of energy, and the surface density of states can be determined from the energy distribution. The interpretation of the data is more complicated than for SPI or UPS.
IRAS	Infrared Reflection Adsorption Spectroscopy	Monoenergetic IR photons are reflected off a surface, and the attenuation of the IR intensity is measured as a function of frequency. This yields a spectrum of the vibrational excitations of adsorbed molecules. Recent improvements in the sensitivity of this technique allow IRAS measurements to be made on single crystal surfaces.

(continued)

TABLE I (continued)

Acronym	Name	Description
IRES	Infra-Red Emission Spectroscopy	The vibrational modes of adsorbed molecules on a surface are studied by detecting the spontaneous emission of infra-red radiation from thermally excited vibrational modes as a function of energy.
ISS	Ion-Scattering Spectroscopy	Ions are inelastically scattered from a surface, and the chemical composition of the surface is determined from the momentum transfer to surface atoms. The energy range is ~ 1 KeV to 10 MeV, and the lower energies are more surface sensitive. At higher energies this technique is also known as Rutherford Back-Scattering (RBS).
LEED	Low Energy Electron Diffraction	Monoenergetic electrons below ~ 500 eV are elastically back-scattered from a surface and detected as a function of energy and angle. This gives information on the structure of the near surface region.

(continued)

TABLE I (continued)

Acronym	Name	Description
LEIS	Low-Energy Ion Scattering	Low-energy ions, below ~ 5 KeV, are scattered from a surface, and the ion "shadowing" gives information on surface structure. At these low energies the surface atom ion scattering cross-section is very large, resulting in large surface sensitivity. Accuracy is limited because the low energy ion scattering cross-sections are not well known.
LEPD	Low Energy Positron Diffraction	Similar to LEED with positrons as the incident particle. The interaction potential for positrons is somewhat different than for electrons, so the form of the structural information is modified.
MEED	Medium Energy Electron Diffraction	Similar to LEED, except the energy range is higher, ~ 300 -1000 eV. LEED calculational methods break down in this energy range. New methods are being developed for glancing angle scattering, which emphasizes forward scattering.

(continued)

TABLE I (continued)

Acronym	Name	Description
MEIS	Medium-Energy Ion Scattering	Similar to HEIS, except that incident ion energies are ~ 50 -500 KeV.
	Neutron Diffraction	Neutron diffraction is not an explicitly surface-sensitive technique, but neutron diffraction experiments on large surface-area samples have provided important structural information on adsorbed molecules, and also on surface phase transitions.
NEXAFS	Near-Edge X-ray Adsorption Fine Structure	A core-hole is excited as in fine-structure techniques (see EXAFS), except the fine-structure within ~ 30 eV of the excitation threshold is measured. Multiple scattering is much stronger at low electron energies, so this technique is sensitive to the local 3-dimensional geometry, not just the radial separation between the source atom and its neighbors. The excitation cross-section may be monitored by detecting the photoemitted electrons or the Auger electrons emitted during core-hole decay.

(continued)

TABLE I (continued)

Acronym	Name	Description
NMR	Nuclear Magnetic Resonance	NMR is not an explicitly surface-sensitive technique, but NMR data on large surface-area samples has provided useful data on molecular adsorption geometries.
NPD	Normal Photoelectron Diffraction	Similar to ARPEFS with a somewhat lower energy range.
RBS	Rutherford Back-Scattering	Similar to ISS, except the main focus is on depth-profiling and composition. The momentum transfer in back-scattering collisions between nuclei is used to identify the nuclear masses in the sample, and the smaller, gradual momentum-loss of the incident nucleus through electron-nucleus interactions provides depth-profile information.

(continued)

TABLE I (continued)

Acronym	Name	Description
RHEED	Reflection High Energy Electron Diffraction	Monoenergetic electrons of ~ 1 -20 KeV are elastically scattered from a surface at glancing incidence, and detected as a function of angle and energy for small forward-scattering angles. Back-scattering is less important at high energies, and glancing incidence is used to enhance surface sensitivity.
SEELFS	Surface Electron Energy Loss Fine Structure	A fine structure technique similar to EXELFS, except the incident electron energies are ~ 100 -3000 eV. SEELFS is surface sensitive because of the lower excitation energy.
SERS	Surface Enhanced Raman Spectroscopy	Some surface geometries (rough surfaces) concentrate the electric fields of incident light sufficiently to enhance the Raman scattering cross-section so that it is surface sensitive. This gives information on surface vibrational modes, and some information on geometry via selection rules.

(continued)

TABLE I (continued)

Acronym	Name	Description
SEXAFS	Surface Extended X-ray Adsorption Fine-Structure	A surface-sensitive version of EXAFS, where the excitation cross-section fine-structure is monitored by detecting the photoemitted electrons (PE-SEXAFS), Auger electrons emitted during core-hole decay (Auger-SEXAFS), or ions excited by photoelectrons and desorbed from the surface (PSD-SEXAFS).
SHG	Second Harmonic Generation	A surface is illuminated with a high-intensity laser, and photons are generated at the second-harmonic frequency through non-linear optical process. For many materials only the surface region has the appropriate symmetry to produce a SHG signal. The non-linear polarizability tensor depends on the nature and geometry of adsorbed atoms and molecules.

(continued)

TABLE I (continued)

Acronym	Name	Description
SIMS	Secondary Ion Mass Spectroscopy	Ions and ionized clusters ejected from a surface during ion bombardment are detected with a mass spectrometer. Surface chemical composition and some information on bonding can be extracted from SIMS ion fragment distributions.
SPI	Surface Penning Ionization	Neutral atoms, usually He, in excited states are incident on a surface at thermal energies. A surface electron may tunnel into the unoccupied electronic level, causing the incident atom to become ionized and eject an electron, which is then detected. This technique measures the density of states near the Fermi-level, and is highly surface sensitive.
SPLEED	Spin-Polarized Low Energy Electron Diffraction	Similar to LEED, except the incident electron beam is spin-polarized. This is particularly useful for the study of surface magnetism and magnetic ordering.

(continued)

TABLE I (continued)

Acronym	Name	Description
STM	Scanning Tunneling Microscopy	The topography of a surface is measured by mechanically scanning a probe over a surface with Angstrom resolution. The distance from the probe to the surface is measured by the probe-surface tunneling current. Also known as Scanning Electron Tunneling Microscopy (SETM).
SXAPS	Soft X-ray Appearance Potential Spectroscopy	Another name for APXPS.
TEM	Transmission Electron Microscopy	TEM can provide surface information for carefully prepared and oriented bulk samples. Real images have been formed of the edges of crystals where surface planes and surface diffusions have been observed. Diffraction patterns of reconstructed surfaces, superimposed on the bulk diffraction pattern, have also provided surface structural information.

(continued)

TABLE I (continued)

Acronym	Name	Description
TDS	Thermal Desorption Spectroscopy	An adsorbate-covered surface is heated, usually at a linear rate, and the desorbing atoms or molecules are detected with a mass spectrometer. This gives information on the nature of adsorbate species and some information on adsorption energies.
TPD	Temperature Programmed Desorption	Similar to TDS, except the surface may be heated at a non-uniform rate to get more selective information on adsorption energies.
UPS	Ultra-violet Photoemission Spectroscopy	Electrons photoemitted from the valence and conduction bands are detected as a function of energy to measure the electronic density of states near the surface. This gives information on the bonding of adsorbates to the surface (see ARUPS).
WF	Work Function measurements	Changes in the work-function during the adsorption of atoms and molecules provide information on charge-transfer and chemical bonding.

(continued)

TABLE I (continued)

Acronym	Name	Description
XANES	X-ray Adsorption Near-Edge Structure	Another name for NEXAFS.
XPS	X-ray Photoemission Spectroscopy	Electrons photoemitted from atomic core levels are detected as a function of energy. The shifts of core level energies gives information on the chemical environment of the atoms (see ARXPS, ARXPD).
XRD	X-Ray Diffraction	X-ray diffraction has been carried out at extreme glancing angles of incidence where total reflection assures surface sensitivity. This provides structural information that can be interpreted by well-known methods. An extremely high x-ray flux is required to get useful data from single crystal surfaces. Bulk x-ray diffraction is used to determine the structure of organo-metallic clusters, which provide comparisons to molecules adsorbed on surfaces. X-ray diffraction has also given structural information on large surface-area samples.

the three-dimensional geometry of the near-surface region. Electron scattering also depends on the chemical identity of the scattering atoms, so electron diffraction techniques are sensitive to both chemical composition and structure throughout the near-surface region. Therefore low-energy electrons are an ideal probe of surface structural chemistry. The main difficulty with electron diffraction methods is that the strong electron-surface interaction makes data analysis difficult -- it is not possible in most cases to "invert" diffraction data to obtain the original surface structure.

2.1.1. Low energy electron diffraction

In a conventional LEED experiment a focused beam of monoenergetic electrons is reflected off an ordered single crystal surface and the elastically backscattered electrons are detected. Several types of information can be extracted from LEED patterns. First, the symmetry of the LEED pattern is related to the symmetry of the surface, so changes in surface symmetry because of reconstruction or chemisorption are immediately detected. Second, imperfections and deviations in long-range order change the shape of diffraction beams. This can be used to study the process of ordering in phase transitions or the growth of ordered domains within overlayers. Finally, the integrated intensity of diffraction beams depends on the detailed bonding structure of the surface. This information is most important for the study of surface chemical bonding. The intensity of LEED beam is a function of the incident electron beam energy and angles of incidence on the surface.

The intensity of a given diffraction beam can be measured as the incident electron energy or beam voltage is varied, producing an intensity-voltage or I-V curve; or as the angle of the incident electron beam relative to the surface is varied, producing an I- θ or rocking curve; or as the crystal is rotated around its own normal at a given angle of incidence, producing an I- ϕ curve. For structure determination LEED data are most often recorded in the form of I-V curves with the incident electron beam at normal incidence or lying in a mirror plane of the surface. This form of data are usually simpler to work with both experimentally and theoretically.

One advantage of LEED is that the diffraction process filters out effects due to local defects or deviations from long-range order. The contribution of defects to I-V curves is proportional to the first power of the number of defects, while the contribution of the part of the surface with long-range order is proportional to the square of the number of atoms involved, so the LEED beam integrated intensity reflects the equilibrium geometry of the ordered surface structure.

LEED has been used to determine the structure of a wide variety of surfaces, including clean and reconstructed surfaces of metals and semiconductors, and atomic and molecular physisorption and chemisorption on many different substrates (see part 5). As the theoretical and experimental tools of LEED have improved, the structure of systems with larger and more complex unit cells have been determined. Successful LEED structure determinations have been carried out for systems with several molecules adsorbed in unit cells up to 16 times larger than the substrate unit cell,^{/1/} and for reconstructed surfaces where the structural rearrangement involves several surface layers.^{/2/}

There are still a number of surface systems where the structure cannot be determined by LEED for theoretical and experimental reasons. High Miller-index surfaces, such as stepped or kinked surfaces, have layers separated by very small distances normal to the surface. The calculational tools normally used for LEED break down in this case, and no new approach has yet been developed to solve this problem. Experimental difficulties restrict the study of insulator surfaces, because of charging problems, and of molecular crystal surfaces, because of beam damage problems.

A reliable LEED structure determination requires a large data base, usually a number of different I-V curves collected at more than one angle of incidence. Electron beam damage to the surface must be prevented during data acquisition.

Over the last decade both the speed and accuracy of data acquisition and the sensitivity of the LEED experiment have been significantly improved. In most structure determination experiments the LEED patterns are displayed on a phosphor screen. LEED I-V curves are then measured by photometric or photographic means. Fast data acquisition systems have been developed that record LEED patterns with video cameras interfaced to computers and generate I-V curves during the experiment.^{/3,4/} The sensitivity of LEED is also being greatly increased with the development of instruments that can detect single

diffracted electrons, which completely solves the problem of electron beam damage./5,6,7/ Such instruments should be able to extend the range of LEED structure determination to delicate systems such as molecular crystals and physisorption systems, and to systems without long-range order, where the diffracted intensity is much lower than for ordered systems.

There are variations of LEED that use positrons (low energy positron diffraction, or LEPD)/8/ or spin-polarized electrons as a probe./9/ The latter technique is especially useful as a probe of magnetic ordering in surfaces. Spin-polarized LEED, or SPLEED, has been used to study surface magnetism and phase transitions on nickel.

At higher energies the surface sensitivity and the importance of multiple scattering is reduced. Diffraction techniques in this energy range have primarily been applied to the study of defects and deviations from long range order, as in the use of reflection high-energy electron diffraction (RHEED) to monitor epitaxial growth on surfaces. The higher-energy diffraction techniques have only infrequently been used for surface structure determination/10/ due to theoretical complications, but new approaches are promising./11/

2.1.2. Diffuse low energy electron diffraction

Conventional LEED experiments are done on systems with long range order. This is not a fundamental restriction. The energy-dependent variation in diffracted intensity at a given point in the Brillouin zone is primarily determined by the local scattering geometry at the surface. Long range order gives rise to sharp diffraction beams which reflect this intensity dependence. If angle resolved intensity data are collected from a system with definite local geometry but without long range order, the local geometry can still be determined by LEED calculations./12/ This "diffuse" LEED experiment will be difficult to interpret unless there is one predominant local scattering geometry. Unlike the conventional LEED experiment, the diffraction process does not filter out the contributions of defects and impurities from the contribution of the equilibrium

structure in the diffuse LEED experiment. If the scattering from different kinds of sites is superimposed in the experimental data it will be difficult to construct a reasonable model of the surface.

There are a number of "lattice-gas" chemisorption systems, where atoms or molecules are adsorbed in well-defined sites on the surface, as determined by vibrational spectroscopy, but where there is no long range order. The adsorption sites and bond lengths for such systems can be determined by diffuse LEED calculations, as has been done for oxygen on the tungsten (100) surface./13/

2.1.3. Photoelectron diffraction

The interference and diffraction of photoemitted electrons can provide structural information, as in angle-resolved photo-electron fine structure (ARPEFS) spectroscopy, angle-resolved x-ray photoelectron spectroscopy (ARXPS), and angle-resolved x-ray photoelectron diffraction (ARXPD). The main advantage of photoemission over LEED is that the initial state of the photoemitted electron is a simple spherical wave, and can be controlled to emphasize particular structural features, especially in chemisorption systems. Because the initial state is simple, in some high-energy cases the data analysis can be more straight forward than a full LEED multiple-scattering calculation.

In photoelectron diffraction experiments monoenergetic photons excite electrons from a particular atomic core level. Angular momentum is conserved, so the emitted electron wave-function is a spherical wave centered on the source atom, with angular momentum components $l \pm 1$, where l is the angular momentum of the core level. If the incident photon beam is polarized, the orientation of the emitted electron wave-function can be controlled. These electrons then propagate through the surface and are detected and analyzed as in LEED experiments. A synchrotron x-ray source normally produces the intense beams of variable energy polarized photons needed for photoelectron diffraction.

In angle-resolved photoemission fine-structure (ARPEFS) experiments electrons are detected at a given angle as a function of energy. Structural information is obtained from the variation in intensity due to interference between different scattering paths for electrons over an energy range of ~ 100 -500 eV. In this energy range the interference effects are dominated by single

scattering, so the scattering amplitude can be readily calculated for a model system. A Fourier transform of the interference pattern will show the distribution of different scattering path-lengths that contribute to the detected intensity. This can be a guide to the proper surface structure, but this result must be confirmed by a calculation of the interference for a model geometry./14/ ARPEFS has been used to solve several surface structures, including sulfur on nickel./15/ Long-range order is not required for ARPEFS experiments. In spite of the name, ARPEFS is not a normal "fine-structure" technique (see below). The variations in the detected intensity as a function of energy are orders of magnitude larger than the fine-structure modulation in core-level excitation cross-sections.

Photoelectron diffraction is most useful for systems where the photoexcited atoms all have the same local geometry, as in a chemisorption problem. If there are source atoms in different local geometries, there will be interference between multiple sets of scattering paths, and the resulting interference spectrum will be harder to interpret. For these cases LEED experiments are probably better, with diffuse LEED used for disordered systems.

2.2. Fine Structure Techniques

There are a large number of "fine structure" techniques, all based on the same physical principle. In all of these techniques an electron is ejected from an atomic core-level by incident photons or other particles. The different names refer to different experimental arrangements for the excitation and detection of core-holes.

As the excitation energy is varied the energy of the emitted electron varies. The emitted electron wave can be scattered back to the source atom from neighboring atoms, where it interferes with the source wave-function with a phase that depends on the electron energy, interatomic distance and the identity of the neighboring atom. This energy dependent interference changes the coupling of the incident excitation to the final state, producing a modulation or "fine-structure" in the excitation cross section.

Fine structure experiments are often carried out with synchrotron sources, since the initial electron state is better defined for photoemission than for electron excitation. When core-hole decay is detected by Auger or secondary electron emission, the technique is surface sensitive. Core-hole decay can also be detected by fluorescence, or by adsorption of the incident photon beam. These methods are not intrinsically surface sensitive, but they are useful when the source atoms are exclusively located at the surface.

If there are different local geometries for source atoms, the different fine structures will be superimposed in the experimental spectrum, which will then be more difficult to interpret. Fine structure techniques are particularly useful when a chemisorbed atom is used as the source atom.

2.2.1. Near-edge fine structure techniques

In the "near-edge fine structure" region emitted electrons have energies up to ~ 50 eV and multiple scattering effects are predominant. An emitted electron wave can scatter several times and still return with a significant amplitude to the source atom. Therefore the variation in the observed cross-section depend not only on interatomic bond distances, but also on bond angles, so the full three-dimensional geometry around the source atom can be determined. The theoretical analysis of near-edge fine structure data is very similar to LEED data analysis.

A few structures have been solved by x-ray adsorption near-edge fine structure (XANES), including oxygen on Ni(100)./16/ This technique is also known as near-edge x-ray adsorption fine structure (NEXAFS).

A variation of XANES or NEXAFS has been used to determine the structure of molecules chemisorbed on surfaces. In this approach photoemitted electrons excite molecular orbitals in the chemisorbed molecules. By varying the polarization of the incident photons, molecular orientation can be determined from selection rules for excitation. The bond lengths can be determined from a quasi-empirical correlation between bond-length and the shift in the molecular orbital excitation energy. This technique has been used to study the chemisorption of several hydrocarbon molecules on different metal surfaces./17/

2.2.2. Extended fine-structure techniques

For emitted electrons above ~ 50 eV, the "extended fine structure" region, the modulation of the excitation cross section is dominated by single backscattering between near-neighbor atoms and the source atom. A Fourier transform of the extended fine structure as a function of momentum transfer gives the distribution of radial distances between the source atom and neighboring atoms. With empirical or theoretical correction for scattering phase shifts, which have been calibrated using results from bulk structures known from x-ray diffraction, this gives chemical bond lengths with an accuracy of better than 0.05 Å.

There are a large number of extended fine-structure results available. These techniques, after LEED, have provided the largest amount of quantitative information on surface structure and chemical bonding. The extended fine structure techniques give quantitative information on surface structure without the need for complex model calculations. In simple systems and when combined with qualitative data from other experiments, knowledge of bond lengths may be sufficient to completely describe the surface geometrical structure. These techniques are most useful in multi-component or chemisorption systems, where atoms of a particular chemical species have only one local geometry. By selectively exciting an appropriate core level, near-neighbor bond lengths are determined. In systems with non-equivalent atomic sites, such as reconstructed surfaces, the extended fine structure will be complicated by a superposition of radial distribution functions for the different sites. Additional data will be needed to solve these structures. Data interpretation is generally simpler with photon excitation, since the polarization and orientation of final-state electrons can be controlled by using single crystal samples and polarized photons from a synchrotron source. One important advantage of extended fine structure techniques is that they do not require long range order or single crystal substrates, so they can be directly applied to many systems of technological importance.

A number of different experimental methods are available to observe fine structure. In extended x-ray adsorption fine structure (EXAFS) experiments x-ray photons excite core levels and the cross section is determined by x-ray absorption

or fluorescence from excited atoms. When Auger or secondary electrons emitted from the excited atoms are detected, the process, now called surface EXAFS (SEXAFS), is surface sensitive. SEXAFS experiments have also been done by detecting ions emitted from surfaces in photon stimulated desorption SEXAFS (PSD-SEXAFS).

There are analogous processes using electrons instead of photons to excite atomic core levels. Diffraction effects may perturb the cross section fine structure when electrons are used to excite core levels or monitor cross section. This is not a problem for systems without long range order. For cases involving long range order it is desirable to integrate over detector angles, and also electron beam incidence angles where this is practical, to average out multiple-scattering effects in the initial and final electron states. In electron appearance potential fine structure spectroscopy (EAPFS) incident electrons at ~ 1 KeV excite shallow core holes, and the cross section is monitored by soft x-ray fluorescence in soft x-ray appearance potential spectroscopy (SXAPS-EAPFS), Auger electron appearance potential spectroscopy, (AEAPS-EAPFS), or by the variation in elastic backscattering in disappearance potential spectroscopy (DAPS-EAPFS), which is also referred to as surface electron energy loss fine structure (SEELFS). With excitation by high energy electrons (60-300 KeV) and detection by fluorescence the process is called extended x-ray energy loss fine structure (EXELFS), or electron energy loss near-edge spectroscopy (ELNES) in the near edge region. This last process, like EXAFS, is not inherently surface sensitive.

2.3. Surface Topography Techniques

Field ion microscopy (FIM), atom diffraction (AD) and scanning tunneling microscopy (STM) provide atomic scale information on surface topography. These techniques produce good qualitative images of surfaces. It is difficult to get atomic coordinates directly, but knowledge of the surface topography can lead directly to structural models of a surface.

2.3.1. Field ion microscopy

Field ion microscopy (FIM) is the oldest of these techniques, developed in the 50's. A sharp, single crystal metal tip with a radius of $\sim 1000 \text{ \AA}$ is maintained at $\sim 10 \text{ kV}$ in a low pressure ($\sim < 10^{-4}$ torr) gas, usually helium. Gas molecules are polarized and attracted to the tip by the strong, inhomogeneous electrostatic fields. The field strength near the tip is several V/\AA . Valence electrons in a gas atom can tunnel into the metal surface as the neutral atom approaches the tip, creating an ion which is repelled by the high field around the tip. The ions project an image of the high field regions of the tip onto a phosphor screen. If the tip is cooled, individual surface atoms can be imaged. Pairs of atoms separated by as little as 1.5 \AA have been resolved.

A field-ion microscopy image is a two-dimensional projection of the outermost surface layer. This image provides a qualitative image of the surface, but very little information on distances normal to the surface. Although the direct information on the surface chemical bond is limited, FIM has added greatly to the qualitative understanding of surface structure. Because of the high field strengths required, application of the FIM has been limited to refractory metals, although some chemisorption systems on these metals have been studied. /19/

2.3.2. Atomic beam diffraction

A thermal energy atomic beam (20-200 meV) has a wavelength on the order of inter-atomic distances. The atomic beam diffracts from a contour of the surface potential corresponding to the beam energy. This contour is located 3-4 \AA above the ion cores in the outermost layer of the surface. Atomic beam diffraction patterns are normally interpreted using model surface scattering calculations, where the scattering is described as a Van der Waals interaction.

The low energy probe of atomic diffraction does not damage even delicate physisorbed overlayers; and it is sensitive to hydrogen, which is an important component of many surface systems of current interest. Electron scattering techniques are relatively insensitive to hydrogen because of its small scattering

cross section. The position of hydrogen chemisorbed on Pt(111) was determined using helium diffraction./20/ Finally, atom diffraction is extremely sensitive to surface order and defects, and it has been very useful in the study of disorder and kinetic processes on surfaces. Because neutral atoms scatter well outside the ion cores of the surface atoms, structural details can be lost and no information on subsurface structure can be obtained.

2.3.3. Scanning tunneling microscopy

The scanning tunneling microscope (STM) is one of the most recently developed surface sensitive techniques./21/ In STM a metal probe is brought close enough to the surface under study for the electron wave functions to overlap. A fixed potential difference between probe and surface is maintained and the probe approaches the surface until a given tunneling current is observed. The probe is mechanically scanned over the surface, and a feedback loop adjusts the vertical spacing to maintain a constant tunneling current. STM has achieved a horizontal resolution of $\sim 2 \text{ \AA}$ and a vertical resolution of $\sim 0.1 \text{ \AA}$ under optimum conditions. By changing the probe-surface potential difference it is possible to map out different surface profiles of wave function overlap. The STM is very flexible and can be applied to all kinds of surfaces. Unlike electron techniques it is not limited to the solid-vacuum interface, although the best resolution has been obtained in vacuum.

The STM can give a direct qualitative image of surface topography. An early STM experiment confirmed the LEED result that the "missing row" model correctly describes the 2×1 reconstruction of the gold (111) surface./22/ Because the tunneling current is a complicated function of the electronic and geometric structure of the tip and surface, so it is difficult to relate a constant tunneling current contour to the geometrical structure of the surface, especially if more than one type of atom is involved. Information on the surface electronic structure is available, however. The lateral resolution of STM images is not good enough to provide accurate information on chemical bond lengths and angles. As the experimental and theoretical tools develop, scanning tunneling microscopy should provide increasingly useful information on surface structure.

2.4. Ion Scattering

At high energies (~ 1 MeV) the interaction of ions with surfaces can be described by classical Rutherford scattering. This simple interaction has been used to study surface structure by directing ion beams along bulk crystal axes at solid surfaces. The "channeling" and "blocking" of these beams is very sensitive to deviations from bulk structure. Ion scattering has been used in particular to study relaxation and reconstruction at crystal surfaces. Measurements of surface relaxation have provided accurate structure determinations, as in the case of reconstructed Au(110).²³ However, if a surface structure involves a large departure from the bulk crystal structure, it can be difficult to solve from ion scattering results.

In any case, because ion scattering is strongly affected by the thermal vibrations of surface atoms, experimental data must be compared to Monte-Carlo simulations for model surfaces to achieve quantitative results. The available data base for structure-fitting is rather small compared to electron spectroscopies, so the sensitivity to structural parameters is sometimes limited. But when the surface structure is close to the bulk structure, ion channeling data can be strongly sensitive to small variations in structural parameters.

2.5. Complementary Techniques

There are a number of other surface probes that are sensitive to the local geometry of the surface or give important information on surface composition, but which do not give direct information on atomic coordinates in the surface region. These techniques provide vital information needed to construct reasonable models of surface structure, which are needed to interpret data from quantitative techniques such as LEED and SEXAFS.

2.5.1. Chemical composition

Chemical composition is the most basic information needed to describe a surface, and a pre-requisite for structure determination. Auger electron spectroscopy is the most generally used techniques for measuring surface composition, and it is sensitive to all elements except hydrogen and helium. Thermal desorption spectroscopy (TDS) is a simple and particularly useful technique for chemisorption studies -- it gives a general idea of the chemical identity of adsorbates, and some information on the type of binding to the surface. Secondary-ion mass spectrometry (SIMS) is another way to get information on surface chemical composition -- its interpretation is generally more complicated, but SIMS is sensitive to hydrogen, and also gives some information on the molecules present on the surface.

2.5.2. Electronic spectroscopy

One group of techniques is sensitive to electronic structure at the surface, and can probe the electronic band structure and density of states near the Fermi level. This electronic information is useful for understanding the bonding mechanisms responsible for chemical process operating at the surface. Structural information can also be obtained by comparing experimentally observed electronic structure with theoretical calculations of electronic structure for model systems (see part 4).

Ultra-violet photoemission spectroscopy (UPS) probes the density of states, and ion neutralization spectroscopy (INS) and surface Penning ionization (SPI) provide similar information with probes of ions and metastable atoms, respectively. Angle-resolved UPS can determine the valence band structure. X-ray Photoelectron Spectroscopy (XPS) provides information on chemical shifts of the atomic core levels, and this can also help in understanding chemical bonding at the surface.

2.5.3. Vibrational spectroscopy

Another class of techniques monitors surface vibration frequencies. High-resolution electron energy loss spectroscopy (HREELS) measures the inelastic scattering of low energy ($\sim 5\text{eV}$) electrons from surfaces. It is sensitive to the vibrational excitation of adsorbed atoms and molecules as well as surface phonons. This is particularly useful for chemisorption systems, allowing the identification of surface species. Application of normal mode analysis and selection rules can determine the point symmetry of the adsorption sites./24/ Infra-red reflectance-adsorption spectroscopy (IRRAS) is also used to study surface systems, although it is not intrinsically surface sensitive. IRRAS is less sensitive than HREELS but has much higher resolution.

2.5.4. Optical techniques

Non-linear optical techniques, such as second harmonic generation (SHG), have recently been used as surface probes. Bulk materials with inversion symmetry do not generate second harmonic signals, while surfaces and interfaces cannot have inversion symmetry, so the total SHG signal will come from the surface region for many systems. The components of the non-linear polarizability tensor have been used to determine the orientation of chemisorbed molecules. /25/ Optical techniques are not limited to solid-vacuum interfaces like charged particle techniques, so their further development can expand the range of surface structural studies to solid-solid, solid-liquid, solid-gas and liquid-gas interfaces.

2.5.5. Electron-stimulated desorption

Observation of the ion angular distribution after electron stimulated desorption of chemisorbed species (ESDIAD) can provide direct quantitative information on the orientation of adsorbed molecules on surfaces. Electrons incident on the surface can excite chemical bonds into non-bonding states, causing molecular decomposition. The excess energy can be converted into kinetic energy, which accelerates an ionic fragment of the molecule along the axis

of the broken bond. The angular distribution of desorbed ions can be related to the orientation of the bonds in the unperturbed adsorbed molecules. This technique gives direct information on the number and symmetry of sites for chemisorption, and approximate information on bond angles.

3. THE THEORY OF MODERN TECHNIQUES FOR SURFACE STRUCTURE ANALYSIS

Although the wide range of experimental techniques described in part 2 have made significant contributions to understanding surface structure and bonding, many of these techniques do not yield explicit information on atomic coordinates in the near surface region, the information required to characterize the surface chemical bond. Other techniques can provide some of this information in certain cases, but can only be applied to a limited range of surface systems, for example ion channeling studies have provided important information on the reconstructions of solid surfaces, but are much more difficult to apply to most chemisorption systems. Optical techniques are being developed which have the potential to contribute direct, quantitative information on surface structure, including surface x-ray diffraction and non-linear optical probes, but these have not yet reached the stage of routine use.

Almost all of the existing quantitative data on surface structure was obtained through experimental techniques that involve the propagation and scattering of electrons in solids. This class of surface probes includes the whole range of "fine-structure" techniques, in addition to LEED and angle-resolved photoemission experiments. This chapter will provide a theoretical description of these techniques and the methods of analyzing the experimental data to determine surface structure.

3.1. General Four-Step Description of Electron-Diffraction Techniques

The most promising techniques for obtaining detailed surface structural information about molecular adsorbates rely on electron diffraction in one way or another. These include LEED,^{/27,28,29/} IV-HREELS,^{/30/} EAPFS,^{/31/} SEELFS,^{/32,33/} EXELFS,^{/34,35/} ARUPS, ARXPS, ARPEFS,^{/36,37,38/} PESEXAFS, SEXAFS, EXAFS, and NEXAFS (XANES). These and other techniques have been discussed above in part 2, and were summarized in Table I. Among these techniques, LEED has been the most productive.

We shall in the following discuss the surface sensitive techniques involving electron diffraction from a common viewpoint. These techniques can all be fit within a four-step description, which will be very useful for comparison. Various techniques are illustrated in terms of this description in Figure 1, and the four steps are defined below.

3.1.1. Step 1: incoming particle

Either a photon or an electron impinges on the surface. This photon or electron may be polarized to yield additional surface information. The electron, part of a well-collimated and monoenergetic electron beam, may be multiply scattered by surface atoms before reaching step 2. Multiple scattering is most marked at kinetic energies below about 200 eV and can make the process particularly sensitive to the surface structure at these lower energies.

3.1.2. Step 2: primary event

A variety of processes may take place at this stage, distinguishing the different techniques -- photoelectron emission, Auger electron emission, ion emission, energy loss due to core-hole, plasmon or phonon excitation, as well as

elastic electron scattering. Thus, in the primary event, the incoming particle generates an outgoing particle. More than one type of particle may be emitted simultaneously, e.g. an electron and a photon in SEXAFS.

From the point of view of obtaining surface structure information, the nature of this primary process is important in two ways. First, the process may be atom-specific, giving chemical selectivity, as in photoelectron emission and Auger electron emission. Second, the process can affect the characteristics of the outgoing particles, especially in terms of angular distribution, and in terms of the exact location within the surface where this primary process takes place. The angular distribution can give direct evidence of the molecular orientation with respect to the surface; this happens, for instance, when an electron is emitted from a valence orbital.

In terms of location, the primary process may be concentrated at one atom, as in an electron-atom scattering in LEED or in electron emission from core levels. It may also be delocalized over many atoms, as in photoelectron emission from a delocalized valence band level. The latter case is again of value to obtain molecular orientations directly. The polarization of the incident electron may also be used to determine molecular orientations, through its effect on the primary process.

3.1.3. Step 3: secondary event

Part of the outgoing electron wave resulting from step 2 will back-scatter from neighboring atoms to the site of emission or initial scattering. If the kinetic energy of the outgoing electrons does not exceed a few hundred eV this results in detectable interference between the outgoing and back-scattered electron waves, which modulates the probability of the primary emission or scattering process. Such modulation is usually called "fine structure" and is the basis of techniques like SEXAFS (EXAFS) and EAPFS (EXELFS, SEELFS), as well as in NEXAFS (XANES). Note that the electrons responsible for this fine structure are rarely collected themselves -- other outgoing electrons or photons (or even ions) are normally detected experimentally.

Two energy regimes are of importance here. At electron kinetic energies above about 50 eV, single back-scattering from neighboring atoms is usually predominant. By contrast, at lower energies electrons can also be multiply scattered by several nearby atoms before returning to the location of the primary process. The single scattering regime modulates the outgoing particle current in a simple oscillatory manner. The near-neighbor interatomic distances can be extracted relatively easily by Fourier transformation given appropriate scattering phase shifts (cf. SEXAFS). When multiple scattering is significant, a multiple-scattering computer simulation is required. This makes the analysis more complex, but gives access to bond angles as well as bond lengths (cf. NEXAFS).

3.1.4. Step 4: outgoing particle

Photons, ions or electrons are detected outside of the crystal. On their way out, electrons may be multiply scattered by surface atoms, especially at the lower energies, which again gives added sensitivities to the surface structure.

3.2. Structural Information

Two modes of electron detection are commonly used, which affect the kind of structural information that can be extracted.




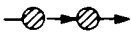

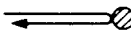



In the angle resolved mode, which selects electrons traveling in well-defined directions, emphasis is laid on the properties of plane-wave diffraction within the surface -- this provides access to all interplanar distances (not only between atomic planes parallel to the surface) and thus, to the complete three-dimensional crystallographic structure (as for example in LEED and in ARPES). Significant structural information can come from steps 1 and 4.

In the angle integrated mode, electrons emitted in many different directions are accumulated simultaneously. To an appreciable extent this averages out the structure-dependent effects of step 4, and therefore emphasizes the information arising from the primary and secondary events of steps 2 and 3, such as the radial distances determined in fine-structure techniques like SEXAFS.

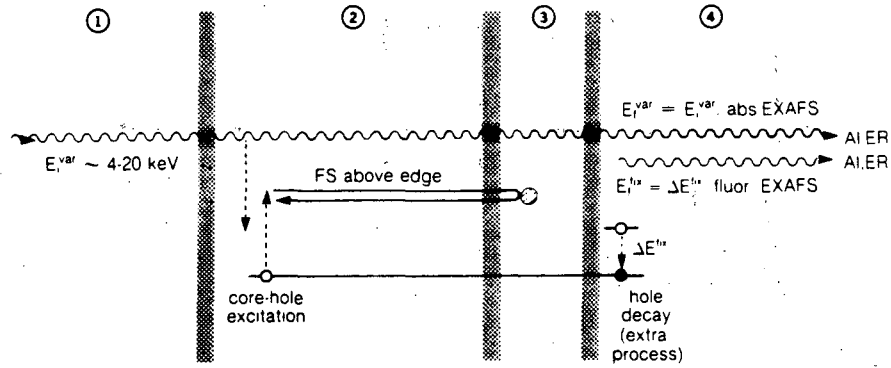
Energy vs. time diagrams

for the event sequences in surface crystallography techniques that use electron scattering/diffraction

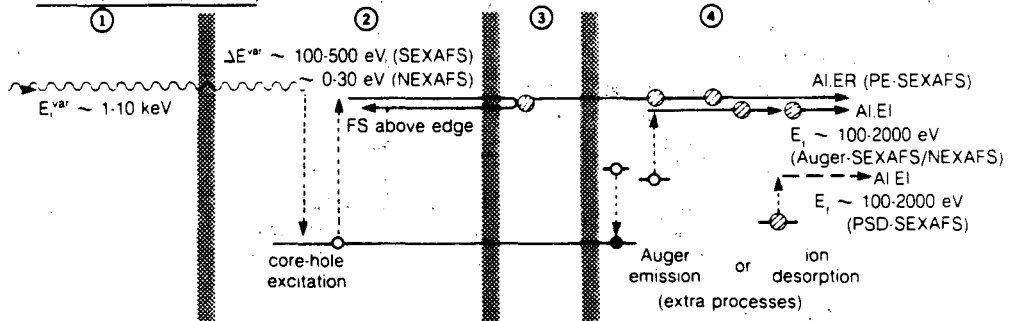
Legend:

	electron propagation
	photon propagation
	ion propagation
	multiple electron forward-scattering by atoms is important
	multiple electron backscattering by atoms is important
	electron backscattering by nearby atoms is important
	bound electron
	electron hole
	energy gain, loss
E_i	incident particle energy
E_f	final particle energy
superscript "fix":	energy is kept fixed in experiment
superscript "var":	energy is varied in experiment
E_b	electronic binding energy
E_A	atomic binding energy in surface lattice
AR	angle-resolved detection
AI	angle-integrated detection
ER	energy-resolved detection
EI	energy-integrated detection
FS	fine structure is important

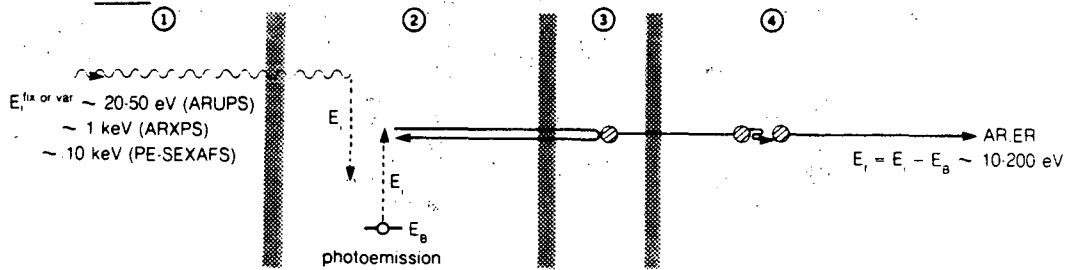
a EXAFS



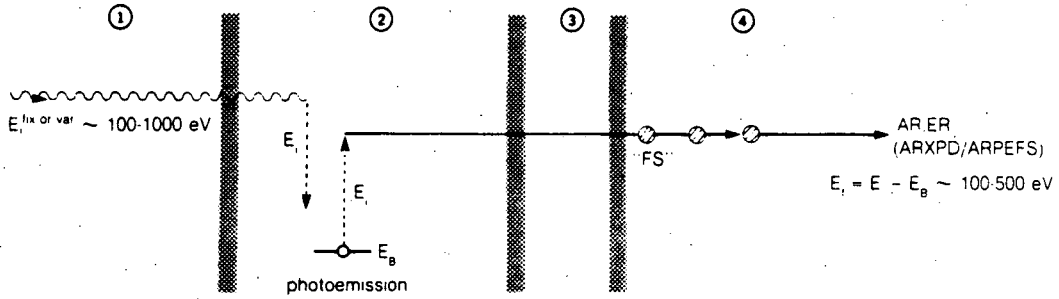
b. SEXAFS/NEXAFS(=XANES)



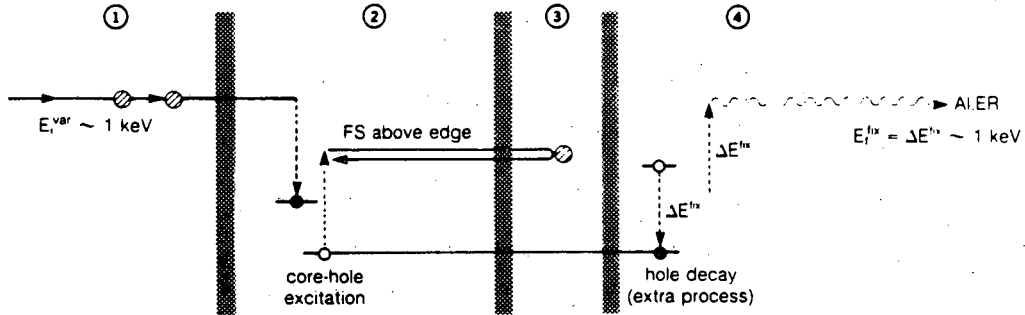
c. ARPES



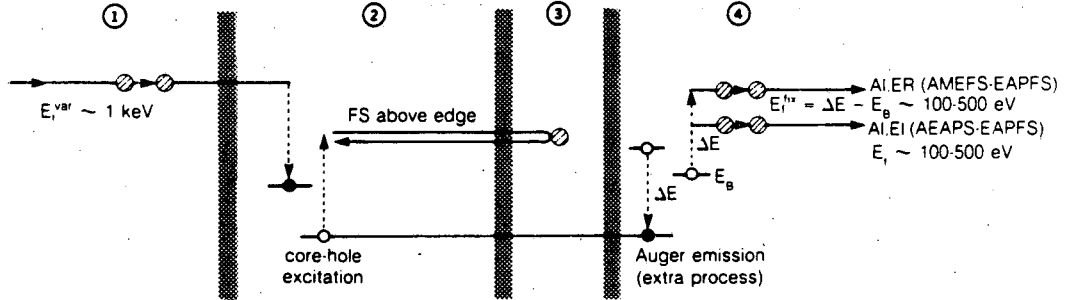
d. ARXPD/ARPEFS



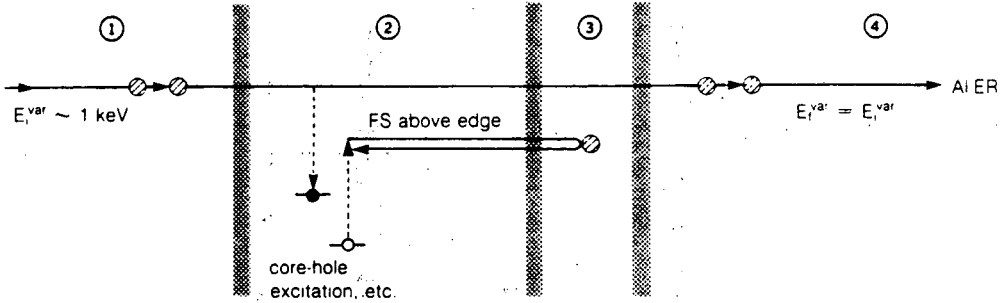
e. SXAPS-EAPFS



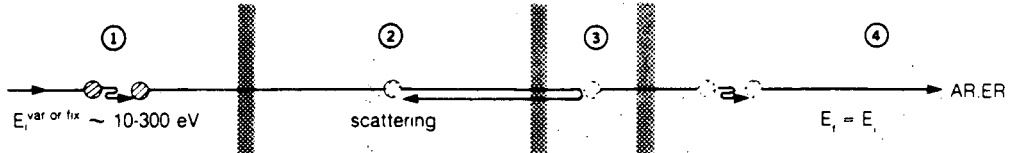
f. AMEFS-EAPFS/AEAPS-EAPFS



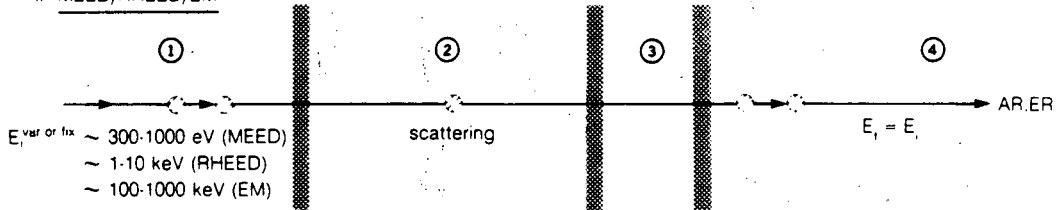
g DAPS-EAPFS



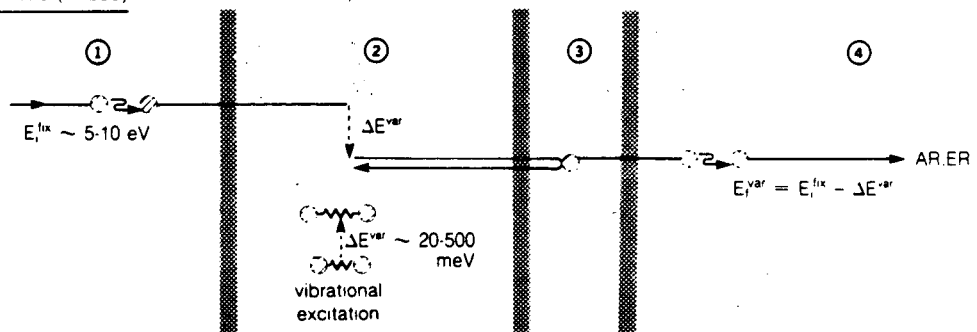
h LEED



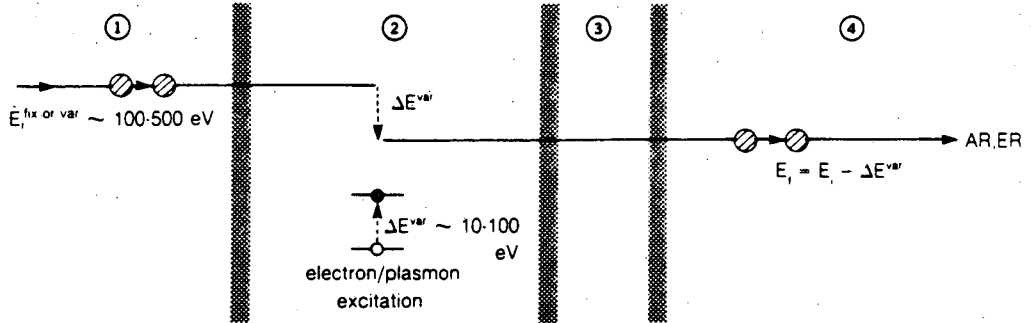
i. MEED/RHEED/EM



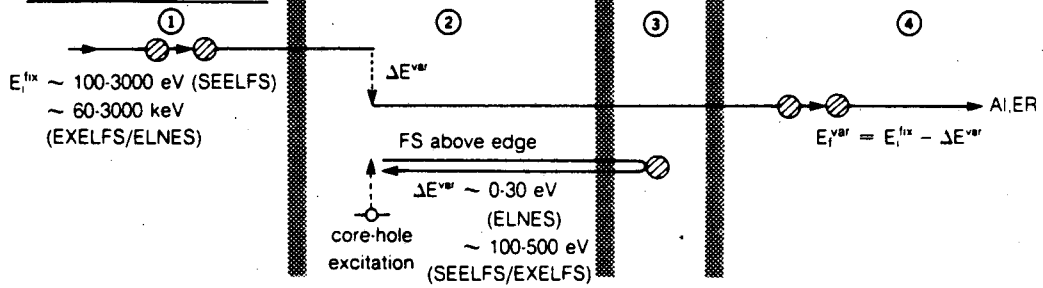
j. HREELS (=EELS)



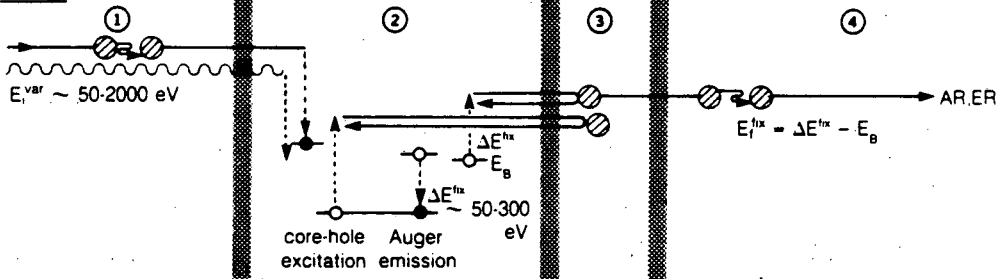
k ELS



l. SEELFS/EXELFS/ELNES



m. ARAES



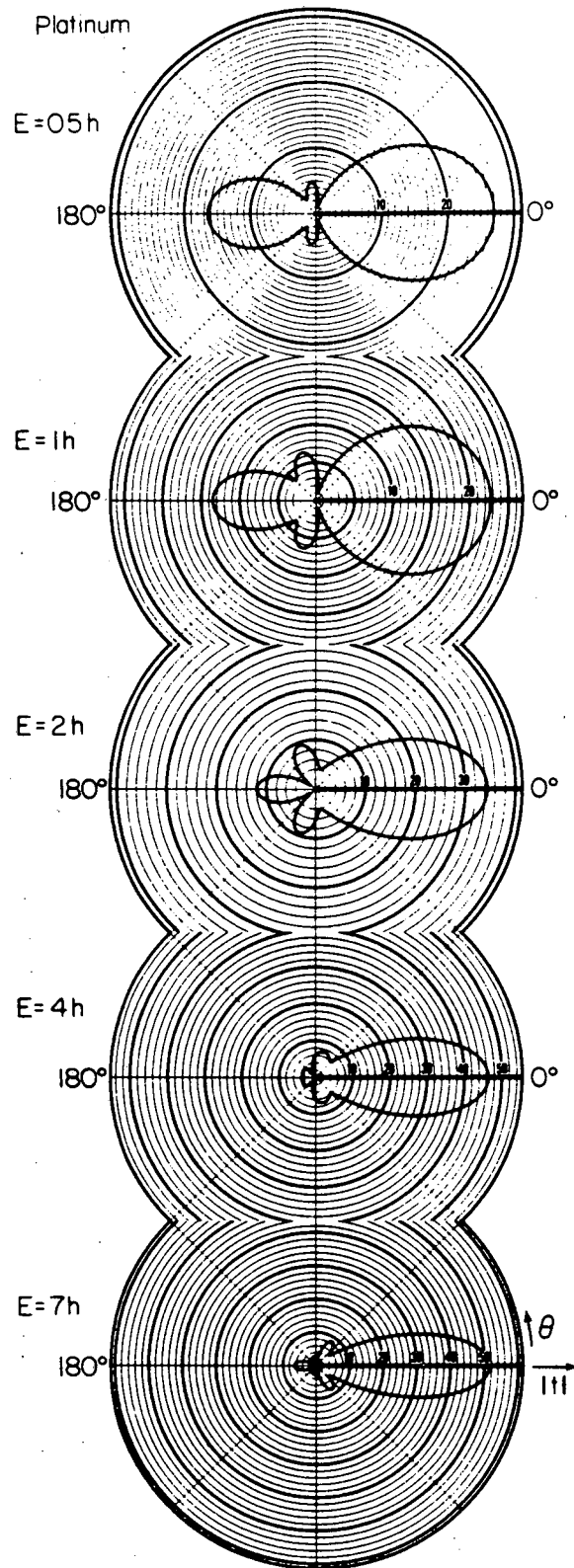
In several techniques an additional process associated with one of the four steps generates the detected particles, e.g. Auger emission in Auger-SEXAFS or ion emission in PSD-SEXAFS. This additional process does not normally provide structure sensitivity, but produces particles that are more conveniently detected. We shall include such processes in the discussion of step 4.

In any of the steps 1, 3 and 4, multiple scattering of electrons can play an important role in the techniques of interest here. On the one hand, multiple scattering provides a greater sensitivity to various aspects of structure; on the other hand, it complicates the theoretical treatment, i.e. it complicates the extraction of the structural information. For the following discussion it will be useful to first describe in more detail a couple of important features of electron scattering by individual atoms in a surface.

At low kinetic energies (10 eV), electrons are scattered strongly but somewhat isotropically by each atom (Figure 2), generating multiple scattering in all directions. As the kinetic energy rises, back-scattering weakens considerably, while forward-scattering remains strong, and multiple scattering remains important only for small scattering angles. This effect is already noticeable around 100 eV and becomes more and more pronounced towards KeV and MeV energies as scattering concentrates in an ever narrower forward cone. This gives the appearance of a more kinematic behavior, i.e. multiple scattering effects becomes less obvious. The reason is that only small momentum transfers occur, which also provides little structure sensitivity. Thus, with rising energy, little back-scattering and therefore, little back-and-forth scattering between any pair of atoms can occur, although multiple forward-scattering along a chain of atoms can be significant. As we shall describe more explicitly in section 3.5.1 one often disregards multiple forward-scattering and talks of a kinematic or single-scattering situation.

3.3. Theoretical Aspects of Individual Techniques

We shall now individually discuss the various techniques in terms of the above four-step description. In all these techniques the flux of outgoing particles is measured as a function of the energy (or sometimes direction) of either the



incident or outgoing particles. The flux (intensity) exhibits variations as a function of energy (or angle), from which the surface structure is extracted. In some cases, the outgoing particles are not energy-analyzed but measured collectively. This is done to enhance weak signal-to-noise ratios, as in SEXAFS.

3.3.1. EXAFS

Extended X-ray absorption fine structure (EXAFS) was the first technique in which "fine structure" was used to obtain structural information./39,35,40/ An incoming photon, penetrating the surface in step 1, undergoes an absorption process creating a core-hole excitation at an atomic site as the primary event (step 2), cf. Figure 1a. This is accompanied by the photo-emission of electrons which back-scatter from near-neighbor atoms as the secondary event (step 3). Interference by the back-scattered electrons modulates (i.e. produces fine structure in) the overall absorption cross-section as their kinetic energy varies in step with the incident photon energy. The fine structure can be observed in the loss of intensity from the incident photon beam ("absorption EXAFS") or instead in the intensity of fluorescence as the core-holes decay ("fluorescence EXAFS"). EXAFS is not intrinsically surface sensitive, and provides surface information only for high-surface-area materials, such as exfoliated graphite or highly dispersed particles, or when the signal comes from atoms which are only present at the surface,/39/ or when total reflection provides surface selectivity.

3.3.2. SEXAFS

To obtain surface sensitivity with EXAFS, thereby creating surface extended x-ray absorption fine structure (SEXAFS), one may monitor instead the outgoing Auger electrons (Auger-SEXAFS), outgoing ions ejected during core-hole decay (PSD-SEXAFS), or outgoing photoelectrons (PE-SEXAFS) instead of a photon signal. Surface sensitivity comes from the short escape depths of electrons and ions./31,41,42,43/ The electron kinetic energies involved in step 3 are sufficiently high (> 50 eV) that single back-scattering prevails over multiple back-scattering. Coupled with angle-integrated detection, this allows a simple Fourier transform

approach to obtain near-neighbor distances (although theoretical or empirical atomic scattering phase-shifts need to be included). Polarization of the incoming photons can be used to obtain additional information about bond directions if valence levels are involved, since the excitation cross-sections include simple selection rules that depend on bond orientations. Chemical selectivity is provided by monitoring only Auger electrons or photoelectrons due to a particular chemical element. One may selectively investigate the structure in the immediate neighborhood of atoms of a particular element. The outgoing particles are normally energy-integrated to provide a measurable signal.

SEXAFS-type fine-structure can be obtained with photo-electrons in the low-energy region ($\sim 100\text{-}300\text{ eV}$). To that end, one must reduce the effect of multiple scattering in step 4 until the effects of step 3 dominate. This can be accomplished with polycrystalline surfaces and with angle-integrated detection, as has been done recently in PE-SEXAFS./44/

3.3.3. NEXAFS and XANES

If in step 3 of EXAFS or SEXAFS, the electron kinetic energy is held within about 50 eV of the excitation edge, one reaches the "near-edge" regime where multiple back-scattering becomes important in the secondary process cf. Figure 1b. This technique is referred to as near-edge x-ray absorption fine structure (NEXAFS) or x-ray absorption near-edge structure (XANES)./45,46,47,48/ Compared to EXAFS and SEXAFS, this multiple scattering gives more complete sensitivity to bond lengths and bond angles in the neighborhood of the atom where the primary process takes place. But model calculations are generally needed to extract this information. As with (S)EXAFS, polarization of the incoming photon can also give direct access to bond directions. Furthermore, combining an empirical correlation between carbon-carbon bond lengths and resonance energies, it appears to be possible to obtain these bond lengths./48/

3.3.4. ARPES, ARUPS and ARXPS

In angle-resolved photoelectron emission spectroscopy (ARPES), incoming photons give rise to the primary event of photoemission (step 2), cf. Figure 1c. This can involve excitation from delocalized electron orbitals (as in angle-resolved ultraviolet photoemission spectroscopy (ARUPS)/49, 50/ from valence levels) or from deeper-lying localized orbitals (as in angle-resolved x-ray photoemission (ARXPS) from atomic core-levels)./51/ If the photoemitted electrons have kinetic energies in the range 10-200 eV, they undergo multiple scattering (similar to that encountered in LEED) in the third and fourth steps, of the four-step process. This yields sensitivity to the surface within a photo-electron mean free path length of the photoexcited atom, which can be chosen with chemical selectivity. Compared to ARUPS, ARXPS is a more convenient approach for the extraction of structural information, since core-level excitations are more easily described than valence-level excitations. Angle-resolved detection is normally used to obtain the most complete structural information, which is interpreted in a procedure very similar to that of LEED with full simulation of the electron emission intensity as a function of energy or angle.

3.3.5. ARXPS and ARXPEFS

If, starting with angle-resolved x-ray photoelectron spectroscopy (ARXPS),/51/ the emitted electron kinetic energy is increased to a few hundred electron volts, the back-scattering of photoemitted electrons to the source atom is considerably reduced, cf. Figure 1b and d. Then the secondary event of step 3 becomes negligible compared to the events of step 4. At the same time, step 4 simplifies to include predominantly single scattering by neighboring atoms, (for convenience, we neglect the multiple forward-scattering in this description, since it yields little structure sensitivity). In this case, electrons reach the detector either directly from the photoemitting atom or after single scattering by atoms that are near the photoemitting atom (again, x-rays, as opposed to ultraviolet radiation, provide the most convenient core-level emission). The interference

between these different outgoing electron paths modulates the detected intensity as a function of the angle of detection: this measurement mode is used in ARXPD.

Similarly, "fine-structure" arises as a function of the emitted-electron kinetic energy in the measurement of angle resolved photoemission extended fine structure (ARPEFS)./37,36,38/ This "fine-structure" is different from that of SEXAFS, EXAFS, etc., since it does not originate from back-reflection to and interference at the electron source atom. It yields the surface structure information relatively easily through Fourier-transformation if angle-resolved detection is used (suitable scattering phase-shifts must be available, however). The full three-dimensional structural information can be so obtained. Sensitivity to a particular structural feature may be emphasized through appropriate selection of the detection angle and and the polarization of the incident photons.

3.3.6. Extended Appearance Potential Fine Structure (EAPFS)

In EAPFS,/31/ incident electrons excite core-level electrons into states above the Fermi level E_F in the primary process cf. Figure 1e-g. This requires a minimum incident energy for any given core-level, namely $E_F - E_1$, where E_1 is the core-level energy (hence the designation "Appearance Potential"). The choice of core-level provides chemical selectivity. The excited electron can then undergo back-reflection from neighboring atoms as the secondary step. This yields fine structure as a function of the incident energy that can be used to obtain structural information by Fourier transformation. Since the incident electrons can undergo multiple scattering prior to the core-level excitation, amorphous materials are preferred to minimize any disturbing LEED-like modulations due to such scattering.

There are three main detection modes for EAPFS within the appearance potential spectroscopy (APS) technique./31/ First, one may monitor soft-x-ray emission due to the decay of the core hole left by the primary process. This is called SXAPS-EAPFS (Figure 1e). Second, it is also possible to monitor Auger electrons due to the same core-hole decay, as in AEAPS-EAPFS and AMEFS-EAPFS, cf. Figure 1f. Third, one may measure the remaining total intensity of

the elastically scattered electrons in DAPS-EAPFS (DA = Dis-Appearance) cf. Figure 1g. Angle-integrated detection removes most of the structural sensitivity of step 4 (especially with amorphous materials). Normally one collects all emitted electrons in these experiments, i.e. energy-integration is used. However, in the Auger-Monitored Extended Fine Structure version (AMEFS-EAPES)/52/ energy resolution is used, which achieves chemical sensitivity at the cost of a lower signal/noise ratio, cf. Figure 1f.

3.3.7. LEED, MEED, RHEED and Electron Microscopy (EM)

In low-energy electron diffraction (LEED) only elastic scattering events are considered, i.e., no energy loss is allowed./27,28,29/ This situation is sometimes referred to as ELEED (Elastic LEED). In LEED, the different steps of the general four-step process are equivalent to each other, in the sense that each step describes possible elastic electron-scattering events in a multiple-scattering chain (which of these scattering events is termed the primary event becomes arbitrary). Figure 1h schematically shows possible scatterings in LEED. The four-step description makes vividly clear that multiple scattering plays a large role in LEED, especially when compared to other techniques described here. This multiple scattering, together with angle-resolved detection, gives LEED a high sensitivity to all details of the surface structure: layer spacings, bond lengths and bond angles throughout the surface to a depth determined by the energy-dependent electron mean free path. To obtain structural information from LEED, the multiple scattering must be simulated on a computer for each plausible geometry until the correct geometry is found by trial-and-error.

At increasingly higher energies, LEED becomes in turn medium-energy electron diffraction (MEED),/53,54,55/ reflection high-energy electron diffraction (RHEED)/56/ and electron microscopy (EM)/57,58/ cf. Figure 1i. Multiple scattering remains important, although the mean distance between successive scatterings increases gradually towards hundreds of Angstroms. On the other hand, to an increasing degree the only significant scattering events at these energies occur near the forward direction. A perfectly ordered surface yields sharp diffracted electron beams, unlike the other techniques which we describe in

this chapter. Any kind of disorder or defects generate diffuse intensities between the sharp diffraction beams. The diffuse intensity contains information not only about deviations from long-range order, but also about the short-range order or local geometry, including chemical bond lengths and bond angles.

3.3.8. ILEED, HREELS and ELS

If at least one of the scattering events in a LEED multiple-scattering chain involves an energy loss, one speaks of inelastic low-energy electron diffraction (ILEED),/59,60/ (multiple losses are possible but infrequent). The lost energy can be transferred to surface vibrations (e.g. molecular vibrations or phonons), as is the case in high-resolution electron loss spectroscopy (HREELS)/61,62,63/ or to electronic excitations (e.g. single-electron excitations or plasmons), as is the case in electron loss spectroscopy (ELS)./64,65/ In ILEED, the primary event of the four-step process is the inelastic electron scattering. It is not necessarily localized at an atomic site (as illustrated for convenience in Figure 1j,k) instead, it is quite often delocalized over many atoms, as with dipole scattering in HREELS or plasmon excitation ELS. In HREELS cf. Figure 1j, multiple scattering is at least as important as it is in LEED, and angle-resolved detection is also used. HREELS can therefore yield potentially the same structural information as LEED, e.g. when intensities are measured as a function of incident energy, at the cost of having to describe an additional inelastic process in the theory./63/ This approach may be called IV-HREELS, since LEED-like IV curves are used. HREELS is however mostly used in a mode where the multiple scattering effects are virtually constant, namely by scanning the energy loss over a small range at fixed incident energy./61,62/ Then all that matters is the occurrence of sharp energy losses at values corresponding to frequencies of surface vibration. This gives a loss spectrum similar to that familiar in infra-red adsorption spectroscopy (IRAS) in the gas phase and at surfaces. This is also the approach with ELS, cf. Figure 1k, although here the wide scan of energy loss allows multiple scattering to significantly modulate the heights of the peaks corresponding to individual excitations. Under these circumstances the structural information is obtained indirectly through the measured vibrational and excitational properties of the surface, rather than through the diffraction effects.

3.3.9. Surface Extended Energy Loss Fine Structure (SEELFS)

Another electron-based energy-loss technique is SEELFS./32,33/ Compared to HREELS and ELS, higher electron energies are used, so that a core-hole excitation-edge and the associated fine structure become available, cf. Figure 11. There is a great similarity between SEELFS and EAPFS. However, in SEELFS the energy-loss is kept small compared to the incident energy, thus, one has a single-electron final-state problem in SEELFS rather than a two-electron final-state problem as in EAPFS. By keeping the incident energy fixed in SEELFS and by angle-integrating the detection, variable diffraction effects in steps 1 and 4 are minimized. This yields fine structure that can be Fourier-analyzed to yield bond lengths around chemically-selected atoms. Complication can arise however, when several spherical waves with different angular momenta are needed to describe the electrons of step 3. This produces in effect several overlapping fine structures, which may not be easy to isolate. Nevertheless, experimental evidence suggests that normally one of the angular momentum components is sufficiently dominant to avoid these complications.

3.3.10. Extended X-Ray Energy Loss Fine Structure (EXELFS)

By substantially increasing the electron kinetic energy in ILEED and SEELFS to 60-300 KeV, one reaches a situation that can resemble EXAFS, with electrons replacing the EXAFS photons, cf. Figure 11. Chemical selectivity. is obtained by choosing an appropriate core excitation edge. And surface sensitivity on the atomic scale exists mainly for high-surface-area materials, as with EXAFS.

3.3.11. Electron Energy Loss Near-Edge Structure (ELNES)

ELNES/66/ is the near-edge equivalent of EXELFS, with the same high-energy (60-300 KeV) electrons as incident particles. It focuses on final energies within about 30 eV of an absorption edge, so that the fine structure arising in step 3 behaves very much as in NEXAFS, cf. Figure 11. Here multiple scattering

is important, giving full structural information in the immediate vicinity of a selected chemical element. However, there is no simplifying dipole selection rule in the primary process, since electrons replace the photons.

3.3.12. Angle-Resolved Auger Electron Spectroscopy (ARAES)

One may directly monitor Auger electrons emitted following core-hole excitation induced by an incident electron or photon beam, using angle resolved detection, cf. Figure 1m./67,68/ Thus the core-hole excitation together with the Auger process constitutes our step 2. At the lower energies used in ARAES (~ 20 -200 eV), multiple scattering is often important as in LEED, especially in step 4. Thus step 3, as in LEED, is not distinguished by convenient fine-structure, but is much more complex due to multiple scattering. In addition, to obtain structural information, the complicated atomic Auger process must be modeled accurately. This has only been done in a few special cases involving atomic orbitals (as opposed to solid state orbitals)./69,70/ As a result, the Auger transition probabilities into the various outgoing spherical waves in step 2 are generally unknown. So far these probabilities have been fit to experiment, with limited success in terms of structural determination. The orientation of adsorbed molecules appears to be accessible with the photon-excited version of this technique, by using photon polarization and symmetry selection rules./71/ Otherwise the angle-resolved detection of ARAES can yield the same relatively complete three-dimensional structural information as does LEED.

3.4. Formalism for Individual Processes

In section 2.3 we have decomposed various surface-sensitive techniques into a small set of more elementary processes. In this section we shall present appropriate formalisms that describe these individual processes. Namely, we shall discuss the theoretical treatment of the propagation of electrons in the surface region, as well as the treatment of elastic and inelastic electron-atom scattering, photoelectron emission and of Auger electron emission. These parts

can then be easily recombined to provide a complete theoretical description of each surface-sensitive technique. Some general features of particular interest will be highlighted in section 3.5.

3.4.1. Overview of process formalisms

We shall deal mainly with the propagation and scattering of electrons through solid surfaces. The most appropriate formalism to describe these processes will depend very much on the situation, as computational efficiency is at a premium. Spherical-wave and plane-wave expansions are frequently used, often side by side within the same theory. Spherical waves are convenient to describe the scattering or emission of electrons by an individual atom. An important quantity will then be the complex amplitude of each spherical wave leaving that atom.

Plane waves are often used when two conditions are satisfied: 1) many (but not necessarily all) atomic layers of the surface have a two-dimensional periodicity, and 2) either a plane-wave incident electron beam is present or angle-resolved electron detection is applied. Computation based on the plane-wave expansion are often much more efficient than those based on the spherical-wave expansion. This explains their frequent use even in problems that do not involve strict two-dimensional periodicity, as with disordered overlayers on an otherwise periodic substrate.

The fate of scattered or emitted electron waves depends on the occurrence of multiple scattering from atom to atom. With strong atomic scattering, a large number of scattering paths must be considered: this applies especially at low energies and with angle-resolved detection, e.g. in LEED and ARPES. At higher energies fewer scattering paths are important, because the atomic scattering is relatively weaker (except for forward-scattering). Paths involving mostly forward-scattering dominate in angle-resolved techniques such as ARPEFS, MEED, RHEED, and EM. By contrast, single back-scattering to the emitting atom dominates in angle-integrated fine structure techniques such as (S)EXAFS, EAPFS and SEELFS. The individual formalisms strongly reflect these different circumstances.

3.4.2. Electron propagation

The interference effects resulting from electron propagation are responsible for providing the desired structural information in all the techniques discussed here. The extraction of structural information, therefore, requires a knowledge of the electron wavelengths and of any phase shifts that may occur in electron emission and electron-atom scattering. Failure to understand these processes can result in quite erroneous results.

The well-known muffin-tin model of the electron atom interaction potential has in most cases proved to be an adequate compromise between accuracy and computational efficiency, at least for electron kinetic energies exceeding ~ 20 eV./27,28,29/ The muffin-tin potential is spherical inside the muffin-tin spheres. This "ion core" usually provides the dominant contribution to electron scattering and emission, to be discussed shortly.

The interstitial region between these spheres is represented by a constant potential value (the muffin-tin constant or muffin-tin zero). This is the region of unscattered electron propagation, in which simple plane-wave or spherical-wave behavior describes the electron wave-field. The plane-wave description is computationally advantageous when dealing with multiple scattering by periodic lattices, since such lattices diffract any plane wave into other well-defined plane waves. This approach is often useful even with non-periodic overlayers adsorbed on an otherwise periodic substrate.

The spherical-wave description has its own great advantages. It is best adapted to the scattering and emission by the spherical ion cores and it does not require the presence of any structural periodicity. In particular, it is well suited to the treatment of multiple scattering between different atoms within any cluster of atoms, in particular within a periodic unit cell as in LEED. It is also convenient for the treatment of fine structure arising from back-scattering by nearby atoms, as in (S)EXAFS, NEXAFS, EAPFS, etc. (i.e. in step 3 in our four-step description).

For energies lower than ~ 20 eV, the muffin-tin model is often inadequate outside the muffin-tin spheres. In the case of surfaces, this applies especially to low-energy studies of adsorbed molecules. For instance, HREELS is normally performed at kinetic energies around 5-10 eV (to benefit from a strong reflection

coefficient from the substrate). HREELS is therefore highly sensitive to the potential in the molecular bonding regions and couples strongly with weakly bound and relatively delocalized electron states. Also, NEXAFS is often measured down to energies of about 10 eV above an emission edge, giving similar sensitivity to bonding details. No satisfactory alternative treatment to the muffin-tin model has yet been applied in the surface context, mainly because excessive computational efforts would be involved (however this problem has been dealt with in the case of low-energy electron scattering by gas-phase molecules/72/).

3.4.3. Single electron-atom scattering

Electron-atom scattering is central to all techniques under discussion here. As we have mentioned, electron-atom scattering at surfaces has been treated almost exclusively by means of the muffin-tin model.

The formalism of electron-atom scattering has been extensively dealt with elsewhere./27,28,29/ We shall only recall its main features here. Because of the assumed spherical symmetry, the partial-wave scattering approach is convenient. Namely, an incoming spherical wave $h_l^{(2)}(kr) Y_l^m(\mathbf{r})$, ($-l \leq m \leq l$) can scatter only into the outgoing spherical wave $h_l^{(1)}(kr) Y_l^m(\mathbf{r})$ (here $h_l^{(1)}$ and $h_l^{(2)}$ are Hankel functions of the first and second kinds, $k = 2\pi/h(2mE)^{1/2}$, E is the kinetic energy and $r = |\mathbf{r}|$). This occurs with amplitude t_l (t_l is an element of the diagonal atomic t -matrix), which is related to the phase shifts δ_l through

$$t_l = -\frac{\hbar^2}{8\pi m} \frac{1}{k} \sin \delta_l e^{i\delta_l} \quad (1)$$

The phase shifts δ_l are calculated by standard partial-wave scattering theory. It involves the electron-atom interaction potential of the muffin-tin model. There are a variety of ways to obtain this potential, which consists of electrostatic and exchange parts (spin dependence may be included, especially when the spin polarization of the outgoing electrons is of interest). One usually starts from known atomic wave functions within one muffin-tin sphere and spherically averages contributions to the total charge density or potential from nearby

atoms. The exchange term may be treated as non-local (e.g. Hartree-Fock) or local (e.g. X_α). The muffin-tin constant with respect to the vacuum zero level is a by product of this approach, however in practice this constant is normally adjusted *a posteriori* to take into account surface-related work function changes.

The t -matrix of Eq. (1) will be useful in describing the scattering of a *plane* wave by an atom. Expansion of the plane wave $e^{i\mathbf{k}\cdot\mathbf{r}}$, with $|\mathbf{k}| = k$, into spherical waves yields the total scattered wave

$$e^{i\mathbf{k}\cdot\mathbf{r}} + f(\theta) \frac{e^{i\mathbf{k}\cdot\mathbf{r}}}{r} \quad (2)$$

at large values of kr . The atomic scattering amplitude $f(\theta)$ depends on the scattering angle θ through the well-known relation

$$f(\theta) = -4\pi \sum_l (2l+1) t_l P_l(\cos\theta) \quad (3)$$

where the functions $P_l(\cos\theta)$ are Legendre polynomials. The scattering amplitude $f(\theta)$ can be used to illustrate the nature of electron scattering in solids. A large scattering amplitude implies strong multiple scattering. To discuss this issue, we need to first include the effect of atomic thermal vibrations. It has been found adequate for this purpose to replace the scattering amplitude $f(\theta)$ by a statistical average over certain atoms, even in the presence of multiple scattering. In the case of diffraction by a periodic lattice, the average is performed over atoms that are equivalent by two-dimensional periodicity, and in the case of back-scattering by shells of vibrating neighbors, around equivalent source atoms. In either case, one ends up multiplying $f(\theta)$ by a Debye-Waller attenuation factor e^{-M} , with

$$M = \frac{1}{2} |\mathbf{s}|^2 \langle (\Delta\mathbf{r})^2 \rangle \quad (4)$$

where \mathbf{s} is the linear momentum transfer and $\langle (\Delta\mathbf{r})^2 \rangle$ is the mean-square atomic displacement.

Note that the product $e^{-M} f(\theta)$ can be expressed in terms of effective phase shifts in direct analogy with Eqs. (1) and (3), then δ_l is replaced by an effective

$\delta_l(T)$ in those relations. These so-called "temperature-dependent" phase shifts $\delta_l(T)$ are commonly used in multiple scattering theory, because the effect of thermal vibrations is felt again and again at each scattering in a chain of scatterings.

The product $e^{-M} f(\theta)$, shown as $|f(\theta)|$ in Figure 2, has a marked lobe structure in its angular dependence. There is always a pronounced lobe of strong scattering amplitude in the forward-scattering direction ($\theta = 0$). This lobe becomes narrower (more forward-focused) with increasing kinetic energy, becoming quite narrow (a few degrees) at energies above 1000 eV. High temperatures also favor a narrow forward scattering lobe since the Debye-Waller factor attenuates forward-scattering less than large angle scattering. In addition, there is usually a lobe centered on the back-scattering direction ($\theta = \pi$). At low energies (~ 10 eV) this lobe is wide and comparable in strength to the forward lobe, yielding nearly isotropic scattering. But at higher energies the back-scattering lobe rapidly loses strength, while also becoming narrower. Finally there are one or more side-scattering conical lobes which are usually of a strength comparable to or smaller than the back-scattering lobe. These become more numerous and narrower with increasing energy. Between lobes there may be directions with vanishing scattering amplitude, when accidental cancellation of partial scattered waves occurs.

3.4.4. Multiple electron scattering

We have just described electron scattering by a single atom. The main feature to remember is the pronounced forward scattering within a more or less narrow forward cone, which occurs especially at the higher energies. The implications for multiple scattering are as follows.

At low energies (~ 10 eV) the scattering is relatively isotropic and relatively strong, so that scattering in any direction is likely to be followed by scattering from another atom that finds itself in the electron path. In fact, several successive scatterings are quite possible, especially with heavy (high-Z) atoms, which scatter most strongly. This includes the possibility of repeated back-and-forth scattering between two or more atoms, which is, when the interference is

constructive, similar to a negative-ion resonance in a molecule. With such strong multiple scattering, a perturbation expansion in terms of the number of scatterings will often fail to converge and a self-consistent solution is then necessary.

At higher energies, back-scattering and side-scattering become increasingly less probable, leaving mainly forward-scattering, which itself remain quite strong. Even for very high energies, e.g. in HEED or EM at $E \sim 10\text{-}1000$ KeV, multiple scattering is still important. But now all scattering paths remain bundled within a few degrees of the incidence direction.

These facts explain many differences between surface-sensitive techniques. Those techniques which use low kinetic energies, such as LEED, ELS, HREELS, ARAES, ARPES and NEXAFS, require a rather complete multiple scattering treatment. Some perturbation theories do apply to them but close attention to multiple forward-scattering as well as to several back-scattering events remain essential. Techniques using higher energies split up in two groups. The fine-structure techniques, such as (S)EXAFS, EAPFS, SEELFS and EXELFS, rely almost exclusively on the (weak) back-scattering from neighboring atoms to the emitting atom. Forward-scattering, though strong, is largely irrelevant in this situation (this is enhanced by angle-integrated detection, which averages over many exit directions). Other high-energy techniques are much more sensitive to multiple forward scattering events, e.g. MEED, HEED, EM and ARPEFS (partly because of their angle-resolved detection mode in the forward direction).

We shall next describe several formalisms used to calculate the effects of multiple scattering. We start with the most accurate formalism in common usage and then introduce simplifications and specializations.

Within the muffin-tin model of spherical scatterers, all multiple scattering can be properly included with the Green function formalism. We already have given the t -matrix for scattering by a single atom. It is now necessary to describe the propagation of the scattered spherical waves in the "near-field" region (without asymptotic forms). Consider the propagation of a wave of angular momentum quantum number $L \equiv (l, m)$ from an atom at location \mathbf{r}_i to an atom at location \mathbf{r}_j . This wave can be expressed in terms of spherical waves $L' \equiv (l', m')$ incident on atom j with amplitudes given by the Green function

$$G_{LL'}^{ij} = -4\pi i \frac{8m}{h^2} k \sum_{L_1} i^{l_1} a(L, L', L_1) h_{l_1}^{(1)}(k|\mathbf{r}_i - \mathbf{r}_j|) Y_{L_1}(\mathbf{r}_i - \mathbf{r}_j) \quad (5)$$

Here $k = |\mathbf{k}|$ and $L_1 = (l_1, m_1)$ extends over all values of l_1 and m_1 compatible with L and L' , namely such that $|l - l'| \leq l_1 \leq l + l'$ and $m + m' = m_1$. This compatibility is manifest as non-zero values of the Clebsch-Gordon (or Gaunt) coefficients

$$a(L, L', L_1) = \int_{\Omega} Y_L^*(\Omega) Y_{L'}(\Omega) Y_{L_1}^*(\Omega) d\Omega \quad (6)$$

With the t -matrix and the Green function we can represent any multiple-scattering path explicitly. For instance, scattering by atom 1 to atom 2, then back to atom 1 and on to final scattering by atom 3 yields a scattering amplitude of

$$t^3 G^{31} t^1 G^{12} t^2 G^{21} t^1 \quad (7)$$

where one should read from right to left (in the fashion of matrix multiplication) and where the superscripts on the t -matrices allow the different atoms to have different scattering properties. When strong multiple scattering occurs, the contributions from all such scattering paths should be included. This can be done self-consistently by replacing the infinite series due to longer and longer scattering paths by a matrix inversion.^{73/} The result is the following expression, for diffraction by a set of N atoms labeled $i = 1, 2, \dots, N$:

$$\begin{pmatrix} T^1 \\ T^2 \\ \vdots \\ T^N \end{pmatrix} = \begin{pmatrix} I & -t^1 G^{12} & \dots & -t^1 G^{1N} \\ -t^2 G^{21} & I & \dots & -t^2 G^{2N} \\ \vdots & \vdots & \ddots & \vdots \\ -t^N G^{N1} & -t^N G^{N2} & \dots & I \end{pmatrix}^{-1} \begin{pmatrix} t^1 \\ t^2 \\ \vdots \\ t^N \end{pmatrix} \quad (8)$$

Here t^i , T^i , G^{ij} and I are matrices indexed by $L = (l, m)$ and $L' = (l', m')$; I is the unit matrix. A multicenter expansion is used, i.e. the spherical waves are centered on the respective atoms. The quantity $T_{LL'}^i$ is the total amplitude of the

spherical wave Y_L that leaves atom i after spherical waves Y_L have initially impinged on every atom of the cluster and multiple scattering within the cluster has been taken into account. The scattered wave accumulated over all terminal atoms i is obtained by simple addition of the T^i values with proper consideration of the relative amplitudes and phases of the initial wave incident on the cluster.

The dimension of the large matrix to be inverted in Eq. (8) is $N(l_{\max}+1)^2$, where l_{\max} is the largest value of l included. This dimension critically affects the required computing effort. The number of spherical waves used, $(l_{\max}+1)^2$ is typically 16 to 64 at LEED energies (l_{\max} is \sim inversely proportional to the electron wavelength). The value of N is in general the number of atoms in the cluster needed to adequately account for all multiple paths involving any given surface atom. At 20 eV this might be several hundred atoms, as defined by a sphere around the given atom and whose radius is a few times the electron mean free path. Thus, matrix dimensions in Eq. (8) of the order of 10^4 would be required within this formalism. This is the situation for NEXAFS, ELNES and diffuse LEED. A similar single-center expansion approach has also been formulated for this problem.^{74,75} It involves a new "wallpapering" scheme that bypasses the larger matrix inversion of Eq. (8); instead it builds up the cluster scattering properties as seen from a central atom in a shell-by-shell iteration, each step of which involves the inversion of a smaller matrix. However, the single-center expansion gives rise to much larger values of l_{\max} (proportional now to the radius of the cluster instead of the muffin-tin radius) which still results in large computation times.

Simplifications can be brought about whenever the surface structure has symmetries. Point-group symmetries help moderately to reduce the matrix dimensions. On the other hand, two-dimensional periodicity can help drastically by reducing the number N to the number of atoms within a single two-dimensional unit cell with a depth perpendicular to the surface of a few times the electron mean free path. For surface crystallography this is, however, not yet sufficient, because surface structural determination requires repeating such calculations for hundreds of different geometrical models of the surface structure.

Great computational advantage can ensue from using the plane-wave expansion between atomic layers. This occurs when such a representation converges, which requires sufficiently large spacings between the layers. Various

calculational methods based on plane waves have been developed over the years, such as the Bloch-wave, Layer Doubling and Renormalized Forward Scattering methods. These have been extensively described previously in the context of LEED, /27,28,29/ but their use in other techniques merits further discussion here. In conventional LEED, the two-dimensional surface periodicity clearly defines a finite set of outgoing plane waves (corresponding to the discrete diffracted beams defined by the two-dimensional reciprocal lattice). Most other techniques do not share this feature -- no sharp electron beams emerge from the surface in photoemission, SEXAFS, diffuse LEED, etc. However, the use of angle-resolved detection is equivalent to defining a finite set of plane waves. This situation has been described as inverse LEED or time-reversed LEED. /76/ The detector essentially singles out an emerging plane wave, which, when time is reversed, acts like a plane wave incident on the surface. This plane wave scatters through the periodic layers as does normal LEED, via the set of plane waves familiar in LEED, until they reach the original source of electrons. The source can be a photoemitting atom, for instance. The calculation need not proceed in this time-reversed manner, however, given the source of emission in the form of amplitudes of outgoing partial waves (which can be corrected for intra-layer multiple scattering), one can deduce the resulting amplitudes of the above-mentioned set of plane waves as they leave the source. From then on multiple scattering through the lattice proceeds as in conventional LEED using the finite set of outgoing plane waves defined by the direction of detection.

Some techniques also involve a well-defined *incident* electron beam, even though the primary process at some point imparts an arbitrary parallel momentum to the electrons. This happens, for example, with energy loss in HREELS and ILEED, with diffuse scattering in LEED and with Auger emission in ARAES. In these cases the direction of the electrons leaving the surface has an arbitrary relationship to the incident beam direction. Up to the primary process, however, conventional LEED can be applied in the plane-wave representation, at least in the ordered part of the surface, using the finite set of plane waves defined by the direction of incidence.

3.4.5. Approximations in multiple scattering

We shall now describe a series of approximations of increasing simplicity which have been developed to reduce computational effort required to describe multiple scattering. These approximations are usually tailored to specific circumstances and are used only in those particular circumstances in order to maintain the highest possible accuracy.

We have mentioned the preponderance of forward scattering of electrons by atoms. Perhaps the earliest method used to exploit this feature was Renormalized Forward Scattering in LEED./27/ This plane-wave method is a perturbation expansion in terms of the number of back-scatterings between atomic layers. It expressly does not count forward scatterings in the expansion. Instead, all forward scattering events that may occur between successive back-scattering events are explicitly included. This approach is very economical and converges well except at the lowest energies (~ 10 eV) where multiple scattering is too strong (as with all plane-wave methods, a sufficiently large interlayer spacing is also required). More recently this idea has been applied to conventional LEED within the spherical-wave representation under the name Reverse Scattering Perturbation./77/ Most recently, this idea has been adapted to a shell-by-shell treatment (as opposed to a layer-by-layer treatment),/78/ similar to the "wallpapering" scheme mentioned above. One then considers spherical waves leaving an atom or cluster and reflecting back from shells of neighboring atoms, including multiple scattering. This approach is particularly useful when long-range order is absent or unimportant, as in NEXAFS/78/ and in one part of a diffuse LEED theory./79/

This diffuse LEED theory consists of three parts:

- 1) multiple scattering of the incident electrons through the ordered region of the surface, yielding to a conventional LEED treatment;
- 2) scattering by a defect site, e.g. an isolated disordered adsorbate, including multiple scattering from shells of neighboring atoms back to the defect site;
- 3) multiple scattering on the way out from the defect site to the detector through the ordered region of the surface, which corresponds to the inverse LEED problem.

Another method based on the number of back-scatterings by atomic layers is Beam Set Neglect in LEED,/80/ which is particularly appropriate for adsorbates on simple substrates. This method takes advantage of the fact that some sets of diffraction beams only affect the intensities of other beams through multiple scattering of third- or higher-order, therefore such sets of beams may be neglected. The method is very efficient both large superlattice unit cells (which create large number of of beams, most of which may be neglected) and also yields an efficient solution to the diffuse LEED problem./79/

As the electron energy increases, back-scattering rapidly becomes weaker and multiple scattering occurs primarily within a narrow cone in the forward direction. This is exploited in the chain method developed for MEED and RHEED./53,54/ In these techniques, grazing incidence is normally used to obtain surface sensitivity and sufficient reflection. These factors favor scattering along chains of atoms oriented parallel to the surface in the direction defined by the incident beam. The chain method uses this as a basis to calculate MEED and RHEED intensities exactly (allowing application to LEED as well). But when back-scattering and side-scattering are very weak, they can be selectively and efficiently neglected in favor of the multiple forward-scattering that occurs within the chains of atoms.

We next turn to the high-energy fine-structure techniques: EXAFS/SEXAFS, EAPFS, SEELFS, EXELFS and ARPEFS. All but one of these involve single scattering back to a source atom, resulting in interference modulation of the primary process (Auger emission, etc.). The exception is ARPEFS, where the source atom emits photoelectrons which are scattered only once by neighboring atoms directly towards the detector (not counting multiple scattering which is insensitive to the structure). The structural information stems from the interference at the detector between the waves directly traveling from the source atom to the detector and the waves scattered emitted from the source atom and scattered into the detector by different neighboring atoms. Furthermore, angle-resolved detection is used in ARPEFS unlike the other fine-structure techniques. The common feature of all these techniques is high electron energies and a diffraction geometry which de-emphasizes forward scattering (although forward scattering effects have been observed)./47/ Under these circumstances substantial simplifications can be considered. First, single

scattering by neighboring atoms may be assumed. Second, one may ignore the finite radius of curvature of the spherical waves reaching the neighboring atoms, yielding the "plane-wave" or "small-atom" approximation. Third, the radial spherical functions may be given their asymptotic form $\frac{e^{ik \cdot r}}{r}$.

These simplifications lead to the following relative intensity modulations for ARPEFS:

$$\begin{aligned} \frac{(I - I_0)}{I_0} &\equiv \chi(k) \\ &= \sum_j \frac{\cos \beta_j}{\cos \gamma} \frac{|f(\pi) + f(\pi)f(0)|}{r_j} \cos[kr_j(1 - \cos \alpha_j) + \phi_j] \end{aligned} \quad (9)$$

Here k is the electron momentum, α_j is the scattering angle at the neighboring atom situated at position \mathbf{r}_j , $|f(\alpha_j)|$ is the corresponding scattering amplitude and ϕ_j the corresponding phase shift (i.e. the phase of $f(\alpha_j)$), while γ is the angle between the polarization direction and the direct emission path to the detector, and β_j is the angle between the polarization direction and the initial path of an electron scattered from site j . (A Debye-Waller factor and an inelastic damping factor may be added to Eq. (9)). This expression may involve many terms j , one for each neighboring atom which contributes. Nevertheless the expression remains simple to analyze in many circumstances. Namely, by suitable choice of the energy, which affects $f(\alpha_j)$, and polarization direction, most terms can be made negligible. Then it becomes relatively easy to extract the structural information in the form of the path length differences $r_j(1 - \cos \alpha_j)$. With the energy scans of ARPEFS, Fourier transformation of the k -dependent data is sufficient, although some care with data manipulation is required. In particular, the phase shifts ϕ_j have to be known from theory. There is also controversy about whether the plane-wave approximation is adequate in ARPEFS.

With the other fine-structure techniques (EXAFS, SEXAFS, EAPFS, etc.), the above mentioned approximations lead to the following general relationship for the intensity modulation at the detector: /41,42,43/

$$\chi(k) = \sum_j \frac{N_j}{kr_j^2} \sin(2kr_j + 2\delta_l + \phi_j) |f_j(\pi)| \quad (10)$$

Here δ_l is the phase shift of the central atom for a partial wave of angular momentum l , while N_j is the number of identical atoms at a distance r_j . (Here again a Debye-Waller and an inelastic damping factor may be added; also a polarization dependence may be included for EXAFS and SEXAFS.) Fourier transformation can yield the distances r_j with proper care. In this case the phase shifts are usually obtained from EXAFS results for bulk materials where the phase shifts are determined from the interatomic distances known from x-ray diffraction. Alternately, the phase shifts may be computed as is done in LEED. Note that multiple forward scattering is not included in Eq. (10).

3.4.6. Photoelectron emission

The first step in photoemission (and some other techniques) involves photon propagation through the surface region to the location of the electron excitation.

3.4.7. Photon propagation

The propagation of electromagnetic waves in bulk solid materials and in molecules is well understood. This understanding is appropriate for bulk EXAFS, for instance, but not necessarily for surface studies. The situation of a solid surface has only been studied recently in terms of atomic-scale phenomena, as is required by techniques such as photoemission. Although photons typically penetrate to a depth of about $1 \mu\text{m}$ into the metal surfaces of interest, the only important photon-induced excitations occur within the electron escape depth of about 5 to 10 Å. Therefore, the shape of the electromagnetic fields should be known in this near-surface region of a few atomic layers.

It has been found that for photon energies near and below plasmon energies ($\sim 20 \text{ eV}$) and near other excitations, the electromagnetic fields are quite structured, both as a function of depth from the surface and as a function of energy.^{/81/} For any quantitative structural studies, this situation is to be

avoided. However, at all other photon energies, the fields are quite uniform and well described by the macroscopic bulk dielectric theory./82,83/ There remains, nevertheless, the unanswered question of where exactly to locate the boundary between solid and vacuum, especially in the case of adsorbed layers: at the substrate-overlayer interface, or at the overlayer-vacuum interface or elsewhere. It has been estimated that this uncertainty leads to errors which do not exceed approximately 20% in absolute emission cross-sections and which do not vary when the polar incidence angle with respect to the surface normal is kept constant./82/

To summarize, for photon energies above the plasmon energies (and away from other excitation energies), the electromagnetic fields can be described adequately with macroscopic dielectric theory.

3.4.8. Photoemission matrix elements

The cross-section for photoexcitation from an initial state ψ_i to a final state ψ_f is: /81/

$$\frac{d\sigma}{d\Omega d\omega} = \frac{2\pi e^2}{hc} \frac{2\pi^3 k}{|\mathbf{A}_0|^2 m\hbar\omega} \left| \int \mathbf{j}_{fi}(\mathbf{r}) \cdot \mathbf{A}(\mathbf{r}) d^3r \right|^2 \quad (11)$$

$$\text{where } \mathbf{j}_{fi} = \psi_f^*(\mathbf{r}) \nabla \psi_i(\mathbf{r}) - \psi_i(\mathbf{r}) \nabla \psi_f^*(\mathbf{r})$$

is the transition current density and $\mathbf{A}(\mathbf{r})$ is the vector potential of the photon field. Assuming that $\mathbf{A}(\mathbf{r})$ is spatially constant within the surface, one obtains the following dipole matrix element, written in the single particle model using the electron potential $V(\mathbf{r})$:

$$\frac{d\sigma}{d\Omega d\omega} = \frac{2\pi e^2}{hc} \frac{2\pi\hbar^2 k}{m\hbar\omega(E_f - E_i)^2} \left| \langle \psi_f | \mathbf{e}_A \cdot \nabla V(\mathbf{r}) | \psi_i \rangle \right|^2 \quad (12)$$

E_f being the kinetic energy of the emitted electron.

In the case of photoexcitation from a bound state ψ_i of a single atom α with a muffin-tin potential, one obtains/82/ the following amplitudes for out going spherical waves $L = (l, m)$:

$$M_L^\alpha = -(-i)^l \int d^3r [e^{i\delta_l^\alpha} R_l'(|\mathbf{r} - \mathbf{R}_\alpha|) - j_l(|\mathbf{r} - \mathbf{R}_\alpha|)] \\ \times Y_L^*(\mathbf{r} - \mathbf{R}_\alpha) - \frac{i\hbar}{2\pi} \frac{e}{mc} \frac{1}{(E_f - E_i)} \mathbf{A} \cdot \nabla V(\mathbf{r}) \psi_i(\mathbf{r}) \quad (13)$$

where the δ_l^α are the phase shifts of atom α , the j_l are Bessel functions and the R_l' are the normalized radial parts of the solutions to Schrödinger's equation inside atom α at energy E_f . If ψ_i is an atomic core state with quantum number l' , then the photoemission dipole selection rule (implicit in Eq. (13)) implies that $l = l' \pm 1$. Usually, one of the two outgoing values of l is by far dominant, as is the case in the gas phase.

Once M_L^α has been computed, one knows the electron waves leaving the source atom and one can proceed to calculate the electron propagation through the surrounding medium, as described in preceding sections (this is the inverse LEED problem). It should be recalled that in this subsequent propagation, scattering by the source atom itself may occur. This is usually treated as if the source atom had already completely relaxed to its initial condition, i.e. as if the hole left by the emitted electron had already been filled. This assumption does not appear to impair the ability to perform structural determination with photoelectrons.

3.4.9. Auger electron emission

The transition matrix element needed to describe Auger electron emission corresponds to the process in which an electron is ejected as a result of the filling of a deeper lying empty level by another electron. This process can be localized on one atom or involve neighboring atoms, especially if valence and conduction levels are involved. The Auger matrix element is/84/

$$M = \langle \psi_c \psi_e | \frac{e^2}{r} | \psi_1 \psi_2 \rangle \quad (14)$$

where ψ_c , ψ_e , ψ_1 and ψ_2 are respectively the wave functions of the core hole being filled, the emitted Auger electron and the initial state wave-functions of the two participating electrons. It is rather difficult to evaluate this matrix element, especially in the solid state. In the gas-phase atomic state, some results have been tabulated./69/ However, the difficulty of obtaining reliable values for the solid state is such that few attempts have been made./67,68/ In addition, there are no selection rules that limit the number of excited partial waves. Therefore, in ARAES the amplitudes of the outgoing partial waves have usually been left as adjustable parameters; and their relative phases have been neglected by assuming incoherent emission into the different partial waves. This inconvenient situation is a major cause for the infrequent use of ARAES in surface structural determination. While some success has been achieved in understanding the angular dependence of AES (and to a limited extent some structural determination has resulted),/67,68,71/ rather more accuracy is needed to achieve structural results that can compete with other techniques.

Note that in AEAPS-EAPFS, the Auger process is not the primary process which is modulated by fine structure since the energies involved in the Auger process are constant. Given the angle-integrated detection mode in EAPFS, the Auger step, therefore, need not be described in any detail.

3.4.10. Inelastic electron-electron scattering

The matrix element for inelastic electron-electron scattering is given by the following golden-rule expression (spin-averaged): /85/

$$\begin{aligned} \langle \rho_I \rangle &= \frac{4\pi^2 N_c}{h} \sum_{\mathbf{k}_1, \mathbf{k}_2 > k_F} \delta(E_i + E_c - E_1 - E_2) \\ &\times \left\{ \frac{3}{4} | -\langle \mathbf{k}_1 \mathbf{k}_2 | V_c | \mathbf{k}_i \gamma_i \rangle_- |^2 \right. \\ &\left. + \frac{1}{4} | +\langle \mathbf{k}_1 \mathbf{k}_2 | V_c | \mathbf{K}_i \gamma_c \rangle_- |^2 \right\} \quad (15) \end{aligned}$$

Here $\langle \dots \rangle$ indicates an average over the possible magnetic quantum numbers of the core-hole; E_c is the core-hole binding energy; γ_c represents the quantum numbers of the core electron, and $\mathbf{k}_1, \mathbf{k}_2$ and E_1, E_2 correspond to the momentum and energies of the electrons in the final state. The + and - subscripts indicate the symmetry of the wave-functions under exchange of the spatial coordinates of the two electrons; N_c is the number of scattering sites, and k_F is the Fermi momentum. The above expression is applicable in particular to the primary process of EAPFS. No strict selection rules emerge in this situation, but a "pseudo-selection rule" does exist:/85/ for nodeless core wave-functions, both final state electrons in the dominant channel have angular momentum increased by one over that of the core state, at least for incident energies which do not exceed the ionization threshold by 500 eV. In addition, it is found that the dipole component in a partial-wave expansion of the Coulomb interaction dominates the matrix elements.

Phase shifts calculated following the above formalism are incorporated into the Fourier-transformation of the experimental EAPFS oscillations, together with phase shifts for back-scattering from nearby atoms./31/ This allows the bond length to be determined with an accuracy on the order of 0.02 Å.

At the high energies E of SEELFS/32,33/ and ELNES,/66/ the final state has only a single "active" electron (the incident electron). One obtains then, for momentum transfer q , a differential cross-section/33/

$$\frac{d^2N(E,q)}{dEdq} \approx -\frac{1}{q^3} \text{Im} \frac{1}{\tilde{\epsilon}_L(E,q)} \quad (16)$$

where $\tilde{\epsilon}_L = \epsilon_1 + i\epsilon_2$ is the longitudinal dielectric function. Moreover, a dipole approximation is valid when the momentum transfer q is sufficiently small. As a result, one obtains a situation very similar to that of (S)EXAFS. By utilizing phase shifts calculated for (S)EXAFS, one may then determine/32/ near-neighbor bond distances with a quoted accuracy of 0.05 Å.

3.4.11. Electron-phonon scattering

We are concerned here with HREELS, /61, 62/ where the probe electrons lose a small amount of energy (≤ 0.5 eV) to atomic vibrations in the surface. Two regimes are commonly discussed. In the case of "small-angle inelastic scattering", also called "dipole scattering", the energy is lost to a long-wavelength phonon with small momentum transfer. The scattered electrons are made to reappear outside the surface by a LEED-type scattering, which supplies the large momentum transfer required for reflection, thus, these electrons emerge within a few degrees of LEED beam directions.

The second case is that of "impact scattering", where the lost energy is transferred to a vibrational mode by a localized impact (distances in the Angstrom range). Impact scattering can occur with small as well as with large scattering angles, but is often overshadowed by dipole scattering at the smaller angles. LEED-type elastic scatterings can occur in addition to impact scattering, but are not essential to obtain a measurable effect. However, they are unavoidable and must therefore be understood. /30/

Dipole scattering does not require an atomistic theory. A phenomenological theory suffices, which includes a response function dependent on dielectric constants. The cross-section for dipole scattering based on these assumptions is given in Eqs. 3.7 and 3.9 of Ibach and Mills. /61/ These formulae include plane-wave reflection coefficients from the surface, which are solutions of the standard LEED problem. Since dipole scattering involves essentially only forward scattering, it is not necessary in practice to adopt the spherical-wave picture of our step 2 (cf. section 3.4.3), the plane-wave approach is adequate in this situation.

In the case of impact scattering, an atomistic description is essential, since a short-range interaction is operative. The cross-section is then (Eqs. 3.77-79 of Ibach and Mills /61/)

$$\frac{dS}{d\Omega} = \frac{2mE_I}{h} \frac{\cos^2\theta_{out}}{\cos\theta_{in}} A |M|^2 \quad (17)$$

where

$$M = (n_s + 1)^{1/2} \left(\frac{h}{2N\omega_s} \right)^{1/2} \frac{\partial f}{\partial Q_s} \quad (18)$$

Here m and h are the electron mass and Planck's constant, θ_{in} and θ_{out} the polar angles of incidence and emergence, A the surface area and n_s the number of vibrational quanta present (following the Bose-Einstein statistics); N is the number of unit cells of the surface, ω_s the frequency of the vibrational mode and $\frac{\partial f}{\partial \theta_s}$ the partial derivative of the atomic scattering amplitude with respect to all the nuclear displacements occurring in the vibrational mode. The latter quantity can be related to the corresponding partial derivative of the atomic scattering potential $V(\mathbf{r})$. If $R_{i\alpha}$ is the nuclear displacement of atom i in vibration mode α , one obtains in the Green function language (Eqs. 3.80-81 of Ibach and Mills/61/)

$$\begin{aligned} \frac{\partial f}{\partial R_{i\alpha}} &= \langle \mathbf{k}_{out} | (G + GT_o G) \frac{\partial V(\{\mathbf{R}\})}{\partial R_{i\alpha}} (1 + GT_o) | \mathbf{k}_{in} \rangle \\ &= \langle \mathbf{k}_{out} | g_{PE} \frac{\partial V(\{\mathbf{R}\})}{\partial R_{i\alpha}} | \psi_{LEED}^{(in)} \rangle \end{aligned} \quad (19)$$

Here $V(\{\mathbf{R}\})$ is the scattering potential for the ensemble of scatters at locations \mathbf{R}_i , G is the free-space electron propagator and T_o the t -matrix for multiple scattering of the electron by the surface.

Eq. (17) clearly exhibits the different steps of the HREELS process: $\psi_{LEED}^{(in)}$ is the LEED wave-function of the electron before the inelastic event; g_{PE} is the photo-electron propagator of the electron following the inelastic event (this includes all multiple scattering paths ending at the detector). Both $\psi_{LEED}^{(in)}$ and g_{PE} provide the sensitivity to surface structure, while $\frac{\partial V}{\partial R_{i\alpha}}$ contains the vibrational properties of the surface. Given the low energies in most HREELS experiments ($\sim 5-10$ eV), the multiple scattering is extremely important and complex. Only a full multiple scattering calculation can properly simulate the diffraction effects.

Nevertheless, as a function of loss energy, the widely used loss peak structure appears./61,62/ This often leads to a relatively simple vibrational mode assignment in the case of adsorbates.

3.5. Unifying and Distinguishing Features

In this section, we shall emphasize some aspects of electron diffraction that are common to or differ among the various experimental techniques mentioned so far.

3.5.1. Single vs. multiple scattering

A clarification of terminology is necessary here. In essence, we shall describe why multiple-forward scattering can often be neglected, leaving only single (back-) scattering. We recall from section 3.2 the relative predominance of forward scattering of electrons by atoms over scattering into other directions, especially at higher energies (this is reinforced by the Debye-Waller factor). It is important to realize that, as a result, multiple forward scattering is always present. For instance, in SEXAFS, where one traditionally speaks of single scattering from shells surrounding the emitting atom, there is in reality also multiple forward scattering from one atom to the next in a radial direction, whether outbound or inbound relative to the source atom. This forward scattering often takes the form of focusing of electrons beyond the scattering atom. In this case, the main effect of forward scattering, as far as structure information is concerned, is to change the effective wavelength of the electron, which can be modeled as a changed inner potential. Otherwise, forward scattering does not produce a position-dependent phase change (since $e^{i\mathbf{s}\cdot\mathbf{r}} = 1$ for forward-scattering where the momentum transfer \mathbf{s} vanishes, whatever the atomic position \mathbf{r}).

This shows how SEXAFS can be described kinematically with a suitable inner potential. Since in SEXAFS the phase shifts are usually empirically determined from other experiments, this corrected inner potential is already

implicitly built into the phase shifts. Consequently, the multiple forward scattering need not be explicitly accounted for and one can use a single-scattering theory in an effective sense.

For the same reason, LEED I-V curves for clean unreconstructed surfaces often have recognizable Bragg peaks, despite strong multiple scattering. These Bragg peaks occur at energies that may be explained kinematically with a suitably adjusted inner potential, which can differ considerably from the muffin-tin constant of a multiple-scattering theory: the difference is due again to the effects of forward scattering./28/

3.5.2. Range of multiple scattering

Multiple scattering samples the environment of any surface atom and gives sensitivity to bond angles in addition to bond lengths within that environment. An important question is therefore how large that environment is. The determining factors are, primarily, the mean free path and, to a lesser degree, the atomic scattering amplitude. At kinetic energies of a few eV the mean free path can be large ($> 10 \text{ \AA}$) which results in a large sampled environment. The sampling radius may then be on the order of 20 \AA in metals, for instance, including many tens of neighboring atoms.

As the energy is raised, the mean free path goes through a minimum near 50-100 eV and slowly increases again, while the scattering amplitude steadily but slowly decreases, especially in non-forward directions and when the Debye-Waller factor is counted in. Then the sampled environment becomes generally smaller.

We must now distinguish between different techniques. In fine-structure techniques (such as SEXAFS, EAPFS, etc.), weak back-scattering combined with the usual $\frac{1}{r^2}$ radial decay of spherical waves limits the range of scattering to a few shells of nearby atoms. In techniques like LEED and ARPES, including ARPEFS and ARXPD, multiple forward scattering can occur along electron paths that leave any atom toward the detector or, in the case of LEED, that arrive toward any atom from the source. Such nearly straight paths extend the

sampling range relative to the fine-structure techniques. Therefore, the range of multiple scattering which matters in these techniques is mainly determined by the mean free path.

It is clear that the larger the range of multiple scattering, the more complex the corresponding calculations become. But it has been found, in the context of LEED calculations, that one may markedly cut the effective range of multiple scattering in the *less dense* materials, especially in molecular overlayers./86/ This approximation is valid because relatively few neighboring atoms are available to interfere with the primary kinematic process near a given atom. For example, in a typical organic molecule, each atom has at most four near-neighbors, compared with a maximum of 12 within a metal lattice. One may approximate the calculation by including only nearest neighbors in the multiple scattering process. This approach has been used successfully in LEED structural determination of adsorbed molecules in the method called "near-neighbor multiple scattering"./86/

3.5.3. Long- vs. short-range order

We address here the question whether LEED samples only long-range order, as is often stated, rather than short range order, as do most other techniques described here. This is an important question, because many surfaces will not take on long-range order, and this might prevent the application of LEED. We shall argue that LEED remains applicable. In the case of LEED we should make the following distinction: on the one hand, there is sensitivity to the long-range order, determined by the periodic lattice which produces the diffraction beams, and on the other hand, there is short-range sensitivity to local geometry, determined by the range of multiple scattering as discussed above. This distinction becomes clearest in the case of diffuse LEED from disordered surfaces. Then, the diffracted intensity can be expressed approximately/79/ as the product of a kinematic structure factor representing the long-range arrangement of the surface and an effective form factor representing the short-range structure, including the sampling by multiple scattering in the neighborhood of any atom.

This factorization into structure and form factors is exact in the limit of dilute identical defects in an otherwise periodic lattice, and only approximate for

dense defects since multiple scattering between defects is neglected. Such a "defect" may be a vacancy or a step in an otherwise periodic surface, or a molecule in an adsorbed layer that has no long range periodicity despite long-range periodicity in the substrate (a "lattice gas"). The error made in the approximation mentioned above can be shown to be small in most cases of interest, since it involves higher-order multiple scattering events, which are relatively weak, as well as long range multiple-scattering paths, which are also relatively weak. Therefore, the main contributions to LEED intensities are due to short-range structure, through the effective form-factor, and to long-range structure, through the kinematic structure-factor, and these terms can be separated out.

This factorization into structure- and form-factors can be applied to ordered surfaces as well (the traditional application of LEED), it then decouples long-range order from short-range order. It is particularly valuable for large unit cells, because one may then simply ignore the long-range order, and also the large number of beams that give rise to very large computational efforts in the more exact traditional formalisms (where all beams are considered coupled). This approach has been implemented and tested in the Beam-Set Neglect method mentioned previously,^{/80/} in which most beams are ignored and only selected sub-sets of beams are included in the calculation. This BSN method has enabled the study of large adsorbed molecules, e.g. benzene, including cases of several molecules per unit cell, with a much reduced computational effort compared to previous methods. In fact, the computational effort in this approach may even be chosen to be independent of the unit cell size, instead of being proportional to its second or third power. The same BSN method has also been programmed and tested for the case of disordered overlayers.^{/79/}

3.5.4. Various forms of disorder

Many kinds of disorder are known at surfaces. "Clean, well-ordered" surfaces present, among others, point defects (impurities, dislocations, etc.) and line defects (steps, crystallite boundaries, etc.). Surfaces with adsorbates or reconstruction-induced superlattices can have a variety of additional defects, e.g.

out-of-phase, rotated or mirrored domains, disordered regions, isolated ad-atoms, etc. Also, different adsorption geometries can occur at substrate defects and at domain boundaries. With adsorbed molecules (including adsorbed clusters), internal degrees of freedom of the molecules can lead to further disorder, e.g. rotational disorder, while chemical reactions can produce a variety of coadsorbed species.

Different surface-sensitive techniques respond differently to the various kinds of disorder. The measurement of LEED beams is unique in largely filtering out all defects that are unrelated to the superlattice periodicity that defines the beams. Other techniques (including diffuse LEED) generally include contributions from all defects, for instance from adsorbates located at undesired steps and crystallite boundaries. Then only a reduction of the defect concentration can remove defect contributions from the experimental data. Rotational disorder of adsorbed molecules does not matter for techniques which measure only bond lengths, and not bond orientations. Thus, NEXAFS is more sensitive to such disorder than SEXAFS.

In the presence of a variety of chemical species, one may distinguish between the species by various means, e.g. by selection of Auger lines in SEXAFS, or core-levels in ARPEFS, or vibrational frequencies in HREELS.

3.5.5. Layer spacings vs. bond lengths

As mentioned earlier, the electron diffraction techniques under discussion in this paper divide into two categories, depending on whether they are primarily sensitive to layer spacings and bond orientations or to bond lengths. The cause of this difference is the source of the structural information. In SEXAFS and EAPFS, for example, the structural information comes primarily from step 3 of the 4-step description, as electrons emitted from the source atom back-scatter from neighboring atoms. Angle-integrated detection is used, which tends to remove all directional information from propagation effects (step 4) and, therefore, leaves only radial information, mainly bond lengths. By contrast, angle-resolved techniques, such as LEED and ARPES, emphasize the behavior of plane waves. In these techniques a lot of the information comes from

propagation effects (steps 1 and 4 of the 4-step description). These plane waves carry structural information through the phase of the interference function $e^{i\mathbf{s}\cdot\mathbf{r}}$ where \mathbf{s} is the momentum transfer between two plane waves. Therefore, only the projection of the atomic position vector \mathbf{r} onto the direction of \mathbf{s} is relevant, and this projection can be viewed as a layer spacing. When many beams are involved and multiple scattering occurs, many values and directions of \mathbf{s} are used simultaneously, such that layer spacings in many orientations are accessible. This gives sufficient information to completely determine a surface structure.

3.5.6. Bond angles vs. bond directions

We have pointed out two methods to obtain bond angles or bond directions. One uses the sensitivity of electron multiple scattering, as in LEED and NEXAFS, and the other uses variable polarization of incident photons, together with selection rules, as in SEXAFS. The first method gives access to bond angles, i.e. the angle between two inter-atomic bonds. The second method gives access to bond directions, i.e. the absolute orientation of a bond with respect to a laboratory coordinate system. The bond angle is the chemically more relevant quantity, which can only be obtained from the bond direction with additional information of assumptions. For example, the direction of the bond between atoms A and B only provides the bond angle between atoms A, B and C if the bond direction BC is also measured or is known from previous work.

4. THE THEORY OF SURFACE CHEMISTRY AND BONDING

The goal of theoretical surface chemistry is to understand the surface chemical bond, and from this to be able to describe and predict the properties of atoms and molecules adsorbed on surfaces. The primary properties of interest include adsorption sites and geometries, bond lengths and angles, the electronic structure of adsorbed species, adsorption energies, diffusion energies, and the

frequencies of vibrational excitations. Other properties that may be derived relate to reaction pathways, kinetics, rates and selectivities as a function of the nature of surface on which the reaction proceeds. Significant progress has been made toward this goal in the last decade using both semiempirical and *ab initio* calculational methods.

The basic approach of chemical theory to surface science is to model a surface with a cluster of a finite number of atoms, with one or more "adsorbate" atoms or molecules bonded to various sites on the cluster. In parallel with the chemical theory there is also the solid state physics approach. This starts from an "extended" surface surface model, where an array of atoms perfectly periodic in two dimensions represents both the substrate and any adsorbates. Many theoretical techniques have been developed for the extended-surface model. We can only refer the interested reader to the literature/87,88,89,90,91,92,93,94/ and remark that the relative merits of the cluster and extended-surface approaches are still very much under active debate. It is clear that certain properties, such as bonding, are very localized in character and are well represented in a cluster. On the other hand, there are properties that have a delocalized nature, such as adsorbate-adsorbate interactions and electrostatic effects, for which an extended surface model is more appropriate.

The cluster approach is, like the extended-surface approach, characterized by many different calculational schemes. A recent review stresses electronic aspects of bonding. In this review we have chosen to concentrate on geometric aspects. We shall discuss a number of major techniques in order of increasing computational complexity: the extended Hückel theory, self-consistent $X\alpha$ scattered wave calculations, and self-consistent *ab initio* Hartree-Fock and valence bond methods. In that order these techniques allow increasing accuracy. However, the cluster size must decrease simultaneously due to calculational complexity, ultimately reducing the degree of analogy with surfaces.

4.1. The Extended Hückel Theory and Applications

The most widely used semiempirical quantum chemistry technique for theoretical chemisorption studies is the Extended Hückel Theory (EHT). The method was first proposed by Hoffmann/95/ in its nonrelativistic form, and by Lohr and Pyykkö/96/ and also Messmer/97/ in its relativistic form, based on the molecular orbital theory for calculating molecular electronic and geometric properties. For a cluster the molecular orbitals are expanded as linear combinations of atomic orbitals

$$\psi_i = \sum_{j=1}^n C_{ij} \phi_j \quad (20)$$

On minimizing the total energy, one obtains a set of secular equations

$$\sum_{i=1}^n [H_{ij} - \epsilon S_{ij}] C_{ij} \phi_j = 0 \quad \text{for } j = 1, 2, \dots, n. \quad (21)$$

Here i and j span the n atomic orbitals in the basis set of valence orbitals (core electrons are neglected) and the coefficients C_{ij} are chosen to diagonalize the Hamiltonian matrix. The quantity S_{ij} is the overlap integral between orbital i and orbital j . EHT approximates the off-diagonal matrix elements H_{ij} by the Wolfsberg-Helmholz formula/98/

$$H_{ij} = \frac{1}{2} K (H_{ii} + H_{jj}) S_{ij}, \quad (22)$$

where the diagonal matrix elements H_{ii} and H_{jj} are approximated as valence state ionization potentials (IP) for atomic orbitals on atom i and atom j . The constant K is commonly taken as 1.75. The total energy is computed as a sum of one-electron orbital energies

$$E_{EHT} = 2 \sum_i \epsilon_i \quad (23)$$

The EHT total energy differs from the Hartree-Fock total energy E_{HF} by the neglect of the nuclear-nuclear repulsion energy E_{NN} and by the overcounting of electron-electron repulsion and exchange. The energy difference is

$$E_{HF} - E_{EHT} = E_{NN} - \sum_{i=1}^{n/2} \sum_{j=1}^{n/2} (2J_{ij} - K_{ij}). \quad (24)$$

Here J_{ij} and K_{ij} are the Coulomb and exchange integrals of the i and j orbital pairs. The sum in Eq. (24) is usually positive.

EHT has the advantage of being computationally an extremely simple method and can be applied to large clusters, up to a few hundred atoms. However, due to the neglect of repulsion terms in Eq. (24), the EHT binding energies for molecules are over-estimated and bond distances are too short./95/ Unrealistic electron charge transfers have also been found for diatomic molecules when the difference between the atomic electro-negativities is large./95/ Improvements can be made by calculating the ionization potential self-consistently/99,100/ or by evaluating the matrix elements more accurately, as is done in the CNDO method./101/

Here we shall discuss a simple method of incorporating the repulsive energy terms as suggested by Anderson and Hoffmann./102/ The method is called Atom-Superposition Electron-Delocalization Molecular Orbital (ASED-MO) theory. It uses the fact that the cluster binding energy can be expressed exactly as the sum of pairwise repulsive energies E_R , due to rigid atom superposition, and attractive electron delocalization energies E_D ./103/

$$E_{ASED-MO} = E_R + E_D \quad (25)$$

It has been shown/103/ that E_D can be approximated by a one-electron molecular orbital energy E_{MO} :

$$E_{ASED-MO} = E_R + E_{MO} \quad (26)$$

E_{MO} is obtained using Eq. (21) with matrix elements

$$H_{ii} = -IP_i \quad (27)$$

$$H_{ij} = 1.125 (H_{ii} + H_{jj}) e^{-0.13R_{ij}} S_{ij} \quad (28)$$

Here $K = 2.5$ has been used in obtaining H_{ij} . An exponential damping factor depending on the inter-atomic distance R_{ij} is introduced which often improves the results. E_R is given as the Coulomb interaction between the nucleus of one atom (usually the more electronegative atom) and the nuclear and electronic charges of the other. It has been shown that the simulation of two-body interactions in this way appreciably improves the calculated molecular binding energies and bond lengths./103/

There is a vast literature on the application of EHT to surface chemistry using model clusters. There are also recent reviews on this subject./104,105/ We shall discuss next specific examples relevant to chemisorption of molecules on metal surfaces for illustrative purposes.

Our first example is the widely discussed problem of CO chemisorption on transition metal surfaces. Ray and Anderson/106/ investigated CO chemisorption on a Pt (111) surface using the ASED-MO theory. In their work, Pt_4 and Pt_{10} clusters were used to model the Pt (111) surface. The bulk Pt-Pt bond distance was used and other theoretical parameters are reproduced in Table II. The calculated Pt-Pt and C-O bond distances and harmonic force constants are within 8% of experimental values for isolated Pt_2 and CO. The results for dissociation energies are less satisfactory: 94.08 and 116 kcal/mole in comparison with experimental values of 84.5 and 256 kcal/mole, respectively.

The calculated binding energy for CO adsorbed on Pt_4 and Pt_{10} is largest for the 1-fold coordinated site ("top-site"), indicating a definite preference for the 1-fold site. With the 3-fold coordinated site ("hollow-site"), there is a small preference for the 3-fold site which has a vacancy in the second metal layer, corresponding to the fcc hollow site of the (111) surface. The binding energies for 2-fold (bridging) and 3-fold sites are similar and the former is favored on the larger cluster. These results are supported by experiment. High-resolution

electron energy loss spectroscopy (HREELS) obtained by Froitzheim et al./107/ for CO adsorbed on the Pt (111) surface indicates sequential occupation of two binding sites with increasing coverage of CO: the 1-fold site is occupied first at lower coverages, and at higher coverages the two-fold sites are also occupied by CO./108/ Infrared reflectance-absorption spectroscopy (IRAS),/109/ XPS and work function measurements/110/ also support these results. In addition the experimental adsorption energy derived from molecular beam experiments (1.52 eV)/111/ is in good agreement with the theoretical value of 1.66 eV. Both the calculated and measured force constants/111/ indicate a weakening of the C-O bond relative to gas-phase CO when adsorbed in the 1-fold site. This can be explained by charge transfer from the *sd* band of Pt to the two antibonding π^*

Table II. Extended Hückel Parameters for CO-Pt

orbital	atom	<i>n</i>	IP(ev)	ζ	C
<i>s</i>	Pt	6	9.0	2.55	-
	O	2	28.48	2.246	-
	C	2	20.00	1.658	-
<i>p</i>	Pt	6	4.96	2.25	-
	O	2	13.62	2.227	-
	C	2	11.26	1.618	-
<i>d</i>	Pt	5	9.6	2.39	6.013
					0.5715
					0.6567

Here *n* = principal quantum number, IP = ionization potential, ζ = orbital exponent and C = *d*-orbital coefficient. To mimic self-consistency in adsorption studies Pt ionization potentials are increased by 1.5 eV, O and C ionization potentials are decreased by 1.5 eV, and O exponents are decreased by 0.1 eV.

CO orbitals. The calculated bond stretch is 0.07 Å. On going to the 2-fold and 3-fold adsorption sites, the C-O force constant is progressively weakened and the C-O bond lengthened.

The interaction of adsorbed CO and adsorbed oxygen has also been studied to estimate the energy of activation for the oxidation of CO on Pt (111) surface. Two mechanisms have been proposed: the Langmuir-Hinshelwood mechanism and the Eley-Rideal mechanism. In the Langmuir-Hinshelwood mechanism, the associatively adsorbed CO interacts with adsorbed oxygen. The activation energy for oxidation is calculated as 1.6 eV for the transition state geometry. This is in reasonable agreement with experimental results of 1 eV./111/ In the Eley-Rideal mechanism, the CO molecule dissociates on the surface and only then interacts with the adsorbed oxygen atoms. The calculated barrier to CO₂ formation is 1 eV greater than that in the Langmuir-Hinshelwood case. Both the experimental evidence and the theoretical results favor the Langmuir-Hinshelwood mechanism.

The chemisorption of hydrocarbon molecules on surfaces presents another class of important and interesting systems for study. We shall discuss the case of acetylene chemisorption on the Ni (111), Rh (111) and Pt (111) surfaces, as they incorporate many features relevant to all hydrocarbon chemisorption systems.

Gavezzotti et al./112,113/ have applied EHT to predict the chemisorption binding energies of acetylene and a number of organic fragments such as CH, CCH₂, CCH₃ and HCCH on the Ni (111), Rh (111), and Pt (111) surfaces. The metal surface was modeled by a four-atom cluster, and the acetylene bond lengths were held constant, although the C-C-H bond angle was allowed to vary. The bond length was 1.2 Å for C-C and 1.06 Å for C-H. They found the behavior of acetylene chemisorbed on these different metals to be similar. Ni, Rh and Pt catalyze the rearrangement of adsorbed acetylene to vinylidene ($>C=C<\frac{H}{H}$), and Ni was also found to catalyze the reverse reaction. However, Ni was found to be the best catalyst for carbon-carbon bond breaking in acetylene. Moreover, adsorbate-adsorbate interactions force the acetylene molecule to tilt out of the plane parallel to the surface on Ni (100), as shown in Figure 3.

Anderson and Hubbard/114/ also performed an ASED-MO calculation for acetylene chemisorbed on the Pt (111) surface. Various adsorption sites were considered in this calculation. The hollow site with the C-C axis parallel to the

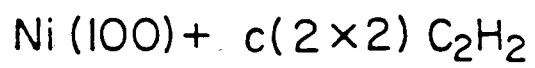
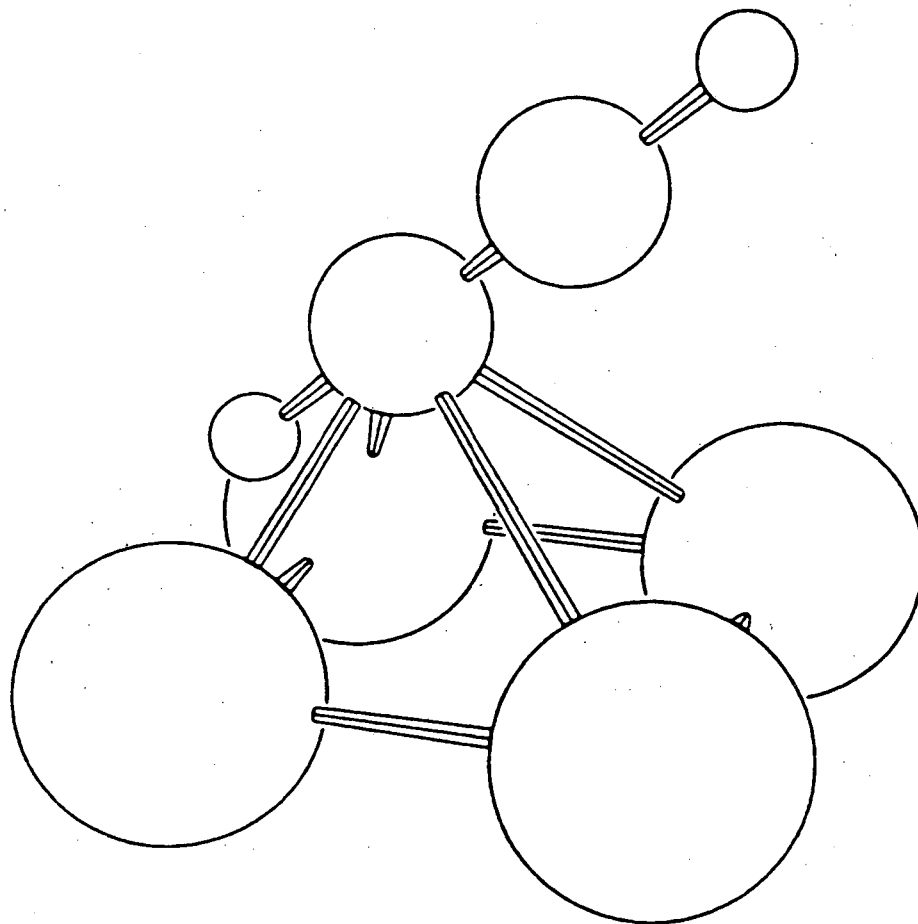


Fig. 3. Perspective view of acetylene over a hollow site of Ni(100), represented by four Ni atoms. The C-Ni bonds are drawn to indicate geometrical relationships only, not the bonding character.

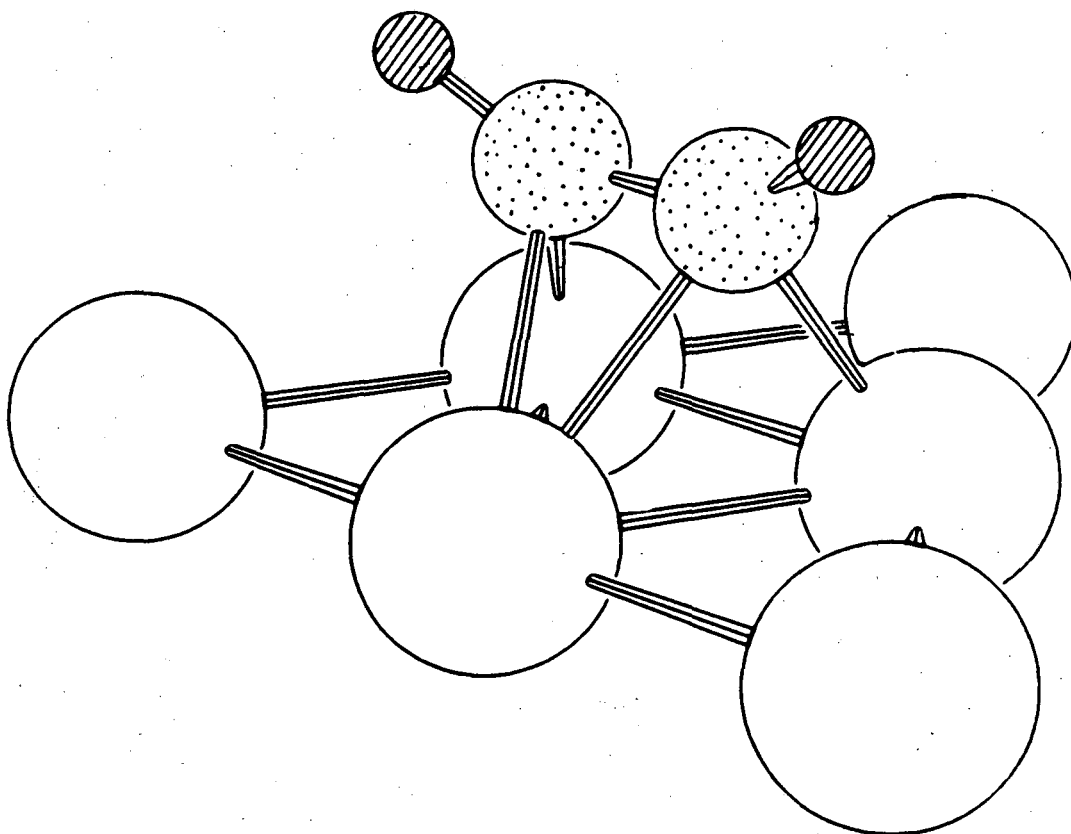
sides of the Pt_3 triangle was definitely preferred, in agreement with the HREELS analysis of Ibach and Lehwald,/115/ (see Figure 4). In most sites the C-H bond axes rotated away from the surface by about 55° and the C-C bond lengthened by about 0.3 \AA relative to the gas-phase. This is in agreement with the bending results of Gavezzotti et al./112/ as well as the HREELS estimates of 60° and 0.24 \AA for these quantities.

A very stable species found on several metal surfaces, including Pt(111), is ethylidyne, CCH_3 . ASED-MO calculations agree that the CCH_3 species does take on the structure deduced from LEED analysis, namely the C-C axis is perpendicular to the surface, with one carbon bonded equally to three metal atoms. The LEED estimates of a 2.0 \AA Pt-C distance and a 1.50 \AA C-C distance agree well with the calculated values of 2.0 \AA and 1.55 \AA (see Figure 5). Ethylidyne is produced either with acetylene co-adsorbed with H_2 or with ethylene adsorption, both of which are unstable relative to ethylidyne. Structures of CCH_2 and CHCH_2 have also been calculated and were found to be less stable than acetylene and CCH_3 when chemisorbed on Pt (111).

We conclude this section with the observation that the extended Hückel method can produce results in good agreement with experiments when used with caution and appropriate parameter searching procedures.

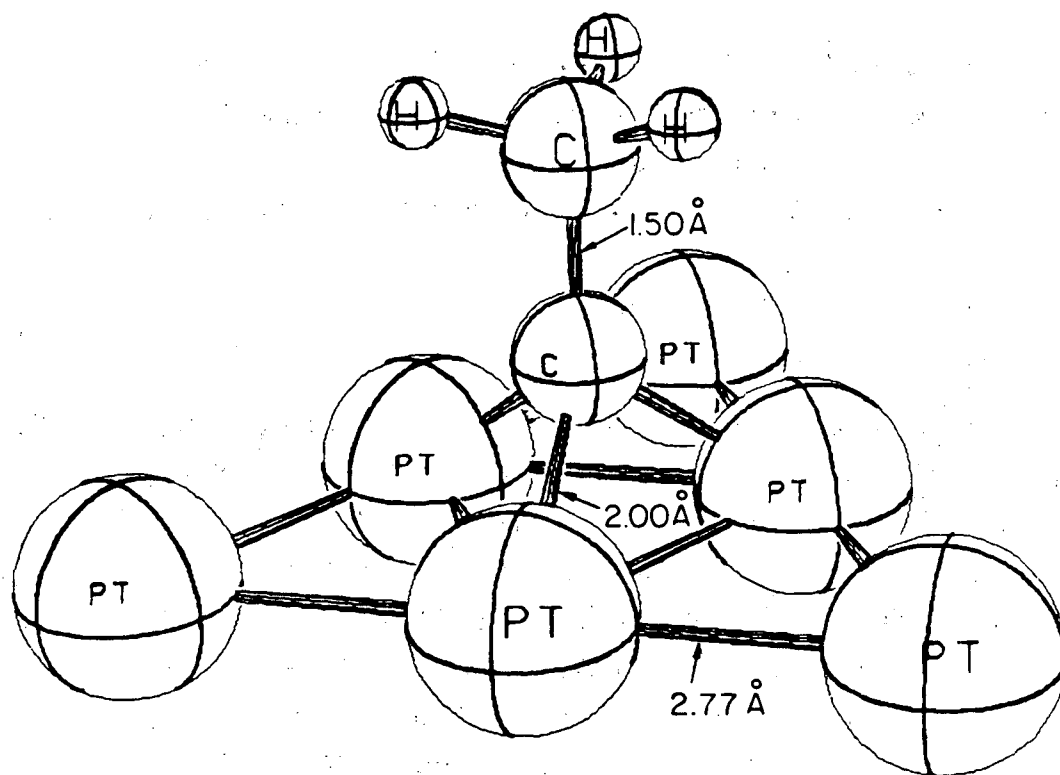
4.2. The SCF $X\alpha$ Scattered Wave Method

The self-consistent-field- $X\alpha$ -Scattered Wave (SCF- $X\alpha$ -SW) method was developed by Johnson/116/ to calculate electronic energy levels and eigenfunctions for polyatomic molecules and solids. In this scheme, the electronic wave functions are solved by a multiple-scattering method, equivalent to the Korringa-Kohn-Rostoker/117, 118/ (KKR) method used for energy band calculations. The method has also been adapted to the calculation of magnetic problems, by use of a spin-polarized formalism,/119/ and to the case of clusters containing heavy elements, by the use of a relativistic formalism./120/ This method has been used quite successfully in correlating the electronic structure of chemisorption systems with the observed experimental photoemission spectrum



Metastable acetylene on Pt(111)

Fig. 4. The structure of acetylene on Pt(111) as determined from HREELS data. The lines between atoms are drawn to indicate geometrical relationships only, not the bonding character.



Pt (III) + ethylidyne

Fig. 5. The adsorption geometry of ethylidyne on Pt(111) as determined by LEED intensity analysis.

assuming known adsorbate binding geometries. It has been less successful in obtaining the adsorption binding energies via total energy calculations.

4.3. SCF- $X\alpha$ -SW Calculations

The SCF- $X\alpha$ -SW method makes the following major assumptions. First one replaces the nonlocal Hartree-Fock exchange potential with the $X\alpha$ local exchange potential that corresponds to the average exchange potential of a free electron gas. The exchange potential is related to the local electronic density by

$$V_{X\alpha}(\mathbf{r}) = -6\alpha \frac{3}{8\pi} \rho^{1/3}(\mathbf{r}) \quad (29)$$

The value of α varies between 2/3 (the Kohn-Sham potential)/121/ and 1 (the Slater potential)./122/ Different methods for determining the value of α have been proposed. Usually the value of α for an isolated atom is determined by requiring that the total energy, using the statistical approximation, should equal the precise Hartree-Fock energy/123/ or the experimental value. The latter takes into account the atomic correlation energy in a phenomenological way. In a molecule or cluster α values are usually chosen in one of two ways. The values of α characteristic of the various atoms may be used within each atomic core, and an average may be used in the region between atoms; alternatively, one may set the parameter α to a universal value in all regions. /124/ Using the statistical approximation, no Slater determinant is required for the electronic wave functions. Instead, we have a one electron equation

$$[-\nabla^2 + V(\mathbf{r})] \psi(\mathbf{r}) = E \psi(\mathbf{r}) \quad (30)$$

where $V(\mathbf{r}) = V_c(\mathbf{r}) + V_{X\alpha}(\mathbf{r})$ and V_c is the Coulomb potential. Once the eigenvalues and eigenfunctions for this problem are determined, one assumes that the orbitals of the lowest energy are occupied up to a Fermi level. From the resulting charge densities, one may compute the total energy of the cluster, using the statistical approximation for the exchange-correlation energy.

The second assumption of the SCF- $X\alpha$ -SW method is the introduction of "muffin-tin" approximation to the potential. Each atom j in the cluster is represented by a sphere of radius b_j where the inside of these spheres constitutes the so-called region I. The potential $V^j(\mathbf{r})$ in each sphere is spherically symmetric and nonoverlapping in the original SCF- $X\alpha$ -SW method. Later, overlapping spheres were introduced to improve the results of total energy calculations./124/ The entire cluster is then surrounded by a sphere of radius b_o , which is the smallest sphere containing all the atomic spheres of region I. The outside of this large sphere defines the region III, in which the potential $V(\mathbf{r})$ is also taken to be spherically symmetric. The space between the small spheres of region I and within the large sphere of region III defines the so-called region II. Within region II, the potential is taken as a constant \bar{V} , which is the volume average of $V^j(\mathbf{r})$ in region II. Assuming that the position of the nucleus of the j th atom is at \mathbf{R}_j , ($j = 1, 2, \dots, N$) and the center of the outer sphere is at \mathbf{R}_o , then:

$$V(\mathbf{r}) = \begin{cases} V^j(r_j) & \text{region I; } r_j = |\mathbf{r} - \mathbf{R}_j| \leq b_j \\ \bar{V} & \text{region II;} \\ V^o(r_o) & \text{region III; } r_o = |\mathbf{r} - \mathbf{R}_o| > b_o \end{cases} \quad (31)$$

The self-consistent field calculation requires that as a first approximation V_j be calculated for each atom j with its associated atomic electron density. The total potential V is then obtained as a superposition of the atomic potentials:

$$V(\mathbf{r}) = \sum_{j=1}^N V^j(r_j) \quad (32)$$

Next the total potential is made spherically symmetric within each atomic sphere and in region III. The constant potential \bar{V} in region II is obtained by

$$\bar{V} = (\Omega_{II})^{-1} \int_{\Omega_{II}} V(\mathbf{r}) d\mathbf{r} \quad (33)$$

where Ω_{II} is the volume of the interatomic region. It should be noticed that the

potential in each atomic region includes not only the contribution of the atom located at its center but also the spherically averaged contribution from all other atoms.

After constructing the $X\alpha$ potentials in each region, the one-electron Schrödinger equation can be solved by matching together separate solutions in regions I, II and III, just as in the KKR method for crystals. The wave matching conditions lead to a determinantal equation, which can be solved only for certain values of E , the eigenvalues. The corresponding wave-functions yield a new electron density, from which the procedure can be iterated.

We will now discuss the advantages and disadvantages of the SCF- $X\alpha$ -Scattered Wave method. The *ab initio* approach is the major advantage of this method, while it has the flexibility of semi-empirical methods through the incorporation of adjustable parameters such as α and the muffin tin radii. It also need not treat the core and valence electrons separately: both are handled as parts of the same calculation. On the other hand, the unrealistic "muffin-tin" approximation is disadvantageous in that the bonding between atoms in the constant potential region is overestimated./125,126/ This results in unreliable total energy values. Although overlapping atomic spheres/127/ and non muffin-tin corrections/128/ have been introduced to compensate for this problem, such corrections increase the computational work considerably.

This shortcoming is avoided in the Hartree-Fock-Slater method by removing the muffin-tin approximation./128/ This will be discussed in section 4.5. The SCF- $X\alpha$ -SW method has nevertheless been able to score successes in the determination of surface structures. This success comes from the sensitivity of the calculated surface density of states (DOS) to the surface geometry. It is true that the orbital energies obtained by the SCF- $X\alpha$ -SW method contain unwanted self-interaction energies and are different from the HF orbital energies./129/ However, by using Slater's transition-state theory,/128/ which assumes that $\frac{1}{2}$ electron is in the initial-state orbital and $\frac{1}{2}$ electron is in the final-state orbital, one obtains good $X\alpha$ orbital energies, since the self-interaction terms partially cancel, and most of the relaxation energy is included. In this way good agreement between the calculated DOS with a given adsorbate geometry and the experimental photoemission spectra is often obtained, so that the most favorable adsorbate geometry may be determined. However, the interpretation of

experimental photoemission spectra presents its own complications, which can induce uncertainties in structural determinations. We shall discuss recent applications of this method in the next section.

4.4. Results of the $X\alpha$ -Method

Determination of the adsorbate bonding geometries for CO chemisorbed on the Cu (100) surface provides an interesting example of the $X\alpha$ -SW method. This example illustrates the problems of interpreting photoemission spectra, since the location of CO on Cu(100) is found to be on a top-site by LEED, while $X\alpha$ -SW calculations either favor a 4-fold hollow site or are inconclusive. Yu/130/ has carried out calculations for CuCO and Cu₅CO clusters with CO bonded to the Cu surface through the carbon atom. In CuCO the CO molecule was put directly on top of a Cu atom and in Cu₅CO it was located in the four-fold coordinated hollow site, simulating CO adsorbed perpendicular to the (100) surface. The calculated valence density of states for the four-fold adsorption site gives a satisfactory interpretation of the two main peaks observed below the copper *d*-band in the UV photoemission spectrum (UPS)./131/ An observed weak third peak can be correlated with a minority of CO molecules adsorbed directly on top of a copper atom.

Messmer and Lamson later calculated core and valence photoemission spectra using the $X\alpha$ -SW method and offered another explanation for the CO-Cu (100) UV photoemission spectra./132/ They pointed out that, in addition to the main photoionization transitions, the outgoing electron can also excite valence electrons. Assuming that a Cu₅ cluster with CO bonded in a four-fold coordinated hollow-site models the Cu (100) surface, they obtained theoretical DOS to compare with the experimental UPS of Norton et al.133

The experimental spectrum was resolved into four peaks. Two of these are assigned to three shake-up transitions labeled $1\pi_+$, $4\sigma_+$ and $5\sigma_+$ arising from a hole in each of the 1π , 5σ , and 4σ orbitals. A third peak is assigned to the 1π and

5 σ ionizations and the fourth peak to the 4 σ transition. Messmer and Lamson conclude that CO adsorption in the four-fold symmetric hollow site is sufficient to explain the observed UPS data.

A theoretical interpretation of the *core-level* satellite structure in the x-ray photoemission spectrum was also offered by Messmer et al./134/ using a larger Cu₉CO cluster and assuming the chemisorption of CO in the one-fold and four-fold sites of the Cu (100) surface. The qualitative differences in the intensity distributions suggest that the Cu₉CO cluster is a better model than the smaller Cu₅CO cluster for the Cu (100) surface.

A three-peak structure of the carbon 1s x-ray photoemission spectrum for CO chemisorbed on Cu (100) is obtained experimentally. The structure is from the photoionization of a carbon 1s electron, where three final ion states with roughly the same energies but different degrees of hole screening are excited. These differences in hole-screening lead to the observed differences in the carbon 1s binding energies.

A molecular orbital study using the X α -SW method suggests that the first peak in the experimental XPS data arises from a transition between the ground state of the neutral chemisorption system and a final state in which a core hole in the CO molecule is created, together with the transfer of an electron from Cu to the 2 $\bar{\pi}_g$ -orbital of the chemisorption system. The other two peaks are caused by shake-up excitations from this core-hole-ion ground state. One of these two peaks can be viewed as a transition from this ground state ion to an excited-state ion via an excitation of electron from the 2 $\bar{\pi}_g$ -orbital to the higher energy 2 $\bar{\pi}_g^*$ -orbital. The other peak is described as a one-electron excitation from the 1 $\bar{\pi}'$ level to the 2 $\bar{\pi}'$ level. Unfortunately the core level shake-up spectra calculated for the 1-fold and 4-fold sites are qualitatively very similar, and this rules out a definite conclusion regarding the CO binding site on the Cu (100) surfaces.

Another way of making geometric structural determinations with X α -SW calculations is to compare the adsorbate photoemission energy level shifts with theoretical level shifts obtained with the assumed binding geometries. An example is the adsorption of ethylene (C₂H₄) on Ni (111).

In the so-called π -bonded model, the C₂H₄ molecule lies flat on the surface and a σ -bond is formed by the overlap of the Ni d_{z^2} orbital and the C₂H₄ $b_{3u}(\pi)$ -

orbital, which donates charge to the nickel atoms. The “ π -back-bonding” refers to charge transfer from the Ni $d_{zz,yz}$ -orbitals into the unoccupied C_2H_4 $b_{2g}(\pi)^*$ -orbital. UPS spectra show an ethylene derived π -level with a bonding shift of 0.9 eV for adsorption on Ni (111), in addition to a relatively uniform relaxation shift for both the π - and σ -type orbitals./135/ The $X\alpha$ -SW calculation of Rösch and Rhodin/136/ for the $Ni_2(C_2H_4)$ cluster gave a 0.72 eV bonding shift for the C_2H_4 $b_{3u}(\pi)$ orbital of the π -bonded complex and a 0.30 eV shift in the di- σ -bonded complex.

Howard and Dresselhaus later did calculations for the π -bonded model using a Ni_{10} cluster and found that the level structure as a whole exhibits slow oscillations in energy from iteration to iteration./137/ An accurate level shift cannot be determined without artificially shifting and aligning the calculated Fermi energy with the experimental one for the chemisorption system. The resulting level structure can explain the reported activation energy difference for ethylene hydrogenation on paramagnetic and ferromagnetic nickel. It is due to shifts in the Ni spd levels relative to the ethylene $b_{3u}(\pi)$ bonding orbital level, via an exchange splitting of ~ 0.1 eV.

Finally we discuss the case of CO bonding to a platinum (100) surface using the relativistic version of the $X\alpha$ -SW method./138/ Adsorption in the top, bridge and four-fold hollow sites with the carbon atom bonded to the metal were examined for $PtCO$, Pt_2CO and Pt_5CO clusters, respectively. In general, the s -band in the transition metals hybridizes with the d -band and at the same time participates in bonding with an adsorbate. However, its hybridization with the d -band is sufficiently weak so the general appearance of the latter remains intact. When relativistic spin-orbit coupling is included the d -band splits into $d_{3/2}$ and $d_{5/2}$ components. Strong $d_{3/2}$ - $d_{5/2}$ hybridization is observed only for the sp or spd orbitals, which are largely responsible for bonding among the Pt atoms. Upon addition of the CO molecule, the metal bands undergo different changes in each model cluster. In all cases, the s -band which overlaps the d -band, and which participates in bonding as well as back-bonding with CO, is partially depleted in the d -band region. The orbitals responsible for bonding between CO and Pt clusters are the 5σ and $2\pi^*$ in the generally accepted bonding picture of 5σ donation and $2\pi^*$ back-donation. The energy position of the 5σ -orbital with respect to the centroid of the d -band remains fixed for all three

clusters. In all cases the C-Pt bond involves at least one antibonding orbital. In the Pt_5CO cluster, but not the other two, one of these antibonding orbitals is occupied. Thus, qualitatively, we expect the four-fold site to have the lowest binding energy among the three sites considered for CO-Pt (100). This prediction is confirmed by HREELS observations.

In the two previous sections, we have discussed the use of the basic SCF- $X\alpha$ -SW method. The advantage of this method is its computational efficiency relative to other *ab initio* methods which allows larger clusters to be handled. The disadvantage is the inadequacy of the "muffin-tin" approximation for systems with low symmetry or open structure, which renders the determination of orbital energies and total binding energies unreliable. In the following section we shall describe an improved method which relaxes the "muffin-tin" approximation and is potentially valuable in adsorbate structure determination.

4.5. The Hartree-Fock-Slater Method and its Applications

In the Hartree-Fock-Slater (HFS) method, one solves the $X\alpha$ one-electron equation (Eq. (21)) directly without using the muffin-tin approximation. Various approaches can be taken. The scheme called discrete variational linear combinations of atomic orbitals (DV-LCAO) uses Slater type orbitals (STO) as variational basis functions./139/ The charge density required to calculate V_c and $V_{X\alpha}$ is cast into a STO-based multipolar form by applying a fitting procedure to each product of orbital pairs. Highly accurate results can be obtained, but the large basis sets are only treated with difficulty. Alternatively, the discrete variation self-consistent charge (DV-SCC) scheme uses numerical atomic-like wave functions as variational basis functions./140/ Since these numerical basis functions can be chosen to form a computationally highly efficient contracted basis set, larger clusters may be treated. To facilitate the calculations, a shape approximation to the charge density is obtained through a Mulliken population analysis/141,142/ of the cluster eigenvectors which leads to

spherically overlapping charge densities and Coulomb potentials. Generally DV-SCC results are found to be of intermediate quality, between $X\alpha$ -SW and full potential DV-LCAO results.

An example of such an application is the calculation of molecular ionization energies for oxygen chemisorbed on Ni (100) surfaces using the DV-SCC method. A Ni_5O cluster was used to model chemisorbed oxygen in the $c(2\times 2)$ configuration in four-fold symmetric hollow sites on the Ni (100) surface. The vertical distance of the oxygen atom to surface plane is taken as 1.7 a.u., a height near that inferred from LEED data. All 148 electrons of Ni_5O were explicitly treated with $\alpha = 0.7$ and basis sets including the 4s and 4p nickel states. At this height the oxygen valence levels (σ and π type) are strongly perturbed by mixing with the metal 3d, 4s, and 4p orbitals of a_1 and e symmetry. The $12e$ orbital of the Ni_5O cluster, which has a dominant oxygen 2p character, was found to have a binding energy of 10.8 eV. The UPS spectra of Eastman and Cashion/143/ and the ion neutralization spectra of Hagstrum and Becker/144/ for oxygen on Ni (100) show a broad peak (~ 2 eV wide) centered 5.5 - 6.0 eV below the Fermi energy. This corresponds well to the calculated oxygen 2p level. In addition, some high lying (4.7 eV above the Fermi energy) antibonding levels can be correlated directly with the HREEL spectrum obtained by Andersson./145, 146/

Rosén et al./147/ and Ellis et al./148/ have carried out calculations using the DV-LCAO method for CO chemisorbed on the Ni (100) surface at various binding sites. They used NiCO and Ni_5CO clusters for the top site configuration, a Ni_2CO cluster for the bridge bonding configuration and a second Ni_5CO cluster for the four-fold hollow site configuration. The experimental HREELS measurements of Andersson for $c(2\times 2)$ CO on Ni (100) show two vibrational losses, which are assigned to the Ni-C and C-O stretch vibrations of CO linearly bonded to nickel atoms (top-sites)./145, 146/ At low coverage, Andersson also found vibrational excitations assigned to CO bridge bonded to two surface nickel atoms.

Total energy calculations of sufficient precision would be able to determine the energetically favorable adsorption site. Such calculations are still much more difficult than the calculation of orbital energy levels and vibrational frequencies. Values of the Ni-Ni bond distance were chosen to correspond to the bulk crystal structure. In the DV-LCAO calculations the C-O and C-Ni bond distances were

taken from known nickel-carbonyl bond distances./149/ The results showed that one-electron binding energies in these clusters are relatively insensitive to the site geometry. The comparison between the theoretical and experimental stretching frequencies for chemisorbed CO did not provide firm evidence for one specific chemisorption site. However, the theoretical results are sensitive to geometrical factors such as the Ni-C and C-O bond distances, and the possible variation of the CO molecular axis from the surface normal. Several LEED results confirm the HREELS observation of top sites without tilting, and support the bond lengths assumed in the DV-LCAO calculations. In addition, a comparison of experimental angle-resolved UPS measurements /150/ with theoretical calculations/151/ showed that CO is chemisorbed with its molecular axis normal to the surface within 5° . A tilted molecule would give a split π level. However, this splitting is estimated to be quite small./151/

The chemisorption of chalcogen atoms on Ni surfaces has been investigated by many techniques (see Table VI). As a result of LEED and other studies the geometrical structure of chalcogens chemisorbed on nickel surfaces is well established. Chalcogen atoms generally adsorb in the site with maximum coordination on close packed nickel surfaces; 4-fold coordinated on the (100) and (110) surfaces, and 3-fold coordinated on the (111) surface. Recently Cao et al./152/ carried out DV-LCAO calculations investigating the spectroscopic and bonding properties of S, Se and Te atoms chemisorbed on Ni (100), (110) and (111) surfaces. The model clusters they used were Ni_5S and Ni_9S_2 for Ni (100), Ni_5S for Ni (110) and Ni_7S for Ni (111) corresponding to the binding sites found by LEED. Their calculations of the variation of adsorbate energy levels with adatom spacing above the metal surface are in good agreement with the results of the LEED structural analyses.

Finally, we conclude this section by drawing attention to the recent development of total energy calculations within the $X\alpha$ approximation. A total energy algorithm specially implemented for calculating small energy differences in large systems has been developed by Ziegler for chemisorption studies./153/ Ellis et al. also developed a method within the HFS approximation to handle this problem and the results for a series of clean copper clusters, namely Cu_2 , Cu_4 ,

Cu₁₃ and Cu₇₉ are very encouraging. Direct binding site determination via accurate total energy calculations for clusters of sufficient sizes is likely to play a more important role in the near future.

4.6. The *ab initio* Quantum Chemical Calculation

In the previous two sections we have discussed the semiempirical extended Hückel theory and the SCF- $X\alpha$ -SW method. We have detailed the advantages and disadvantages of these methods for surface structure determination. However, there exists a vast literature of *ab initio* quantum chemical methods which are described in terms of either the molecular orbital (MO) or valence bond (VB) schemes for determining the electronic and geometric structure of molecules. The application of these methods to surface problems has advanced rapidly in recent years, as we shall discuss in this section.

The most commonly used *ab initio* method is the self-consistent field Hartree-Fock (SCF-HF) scheme with or without configuration interaction (CI). In the Hartree-Fock method, the wave function for a closed shell singlet state has the antisymmetrized form

$$\psi_i = A(\phi_1\alpha\phi_1\beta\phi_2\alpha\phi_2\beta \cdots \phi_n\alpha\phi_n\beta) \quad (34)$$

with each orbital appearing twice for the two spin states α and β . The equation satisfied by the one-electron orbital ϕ_i is written as

$$[h_{eff} + \sum_j (2J_j - K_j)] \phi_i = \epsilon_i \phi_i \quad (35)$$

Here h_{eff} contains the kinetic energy operator and the electron-nucleus attraction interaction. J_j and K_j are the usual Coulomb and exchange operators. Eq. (35) can be solved by a self-consistent iteration procedure within the LCAO approximation. Filling these molecular orbitals up to the Fermi energy gives the ground state electronic configuration for the system. For open-shell systems when a few determinants of the form of Eq. (34) are combined, the resulting one-

electron equations can be solved using the multiconfiguration SCF (MCSCF) method. The SCF-HF results neglect electron-electron correlation effects. The configuration interaction includes these effects by formulating a multiconfiguration electron state as

$$\Psi = \sum_i c_i \psi_i \quad (36)$$

where the c_i 's are coefficients to be determined variationally.

Numerous studies have applied SCF-HF, MCSCF and SCF-HF-CI methods to surface problems./154, 155, 156, 157, 158, 159, 160, 161, 162, 163/ One particularly interesting example is an explanation of the origin of the coverage-dependent vibrational frequency shift for oxygen on Ni (100). Bauschlicher and Bagus have carried out SCF studies for the Ni_{25}O and Ni_{25}O_5 clusters to model the p(2x2) and c(2x2) structures of O on Ni (100), respectively./164/ The cluster contains a four-atom by four-atom square top layer and a three-atom by three-atom second layer. Four oxygen atoms are located in hollow sites for the (2x2) arrangement and a fifth centered atom is added for the c(2x2) arrangement. The spacing between the oxygen atoms and the first Ni layer is varied. For the Ni_{25}O_5 cluster, the four atoms placed at the outer four-fold sites are given an equilibrium spacing determined from Ni_{25}O calculations where only one oxygen is present, centered on the square top layer. The spacing of the central atom is then allowed to vary.

The Ni atoms are treated as one-electron systems in which the effects of the Ar-like core and the nine 3d electrons are replaced by a modified effective potential (MEP) as suggested by Melius et al./165/ A contracted gaussian basis set is used for Ni, which includes two functions to describe the 4s and one to describe the 4p atomic orbitals. Since a previous study/159/ found the O-Ni spacing and the vibrational frequency ω_e insensitive to correlations in this open-shell system, the authors have adopted the SCF calculation scheme. To check the approximation of treating the Ni atoms as a one-electron system, they performed both the MEP and an all electron SCF calculation for the Ni_5O cluster. They found that the MEP spacing is 0.37 Å or 35% smaller than the all-electron value; the MEP ω_e value is 90 cm^{-1} or 24% smaller. Since the 3d

orbital extends into the valence region where the 4s electron density is substantial, a correction needs to be added to the MEP calculation to take the 3d penetration into account. This was done phenomenologically by replacing the core charge of +1 by a distance-dependent $Z_{eff}(R)$. When this correction is included, the resulting spacing and ω_e values are in good agreement with the all-electron values. They found that for Ni₂₅O, the spacing is 0.83 Å and for Ni₂₅O₅ it is 0.72 Å. The ω_e values are 400 and 315 cm⁻¹, respectively./166/ The ω_e values measured in HREELS experiments are 430 and 310 cm⁻¹ for p(2x2)-Ni(100)-O and c(2x2)-Ni(100)-O. The spacings obtained from EXAFS experiments are 0.86±0.07 Å for both p(2x2)-Ni(100)-O and c(2x2)-Ni(100)-O./167/ LEED analyses have yielded a spacing of 0.9±0.1 Å for both coverages./168,169/ These calculations do not support the possibility of having two states, i.e., an O radical state for p(2x2) and an oxide state for c(2x2) coverages. The two states were previously suggested by Upton and Goddard/170,171/ as an explanation for the two different Ni-O vibration frequencies.

Another interesting example of MCSCF calculation is the determination of the oxygen binding site on Si(100). Batra et al performed this work for a few model clusters for oxygen chemisorbed at one, two and four-fold coordinated sites on Si₃H₆, Si₆H₁₂, and Si₇H₈ clusters./172/

They attempted to resolve the controversy regarding the dissociative chemisorption of oxygen on semiconductor surfaces. The energy-minimized geometries and absolute binding energies are listed in Table III. Since the binding energy of O₂ is 2.6 eV per oxygen, dissociative chemisorption is found to be energetically favorable and is exothermic by 3 eV. Moreover, the two-fold bridge site is calculated to be more stable than the one-fold top and four-fold hollow sites. The calculated interatomic distance for the on-top site, 1.64 Å, is in good agreement with the value obtained by Goddard et al., of 1.69 Å./173,174/ Since the treatment of correlation effects in MCSCF is limited, the dissociation energies are expected to increase when a more accurate configuration interaction calculation is performed.

Comparing the calculated vibrational frequencies with the HREELS data/175/ also yields a reasonable interpretation. For Si(100) at low O₂ exposures at 700 K, two major EELS peaks were reported, one at 1060 cm⁻¹ and

Table III. Oxygen on Si(100)

coordination	1-fold	2-fold	4-fold
model cluster	Si ₃ H ₆ O	Si ₆ H ₁₂ O	Si ₇ H ₃ O
spacing (Å)	1.64	0.06	0.96
bond length (Å)	1.64	1.92	2.88
energy (eV)	3.81	4.28	0.27
ω_e (cm ⁻¹)	866	288	106

All silicon atoms which are not involved in Si-O bonding are 4-fold coordinated, with all dangling (non Si-Si) bonds taken up by Si-H bonds.

the second at 866 cm⁻¹. A third low intensity peak is at 370 cm⁻¹. The authors assigned the high-frequency peak to the top-site and the lower frequency 866 cm⁻¹ peak to the bridge site. The third low intensity peak can be associated with adsorbed O₂ or O atoms in an initial or intermediate stage of oxidation of Si to form SiO₂.

While the above mentioned *ab initio* calculations produced good results for surface structure determinations, their computational cost is often high. In most formulations, the cost arises from the large number of two-electron integrals to be evaluated. The number of integrals increases as n^4 for n basis functions, so that computations become lengthy when large basis sets are required to achieve accuracy. This places practical restrictions on the applicability of *ab initio* techniques. One possible simplifying approach is to consider exact evaluations of certain important integrals in the n^4 list and to approximate the remainder. This idea was first applied to molecular problems by Whitten.¹⁷⁶ He introduced the notation

$$\langle g_i(1)g_j(1) | \frac{1}{r_{12}} | g_k(2)g_l(2) \rangle = [\phi_{ij} | \phi_{kl}] \quad (37)$$

for electron repulsion integrals where g denotes an arbitrary basis function. He then showed that

$$| [\phi_{ij} | \phi_{kl}] - [\phi_{ij}' | \phi_{kl}'] | \leq \delta \quad (38)$$

where

$$\delta = \epsilon_a^{1/2} \epsilon_b^{1/2} + \epsilon_a^{1/2} K_b^{1/2} + \epsilon_b^{1/2} K_a^{1/2} \quad (39)$$

$$\epsilon_m = [\phi_m - \phi_m' | \phi_m - \phi_m'] \text{ and } K_m = [\phi_m | \phi_m'], \quad m = a, b \quad (40)$$

Here $\phi_{ij} = g_i g_j$ and $\phi_{kl} = g_k g_l$ are used to approximate the electron densities ϕ_{ij}' and ϕ_{kl}' . The attractiveness of this approach is due to the simple structure of the error bound δ which can be calculated separately for the pair of densities ϕ_{ij} and ϕ_{kl} , yielding a number of integrals proportional to n^2 . One can then obtain the approximated density by minimizing δ with respect to all parameters in ϕ_{ij} and ϕ_{ij}' . This method is called the error bound method. Its results have been shown to be quite successful in many cases.

In addition to the error bound method to approximate two-electron integrals, Whitten and Pakkanen also proposed a new embedding theory to increase the cluster size that could be used for chemisorption studies.¹⁷⁷ Let us assume that molecular adsorption is taking place at a chosen site of well-defined geometry. Let the adsorbate be characterized by a set of orbitals $\{\phi_k^A\}$ with energies $\{\epsilon_k^A\}$ and let the metal substrate be characterized by another set of orbitals $\{\phi_l\}$ with eigenvalues $\{\epsilon_l\}$. For large metal clusters, the number of orbitals in $\{\phi_l\}$ is very large and the energy levels $\{\epsilon_l\}$ are densely spaced. Whitten and Pakkanen proposed a so-called "localization" scheme in which the interaction of the adsorbate levels with the large number of metal levels can be described by those orbitals for which the interaction $|\langle \phi_k^A | H_{eff} | \phi_l \rangle|$ is large. A unitary transformation can be introduced such that $|\langle \phi_k^A | H_{eff} | \phi_l \rangle|$ is maximized. This procedure yields one set of functions which physically represent orbitals localized on the designated surface atoms, bonds between these atoms, as well as bonds linking the designated atoms with the remainder of the cluster. A second set of functions consists of so-called interior orbitals. They are treated as an invariant core in each configuration for the step of the configuration

interaction. Thus, for an n -electron chemisorption system the interior orbitals contribute a fixed Coulomb and exchange field acting on the n electrons included explicitly.

The application of the error bound method and the embedding theory may be illustrated by a SCF-HF-CI calculation for H_2 on Ti (0001)./178/ It was found by this method that dissociative adsorption of H_2 occurs for the Ti_7H_2 , $Ti_{10}H_2$ and $Ti_{38}H_2$ clusters. The top, bridge and three-fold hollow sites were considered. H_2 was allowed to approach the surface with its axis parallel and perpendicular to the surface plane and the H-H bond was also allowed to stretch. The authors found that dissociative chemisorption occurs and the most stable adsorption geometry is in the 3-fold symmetric site with H spaced 1.3 Å above the surface. Adsorption of two hydrogens in adjacent 3-fold sites (about 1.5 Å apart) is less stable than in next-nearest 3-fold sites or more distant sites. The calculated adsorption energy of 45 kcal/mol for $Ti_{38}H_2$ compares favorably with experiment (the adsorption geometry is otherwise not known, but by analogy with Ni (111), 3-fold hollow sites are likely). The chemical bond involves mainly the 4s electrons of the metal interacting with the hydrogen and a polarized substrate electron distribution, but d -electron bonding and correlation significantly increase the binding energy. The binding energies calculated for the smaller clusters are in most cases a few tenths of an eV larger than those calculated for the larger clusters. Similar calculations have also been carried out by Madhavan and Whitten for the chemisorption of H_2 on Cu (100) using a $Cu_{38}H_2$ cluster./179/ They found that H_2 dissociative chemisorption is activated in that case. The H_2 binding energies are in the range of 13-22 kcal/mol. The activation barrier is about 35-40 kcal/mol due to the repulsion of molecular H_2 by the surface and the difficulty of stretching H_2 at a significant distance above the surface. It was also concluded from these calculations that the effect of the 3d-electrons, either in terms of direct 3d-4d mixing or in terms of 3d-4s promotion is unlikely to assist the dissociation of H_2 on the Cu surface.

Finally we discuss the Generalized Valence Bond (GVB) method as proposed by Hunt, Hay and Goddard./180,181,182/ This is a method aimed at improving some of the HF procedures, for instance to obtain the correct dissociation limit, and to partially include correlation effects. The basic idea is that the $\phi_i\alpha\phi_i\beta$ type of orbitals in Eq. (34) be replaced by

$$\phi_{ia}\alpha\phi_{ib}\beta, \quad (41)$$

such that each spin can have a different spatial orbital ϕ_{ia} or ϕ_{ib} , instead of having the same spatial orbital ϕ_i for both spins. This yields the wave function

$$\begin{aligned} \psi_i &= A(\phi_{1a}\alpha\phi_{1b}\beta\phi_{2a}\alpha\phi_{2b}\beta \cdots \phi_{Na}\alpha\phi_{Nb}\beta) \\ &= (\phi_{1a}\phi_{1b}\phi_{2a}\phi_{2b} \cdots \phi_{Na}\phi_{Nb}\chi) \end{aligned} \quad (42)$$

where χ is a general N -electron spin function and the orbitals ϕ_{ia} and ϕ_{ib} are solved for self-consistently. The dependence of the energy upon the orbital pair i has the form

$$\begin{aligned} E &= E_{(i)} + f_{1i}\langle\phi_{1i}|2h_{eff} + J_{1i}|\phi_{1i}\rangle + f_{2i}\langle\phi_{2i}|2h_{eff} + J_{2i}|\phi_{2i}\rangle \\ &\quad + C_{1i}C_{2i}\langle\phi_{1i}|K_{2i}|\phi_{1i}\rangle \end{aligned} \quad (43)$$

where $i = a, b$; h_{eff} is the usual HF Hamiltonian excluding the orbital pair i , $E_{(i)}$ is independent of the orbitals in pair i and f_k is a constant which depends on the orbital occupancy. Separating from $E_{(i)}$ the terms involving the other pairs, the authors obtained the general expression

$$E = \sum_k f_k h_k + \sum_{k,l} (a_{kl} J_{kl} + b_{kl} K_{kl}) \quad (44)$$

which gives, upon using the variation principle

$$\bar{H}_k \phi_k = [H_k - \sum_{j \neq k} |j\rangle\langle j| H_j] \phi_k = \epsilon_k \phi_k, \quad k = 1, 2, \dots, n \quad (45)$$

where

$$H_k = f_k h + \sum_l (a_{kl} J_l + b_{kl} K_l) \quad (46)$$

and n is the number of distinct orbitals. J and K are the usual Coulomb and exchange operators from HF theory. Eq. (46) can be solved self-consistently. Since the GVB method allows paired electrons which have different spins to occupy different spatial orbitals, some correlation is included in solving the GVB equation, which removes many difficulties and inconsistencies of the HF method. Using the GVB wave functions one can include further correlation via the configuration interaction in the so-called GVB-CI method.

To illustrate applications of the GVB-CI method we shall first discuss the recent theoretical studies of CO on Ni (100) of Allison and Goddard./183/ They investigated CO adsorption at a top site having one-fold coordination to one Ni metal atom (see Figure 6). A Ni₁₄ cluster was used to represent Ni (100). The Ar-like core of the Ni atom was replaced by an effective potential,/184/ while the nine 3d electrons were kept frozen, producing another electrostatic potential as discussed previously. The GVB calculation produced a CO dipole moment of 0.124 Debye in excellent agreement with the experimental value./185/ The best calculated geometry for Ni₁₄CO has bond lengths $R_{\text{Ni-C}} = 1.94 \text{ \AA}$, $R_{\text{C-O}} = 1.14 \text{ \AA}$ and an Ni-C-O bond angle of 180° , in good agreement with LEED results. Calculations for CO tilted away from the normal showed this geometry to be energetically less favorable. The dissociation energy, after correcting for the zero-point energy and temperature dependence of the enthalpy, is 1.29 eV. The binding energy obtained for the Ni₄OC geometry, i.e. with the O end toward the surface, was much lower, only 0.39 eV. The optimum Ni-O bond length is then 2.03 Å. The GVB results agree well with the experimental heat of adsorption of 1.30 eV found by Tracy at low coverages./186/ Good agreement is also found for vibrational frequencies. The calculated frequencies are 49.7 meV for the Ni-CO stretch, 264.0 meV for the C-O stretch, and 40.5 meV for the Ni-CO bend. The calculated frequencies on the Ni₅CO cluster are 54.2, 258.9 and 50.9 meV for these modes.

Another application of the GVB-CI method is the determination of the chemisorption geometries of oxygen and aluminum on the GaAs (110) surface by Barton et al./187/ The 28 core electrons of Ga and As are replaced by model effective core potentials./184/

The bulk GaAs zincblende structure involves tetrahedral bonding about each atom. Each Ga atom is bound to four near As atoms and vice versa. The

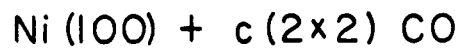
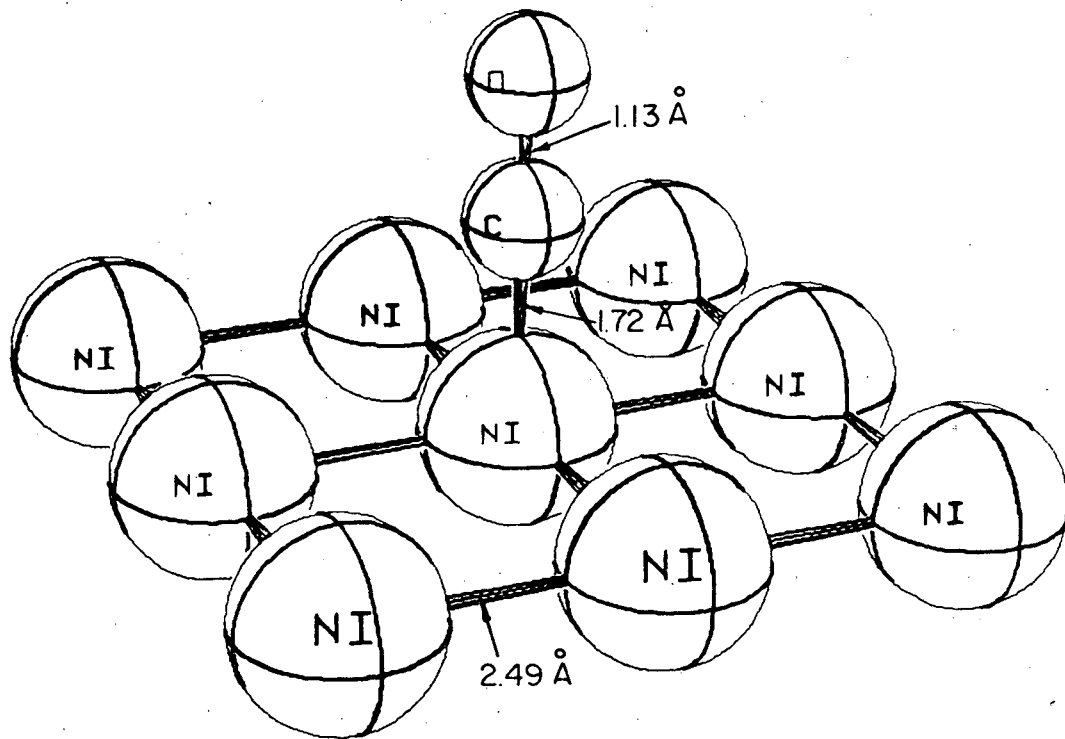
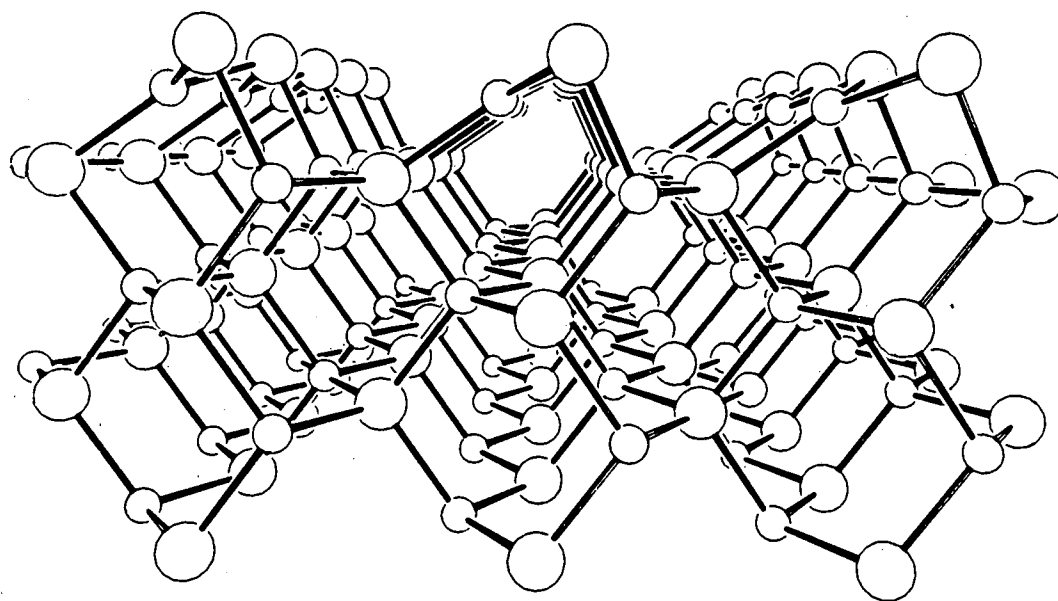


Fig. 6. The structure of carbon monoxide chemisorbed on Ni(100) in a c(2x2) periodic arrangement. The carbon atoms are bonded to single metal atoms.

unreconstructed GaAs (110) face consists of parallel zigzag chains of atoms. Each Ga is bound to two As atoms in the surface layer and one As atom in the layer below. GVB calculations by Goddard et al./188/ showed that the two dangling bonds broken at the surface, one on a Ga atom and one on an As atom, coalesce into one lone pair of electrons localized on the As center. The surface As has the character of normal trivalent As with a $(4s)^2$ lone pair. Such an As atom bonds to the p -orbitals leading to optimum bond angles near 90° . In contrast, the surface Ga has three bonds with no electron in the fourth valence orbital. The best configuration for Ga is therefore planar, with bond angles near 120° (see Figure 7). Such bond angles around both Ga and As can be accommodated by a reconstruction involving a simple rotation of the surface zig-zag chains by about 27° . With such a reconstruction, the GVB results indeed gave an average bond angle of 119.4° at the Ga site and 94.9° at the As site, consistent with the above local bond analysis. If we define the surface strain as the projection normal to surface of the total displacement of the surface As relative to the surface Ga, the theoretical value of 0.67 \AA is found to be in good agreement with the experimental value of $0.65\text{-}0.70 \text{ \AA}$ obtained by LEED./189,190,191,192/

When oxygen chemisorbs on GaAs (110), the authors predicted that the O atom would be promoted to the singlet state, creating a configuration with an empty p -orbital prepared to accept an electron pair. They also showed that the energy gained by the O-As bond is larger ($\sim 2.2\text{eV}$ for H_3AsO) than the promotion energy of the O atom from the ^3P to the ^1D state. Therefore, the only way oxygen can bond to the GaAs (110) surface without disrupting Ga-As bonds is for the O atoms to attach to As atoms. The computed As-O bond length is 1.63 \AA (the As-O single bond length is 1.8 \AA), in good agreement with the EXAFS value of $1.70 \pm 0.05 \text{ \AA}$./193/ The calculated dipole moment and vibrational frequency for the As-O bond are 1.00 Debye and 125 cm^{-1} . Experimentally, $(\text{H}_3\text{C})_3\text{AsO}$ has an As-O bond length of 1.63 \AA ./194/ a vibrational frequency of 110 meV /195/ and a dipole moment of 1.14 Debye ./196/ The chemical shifts of the Ga ($3d$) and As ($3d$) levels were also calculated for the As=O case. The authors found that Ga ($3d$) shifts by 0.8 eV and the As ($3d$) shifts by 2.6 eV , both to higher binding energy. The experimentally reported values for the core-level shifts are 0.8 eV for Ga ($3d$)/197/ and 2.9 eV for the As ($3d$)/198,199,200/



Ga As (110)

Fig. 7. Perspective view of the structure of the GaAs(110) surface which exhibits the 27 rotation of the zig-zag chains of surface atoms.

The chemisorption of Al on GaAs (110) proceeds in a different way. The Al atom is an electron donor since it is not very electronegative, with a value of 1.5 on the Pauling electronegativity scale./201/ GVB energy minimization for the Al position finds the Al 2.95 Å above a Ga site, tipped very slightly towards an adjacent As (3.90 Å). At the same time it was found that the Ga site reconstructs (the surface strain decreases from 0.67 to 0.55 Å) leading to a 40% increase in net binding energy. When an Al atom binds to a surface Ga atom, the Ga atom will prefer a more tetrahedral geometry to make more use of the electrons available for bonding to its neighbors. This increases the strength of the Al-surface bond.

4.7. Conclusion

The techniques of theoretical surface chemistry have advanced sufficiently to make a significant contribution to the understanding of surface structural chemistry. Even with the simplified "muffin-tin" potential, $X\alpha$ -scattered wave calculations do a good job of predicting photoemission spectra and their variation with adsorbate geometry. Fully self-consistent *ab-initio* total-energy calculations have been able to successfully determine the structure of adsorbate bonding geometries. These calculations are still very complex, and therefore limited to small clusters. However a number of approaches to increase the efficiency of such calculations are being pursued, and over the next few years such work should make an increasing contribution to the understanding of surface structural chemistry.

5. RESULTS OF SURFACE CRYSTALLOGRAPHY

In this section, we present and discuss the accumulated results of surface structure determination. We give a comprehensive tabulation of published results. Only those structures which provide three-dimensional geometrical

information, including bond lengths, bond angles and layer spacings are included. They are brought together in Tables IV to XII, classified by type of surface: clean, unreconstructed metals (Table IV), alloys and reconstructed metals (Table V), chalcogens chemisorbed on metals (Table VI), other atoms adsorbed on metals (Table VII), clean semiconductors (Table VIII), atoms adsorbed on semiconductors (Table IX) and insulators (Table X), carbon monoxide chemisorbed on metals (Table XI) and other molecular adsorption on metals (Table XII). It must be stressed that not all these structures can be termed final or even reliable. However, the vast majority are most likely qualitatively correct.

A variety of surface analytical techniques have contributed to these results, as detailed in the tables. Their names, acronyms and characteristics were summarized in Table I and further described in sections 2 and 3.

We first discuss some basic aspects of surface structures, including ordering principles and notations, followed by an overview of the number and types of surface structures that have been investigated. Finally we shall highlight a few major trends emerging from the structural results.

5.1. Ordering Principles

The vast majority of solved surface structures have long-range two-dimensional ordering parallel to the surface. This means that the structures periodically repeat themselves in the two surface dimensions. There are several reasons for this. First, single crystals have been chosen in most cases as substrates, exposing a simple periodic lattice as a template. Second, a surprising number of surface structures can be easily prepared to remain periodic on the experimental time scale, whether in the clean state or after adsorption of atoms or molecules. Third, ordered structures are desirable for investigation because they provide the greatest simplicity in the interpretation of results. And fourth, structural determination itself is simplest in ordered cases.

The driving force for ordering originates, just as with three-dimensional crystal formation, in the mutual atomic interactions. With adsorbates, an important distinction must be made between adatom-adatom and adatom-substrate interactions. In chemisorption the adatom-adatom forces are usually

small compared to the adatom-substrate binding forces, so the adatom locations or sites are determined by the optimum adatom-substrate bonding. But the adatom-adatom interactions still manage to dominate the long-range ordering of the overlayer. These interactions can be studied by examining the phase transitions of the overlayer as a function of temperature or coverage.

The surface coverage of an adsorbate is another important parameter in ordering. We shall use the common definition of coverage where one monolayer corresponds to one adsorbate atom or molecule for each unit cell of the clean, unreconstructed substrate surface. Thus, if an adsorbed undissociated carbon monoxide molecule bonds to alternating top-layer metal atoms exposed at the Ni(100) surface, we have a coverage of a half monolayer.

At very low coverages some adsorbates bunch together in two-dimensional islands. This results from short-range attractive adsorbate-adsorbate interactions combined with easy diffusion along the surface. Other adsorbates repel each other and form disordered overlayers with atoms or molecules adsorbed in sites of a given type (a "lattice gas"). When the coverage is increased so that the mean interadsorbate distance decreases to about 5-10 Å, the mutual interactions often strongly influence the ordering, favoring certain adsorbate configurations over others. As a result, the structure can develop a unit cell that repeats periodically across the surface. This is very evident in the LEED patterns, which depend directly on this unit cell. For example, atomic oxygen on Ni(100) orders very well at a quarter of a monolayer. The oxygen atoms then occupy one quarter of the available "hollow" sites of Ni(100) in a square array labeled (2x2). When the coverage is doubled to a half monolayer, the extra oxygen atoms occupy the empty hollow sites at the center of each of the (2x2) squares, thereby creating a new pattern labeled c(2x2) (c=centered). The corresponding LEED patterns are fundamentally different in that the (2x2) diffraction pattern has twice as many spots as the c(2x2) pattern, which in turn has twice as many spots as the clean-surface pattern, labeled (1x1).

Most nonmetallic adatoms will not compress into a one-monolayer overlayer on the closest-packed metal substrates. There appears to be a short-range repulsion that keeps adatoms apart by approximately a Van der Waals distance. Attempts to compress the overlayer further by increasing the coverage (which is

done by exposing the surface to the corresponding gas) result either in no further adsorption or in diffusion of the adatoms into the substrate, forming compounds.

Some adsorbates do not form strong chemical bonds with substrate atoms. This case is called physisorption. For these adsorbates the adsorbate-adsorbate interactions can dominate the adsorbate-substrate interactions, and the optimum adatom-substrate bonding geometry can be overridden by the lateral adatom-adatom interactions, yielding for example incommensurate structures, in which the overlayer and the substrate have independent lattices. When adsorbates are used which physisorb rather than chemisorb (at suitably low temperatures), one also finds that the Van der Waals distance determines the densest overlayer packing. In this case, Furthermore, with physisorption a larger coverage is possible through multilayer formation.

With metallic adsorbates very close-packed overlayers can be formed, because metal adsorbate atoms attract each other relatively strongly and coalesce with covalent interatomic distances. When the atomic sizes of the overlayer and substrate metals are nearly the same, one observes one-monolayer (1x1) structures, where adsorbate atoms occupy every unit cell of the substrate. With less equal atomic radii, other structures are formed, dominated by the covalent closest packing distance of the adsorbate. Beyond one close-packed overlayer, metal adsorbates frequently form multilayers or also three-dimensional crystallites. Alloy formation by interdiffusion is also observed in a number of cases, even in the submonolayer regime.

5.2. Notation for surface lattices

In Tables IV to XII the substrate surface is defined by the Miller indices of the corresponding crystallographic plane.

Unless there is reconstruction, this clean surface is labeled (1x1) to denote that the surface lattice is the same as it would be if the bulk lattice were cut along a crystallographic plane (the "terminated bulk surface"). In the case of reconstruction or with overlayers, the surface symmetry and periodicity is often different from the (1x1) lattice. Often this new periodicity is "commensurate"

with the (1x1) substrate lattice, i.e. there is a simple rational relationship between the two lattices. Such a "superlattice" may be labeled by the notation

$$c(vxw)R\alpha \text{ or } p(vxw)R\alpha \quad (47)$$

Here v and w are elongation factors of the (1x1) lattice vectors; they indicate that the non-centered (vxw) lattice has unit cell edges that are v and w times the lengths of the (1x1) unit cell edges. The quantity α is an angle through which the (1x1) lattice must be rotated to coincide with the superlattice (the $R\alpha$ is omitted when $\alpha=0$). The prefix p denotes a primitive lattice (it is often omitted), while c denotes a centered lattice. As an example, the above-mentioned (2x2) lattice can also be written $p(2x2)$, whereas the $c(2x2)$ lattice can be given equally by $(\sqrt{2}x\sqrt{2})R45^\circ$ or $p(\sqrt{2}x\sqrt{2})R45^\circ$. This so-called Wood notation assumes that the rotation angle α is the same between the different lattice vectors of the (1x1) lattice and the non-centered (vxw) lattice. For instance, it assumes that the (vxw) lattice is rectangular when the (1x1) lattice is rectangular. (Some authors use the Wood notation even when the rotation angle for the two superlattice vectors is *not* the same. In this case the notation is not well defined. The matrix notation described below should be used for such cases.)

The more general case can be handled with a "matrix notation", which we will not need here. But there is a frequently occurring case which has its own notation. On a substrate with a six-fold rotationally symmetric (1x1) lattice (such as with fcc(111) surfaces), one often finds rectangular superlattices. These can be labeled

$$c(v\sqrt{3}xw)rect \text{ or } p(v\sqrt{3}xw)rect \quad (48)$$

indicating that the superlattice unit cell is rectangular and has edges of lengths $v\sqrt{3}$ and w times the (1x1) cell edges.

5.3. Numbers and types of solved surface structures

If we limit ourselves to observed LEED patterns, we find that over the years about 2000 ordered structures have been reported./202/ Among these, perhaps 180 have been structurally solved by various techniques of surface crystallography. Intensity analyses of low-energy electron diffraction have contributed about 150 of these. The remaining 30 structures were obtained primarily with ion scattering (MEIS, HEIS), SEXAFS or photoelectron diffraction (NPD, ARXPS).

A breakdown of the structural results by type of surface shows results for nearly 50 clean, unreconstructed metal surfaces and about 10 alloys and reconstructed metal surfaces. The structures of about 65 atomic overlayers on metal surfaces have been determined, some 40 of these involving chalcogen atoms. Just over 20 molecular structures have been determined for metal surfaces, half of these being overlayers of undissociated carbon monoxide and the others various hydrocarbons. Turning to semiconductors, some 13 clean, usually reconstructed structures were determined, against nearly 10 atomic overlayer structures. In addition, about 15 insulator surface structures have been investigated.

5.4. Major trends among surface structures

5.4.1. Bond length contractions and reconstructions

A general observation at surfaces is a tendency for bond lengths to decrease as the bonding coordination number decreases. This trend fits long-established principles (cf. Pauling), if one relates coordination number to bond order (cf. Mitchell). The clearest manifestation is provided bond length relaxations at clean metal surfaces. As one compares close-packed with less close-packed surfaces of metals, one finds that the latter present a smaller interlayer spacing between the topmost and the second atomic layers, compared with bulk values. The

corresponding bond length contraction is of the order of 2 to 3%. Moreover, the perturbation caused by this surface relaxation propagates a few layers down into the surface. In fact, there is a compensating expansion between the second and third metal layers of the order of 1%, and a small but detectable change in the next layer. Appropriately, such relaxations are largely removed by the chemisorption of atoms on top of these surfaces.

Another manifestation of bond length contractions at surfaces compared to the bulk metal are certain reconstructions, where the topmost metal layer adopts a different structure and symmetry than the underlying layers. For instance, with Ir, Pt and Au(100), the interatomic distance in the topmost layer shrinks by a few percent parallel to the surface. It then becomes more favorable for this layer to collapse into a hexagonally close-packed layer rather than maintaining the square lattice of the underlying layers. Many adsorbates can reverse this reconstruction by removing the driving force towards smaller bond lengths.

In the case of semiconductor surfaces, a more dominant disturbance is the difficulty of surface atoms to compensate for the loss of nearest neighbors. The "dangling bonds" created at the surface cannot easily be satisfied by bonding to neighboring surface atoms, except through more drastic rearrangements of these atoms. Therefore, most semiconductor surfaces reconstruct. Major rebonding between surface atoms occurs in this process. The associated perturbation propagates several layers into the surface until the bulk lattice is recovered. Here again, adsorbates can reverse the reconstruction and induce a return to the bulk structure.

5.4.2. Atomic penetration into substrates

Of major interest for such processes as oxidation and compound formation are results that show several stages of atomic penetration into the substrate lattice. At metal surfaces, this appears to occur mostly with small atoms: oxygen, nitrogen, carbon, as well as hydrogen. In some instances, as the coverage is increased, first an overlayer is formed (e.g. O on Ni(100)). Usually, the adatom occupies high-coordination sites such as "hollow" sites. On less close-packed surfaces, this site puts the adatom nearly coplanar with the surface metal atoms

(e.g. O on Fe(100)). This may be viewed as a single layer of the metal-adatom compound. The next stage of penetration is illustrated by N on Ti(0001), where the adatom occupies interstitial sites between the first and second metal layers, thereby forming a three-layer film of the bulk compound TiN. Deeper penetration is often observed in the form of thicker compound films which show no trace of the structural properties of the parent metal.

In the case of semiconductors, there is more interstitial space available for diffusion of adatoms into the surface. The very few cases whose structure is known show, however, that a substitutional arrangement may be the more stable equilibrium configuration. Thus, with Al on GaAs(110), Al atoms tend to occupy the original Ga and As positions.

5.4.3. Molecular adsorption

In the case of molecules adsorbed at surfaces, it must be first stated that much important information is obtained from high-resolution electron energy loss spectroscopy (HREELS). This technique measures vibration frequencies of surfaces, in a way similar to infra-red absorption spectroscopy in the gas phase. HREELS allows the identification of the molecular species present on the surface, which no surface crystallography method can do.

Carbon monoxide has proved a popular and convenient molecular adsorbate. It provides a rich variety of behavior at surfaces, while being relatively easy to study by various methods. Toward the left of the periodic table, metal surfaces increasingly tend to dissociate CO, then separate C and O atoms bond directly in individual hollow sites, as in atomic adsorption. On other metal substrates, CO remains intact and bonds through its carbon end to the surface, with the C-O axis perpendicular to the surface. However, the adsorption site varies considerably. CO most commonly adsorbs in one-fold coordinated top sites or two-fold coordinated bridge sites. Occasionally, three-fold coordinated hollow sites are also found. The site depends on several factors: the metal, the crystallographic face and the CO coverage. Another factor has recently been found to influence the CO adsorption site -- coadsorbed atomic or molecular species which donate charge to the CO can shift CO to a higher-coordination site.

An example is the coadsorption of benzene, whose π -orbitals give up charge to the metal and to nearby CO species. On Rh(111) this shifts CO adsorption to three-fold sites.

There is a close similarity between the bonding geometry of CO on metal surfaces and in metal-carbonyl complexes. In both cases, for example, the metal-carbon bond length increases markedly with the coordination number of the site where the CO molecule bonds to the metal. The C-O bond length tends to increase slightly at the same time, indicating a C-O bond weakening, which is amplified by nearby electron donors.

If we consider hydrocarbons at surfaces, we must set the saturated ones aside. These do not chemisorb at metal surfaces, but rather physisorb at low temperatures. No detailed structural determination has been performed for saturated hydrocarbons on metals. However, some structures have been obtained using the graphite basal plane as a substrate (cf. Suzanne etc) which give information about Van der Waals packing of such molecules, but no chemical reactions are involved.

With unsaturated hydrocarbons, whether straight-chain or aromatic, two basic types of surface structure can be distinguished. The first consists of the intact molecule bonding to the metal surface by sharing its C-C multiple bonds with the metal. Thus, acetylene and ethylene adsorb with their C-C bonds parallel to the metal surface. The C-C bond is believed to be considerably lengthened, indicating bond-order reduction in favor of the newly formed metal-carbon bonds. The associated rehybridization around the carbon atoms may also result in the hydrogen atoms bending away from the metal. Similarly, benzene bonds with its carbon ring parallel to the surface, and large expansions of the C-C distances have been observed. Such distortions may be a forerunner of molecular dissociation.

The second type of structure for unsaturated hydrocarbons is the result of a hydrogen rearrangement in straight-chain molecules. Alkylidynes are formed, in which a terminal carbon bonds to three metal atoms, while the rest of the chain is saturated and points away from the metal (extra hydrogen atoms may be necessary for these species to form). These alkylidynes, foremost among which is ethylidyne (C_2H_3), are quite stable in comparison to other organic species formed at room temperature transition metal substrates. However, at higher

temperatures, a progressive dehydrogenation occurs, leaving CH and CCH fragments, then carbonaceous fragments and ultimately graphite and bulk carbides on the surface.

Both types of hydrocarbon adsorption are also encountered in organometallic complexes. Here again, the geometries found at surfaces often correspond closely to those observed in complexes, including agreement of bond lengths and bond angles. There probably are larger differences between surfaces and complexes in the relative occurrence of the various species.

TABLE IV. Clean Metal Structures (unreconstructed)

(Where multiple layer spacing changes have been investigated these are listed in the table on successive lines.)

Substrate Face	Bulk Spacing(Å)	Surface Spacing(Å)	Expansion(%)	Method
Ag (110) fcc	1.44	1.34	-7	LEED/1/
Ag (110) fcc		1.33±0.04	-7.6	HEIS/2/
		1.50±0.04	4.2	
Ag (111) fcc	2.35	2.35±0.1	0	HEIS/3/
Al (100) fcc	2.02	2.025±0.10	0.0	LEED/4/
Al (100) fcc		2.02	0.0	LEED/5/
Al (100) fcc		2.052	1.0	MEED/6/
Al (110) fcc	1.43	1.30	-9.1	LEED/5/
Al (110) fcc		1.304±0.012	-8.8	LEED/7/
		1.499±0.15	4.8	
		1.404±0.017	-1.8	
		1.429±0.018	0.0	
Al (110) fcc		1.310±0.014	-8.4	LEED/8/
		1.510±0.016	5.6	
		1.463±0.019	2.3	
		1.455±0.022	1.7	
Al (111) fcc	2.33	2.350±0.012	0.9	LEED/9/
Al (111) fcc		2.41±0.05	3.1	LEED/10/
Al (311) fcc	1.23	1.68±0.01	-13.0	LEED/11/
		1.335±0.02	8.8	
Al (331) fcc	0.93	0.82±0.02	-11.7	LEED/12/
		0.89±0.03	-4.1	
		1.05±0.03	10.3	
		0.88±0.03	-4.8	

First-layer registry shifts of $\sim 0.06 \pm 0.08$ found

(continued)

TABLE IV (continued)

Substrate Face	Bulk Spacing(Å)	Surface Spacing(Å)	Expansion(%)	Method
Au (100) fcc (metastable)	2.04	2.04	0.0	LEED/13/
Cd (100) fcc	2.81	2.81	0	LEED/14/
Co (100) fcc	1.77	1.70	-4.0	LEED/15/
Co (111) fcc	2.05	2.05±0.05	0.0	LEED/16/
Co (0001) hcp	2.05	2.05±0.05	0.0	LEED/16/
Co (11 $\bar{2}$ 0) hcp	1.25	1.14±0.04	-8.8	LEED/17/
Cu (100) fcc	1.81	1.785	-1.1	LEED/18/
		1.836	1.7	
		1.832	1.5	
Cu (110) fcc	1.28	1.159	-9.2	LEED/18/
		1.305	2.3	
Cu (110) fcc		1.21±0.02	-5.3	MEIS/19/
		1.32±0.02	3.3	
Cu (110) fcc		1.170±0.008	-8.5	LEED/20/
		1.307±0.010	2.3	
Cu (111) fcc	2.09	2.076±0.02	-0.7	LEED/21/
Cu (311) fcc	1.09	1.035±0.02	-5.0	LEED/22/
Fe (100) bcc	1.43	1.41±0.04	-1.6	LEED/23/
Fe (110) bcc	2.02	2.04±0.04	0.5	LEED/24/
Fe (111) bcc	0.83	0.70±0.03	-15.4	LEED/25/
Fe (111) bcc		0.69±0.025	-16.6	LEED/26/
		0.75±0.025	-9.3	
		0.86±0.03	4.0	
		0.81±0.025	-2.1	
Fe (210)* bcc	0.64	0.50±0.03	-21.9	LEED/27/
		0.57±0.03	-10.9	

(continued)

TABLE IV (continued)

Substrate Face	Bulk Spacing(Å)	Surface Spacing(Å)	Expansion(%)	Method
		0.61±0.03	-4.7	
		0.64±0.03	0.0	
Fe (211)* bcc	1.17	1.05±0.03	-10.3	LEED/28/
		1.23±0.03	5.1	
		1.15±0.04	-1.7	
Fe (310) bcc	0.906	0.76±0.03	-16.1	LEED/29/
		1.02±0.03	12.6	
		0.87±0.04	-4.0	
Ir (100) fcc (metastable)	1.92	1.85±0.01	-3.6	LEED/30/
Ir (110) fcc	1.36	1.26±0.10	-7.4	LEED/31/
Ir (111) fcc	2.22	2.16±0.10	-2.6	LEED/32/
Na (110) bcc	3.03	3.03	0.0	LEED/33/
Na (110) bcc		3.0±0.01	-1.0	LEED/34/
Na (0001) hcp	2.87	2.87	0.0	LEED/35/
Ni (100) fcc	2.22	1.78±0.02	1.1	LEED/36/
Ni (100) fcc		1.604±0.008	-8.9	MEIS/37/
Ni (110) fcc	1.25	1.195±0.01	-4.0	MEIS/38/
Ni (110) fcc		1.18±0.02	-4.8	HEIS/39/
		1.27±0.02	2.4	
Ni (110) fcc		1.14±0.01	-8.1	LEED/40/
		1.28±0.01		
Ni (110) fcc		1.123±0.02	-9.8	LEED/41/
		1.292±0.02	3.8	
Ni (110) fcc		1.138±0.006	-8.6	LEED/42/
		1.284±0.007	3.1	
		1.240±0.009	-0.4	

(continued)

TABLE IV (continued)

Substrate Face	Bulk Spacing(Å)	Surface Spacing(Å)	Expansion(%)	Method
Ni (110) fcc		1.121±0.012	-9.0	MEIS/43/
		1.290±0.019	3.5	
Ni (111) fcc	2.03	2.005±0.025	-1.2	LEED/36/
Ni (111) fcc		2.033±0.020	0.0	HEIS/44/
Ni (311) fcc	1.06	0.894±0.010	-15.9	LEED/45/
		1.106±0.016	4.1	
		1.045±0.017	-1.6	
Mo (100) bcc	1.25	1.424±0.03	-9.5	LEED/46/
Mo (110) bcc	2.22	2.19±0.04	-1.6	LEED/47/
Pd (100) fcc	1.94	1.95±0.05	0.3	LEED/48/
Pd (110) fcc	1.37	1.29±0.03	-5.8	LEED/49/
		1.38±0.03	0.7	
Pd (111) fcc	2.246	2.25±0.05	0.0	HEIS/50/
Pd (111) fcc		2.276	1.3	LEED/51/
		2.216	-1.3	
		2.296	2.2	
		2.296	2.2	
Pt (100) fcc (metastable)	1.96	1.96	0.2	SPLEED/52/
Pt (100) fcc (metastable)		1.963	0.2	HEIS/53/
Pt (100) fcc (metastable)		1.96	0.0	LEED/13/
Pt (111) fcc	2.26	2.29±0.10	1.1	LEED/54/
Pt (111) fcc		2.30±0.02	1.4	HEIS/55/
Pt (111) fcc		2.276±0.02	0.5	SPLEED/56/
Pt (111) fcc		2.265±0.05	0.0	LEED/57/

(continued)

TABLE IV (continued)

Substrate Face	Bulk Spacing(Å)	Surface Spacing(Å)	Expansion(%)	Method
Re (10 $\bar{1}$ 0) hcp		0.67	-16.3	LEED/58/
Rh (100) fcc	1.90	1.91±0.02	0.5	LEED/59/
Rh (110) fcc	1.34	1.33±0.02	-0.7	LEED/59/
Rh (111) fcc	2.19	2.16±0.02	-1.4	LEED/59/
Rh (111) fcc		2.192±0.10	0.0	LEED/60/
Ru (0001) hcp	2.14	2.10±0.02	-1.9	LEED/61/
Sc (0001) hcp	2.64	2.59±0.02	-1.9	LEED/62/
Ta (100) bcc	1.65	1.47±0.03	-10.9	LEED/63/
		1.67±0.03	1.2	
Te (10 $\bar{1}$ 0) hcp		0.34±0.10		LEED/64/
Ti (0001) hcp	2.34	2.29±0.05	-2.1	LEED/65/
V (100) bcc	1.51	1.41±0.01	-6.6	LEED/66/
V (110) bcc	2.14	2.13±0.10	-0.5	LEED/67,68/
W (100) fcc	1.58	1.46±0.03	-7.6	LEED/69/
W (110) fcc	2.23	2.23±0.10	0.0	LEED/70/
Zn(0001) hcp	2.44	2.39±0.05	-2.0	LEED/71/
Zr (0001) hcp	2.57	2.54±0.05	-1.2	LEED/72/

* There are relaxations in the layer registries for the stepped iron (211) and (210) surfaces in addition to layer spacing relaxations.

REFERENCES

1. Zanazzi, E., Jona, F., Jepsen, D. W., and Marcus, P. M. (1977) *Journal of Physics C* **10**, 375.
2. Kuk, Y. and Feldman, L. C. (1984) *Physical Review B* **30**, 5811.
3. Culbertson, R. J., Feldman, L. C., Silverman, P. J., and Boehm, H. (1981) *Physical Review Letters* **47**, 657.
4. Van Hove, M. A., Tong, S. Y., and Stoner, N. (1976) *Surface Science* **54**, 259.
5. (1977) *Surface Science* **62**, 567.
6. Masud, N., Baudoing, R., Aberdam, D., and Gaubert, C. (1983) *Surface Science* **133**, 580.
7. Andersen, J. N., Nielsen, H. B., Petersen, L., and Adams, D. L. (1984) *Journal of Physics C* **17**, 173.
8. Noonan, J. R. and Davis, H. L. (1984) *Physical Review B* **29**, 4349.
9. Nielsen, H. B. and Adams, D. L. (1982) *Journal of Physics C* **15**, 615.
10. Martinez, V., Soria, F., Munoz, M. C., and Sacedon, J. L. (1983) *Surface Science* **128**, 424.
11. Noonan, J. R., Davis, H. L., and Erley, W. (1985) *Surface Science* **152/153**, 142.
12. Adams, D. L. and Sorensen, C. S. (1986) *Surface Science* **166**, 495.
13. Lang, E., Grimm, W., and Heinz, K. (1982) *Surface Science* **177**, 169.
14. Shih, H. D., Jona, F., Jepsen, D. W., and Marcus, P. M. (1977) *Physical Review B* **15**, 5561.
15. Maglietta, M., Zanazzi, E., Jona, F., Jepsen, D. W., and Marcus, P. M. (1978) *Applied Physics* **15**, 409.
16. Lee, B. W., Alsenz, R., Ignatiev, A., and Van Hove, M. A. (1978) *Physical Review B* **17**, 1510.
17. Weltz, M., Moritz, W., and Wolf, D. (1983) *Surface Science* **125**, 473.
18. Davis, H. L. and Noonan, J. R. (1983) *Surface Science* **126**, 245.
19. (1983) *Surface Science* **128**, 281.
20. Adams, D. L., Nielsen, H. B., and Andersen, J. N. (1983) *Surface Science* **128**, 294.

21. Lindgren, S. A., Walldén, L., Rundgren, J., and Westrin, P. (1984) *Physical Review B* **29**, 576.
22. Streater, R. W., Moore, W. T., Watson, P. R., Frost, D. C., and Mitchell, K. A. R. (1978) *Surface Science* **72**, 744.
23. Legg, K. O., Jona, F., Jepsen, D. W., and Marcus, P. M. (1977) *Journal of Physics C* **10**, 937.
24. Shih, H. D., Jona, F., and Marcus, P. M. (1980) *Journal of Physics C* **13**, 3801.
25. Shih, F. E., Jona, F., Jepsen, D. W., and Marcus, P. M. (1981) *Physical Review Letters* **46**, 731.
26. Sokolov, J., Jona, F., and Marcus, P. M. (1986) *Physical Review B* **33**, 1397.
27. Sokolov, J., Jona, F., and Marcus, P. M. (1985) *Physical Review B* **31**, 1929.
28. Sokolov, J., Shih, H. D., Bardi, U., and Jona, F. (1984) *Journal of Physics C* **17**, 371.
29. Sokolov, J., Jona, F., and Marcus, P. M. (1984) *Physical Review B* **29**, 5402.
30. Heinz, K. and Besold, G. (1983) *Surface Science* **125**, 515.
31. Chan, C. M., Cunningham, S. M., Luke, K. L., Weinberg, W. H., and Withrow, S. P. (1978) *Surface Science* **78**, 15.
32. Chan, C. M., Cunningham, S. L., Van Hove, M. A., Weinberg, W. H., and Withrow, S. P. (1977) *Surface Science* **66**, 394.
33. Echenique, P. M. (1976) *Journal of Physics C* **9**, 3193.
34. Andersson, S., Pendry, J. B., and Echenique, P. M. (1977) *Surface Science* **65**, 539.
35. Lindgren, S. A., Paul, J., Walldén, L., and Westrin, P. (1982) *Journal of Physics C* **15**, 6285.
36. Demuth, J. E., Marcus, P. M., and Jepsen, D. W. (1975) *Physical Review B* **11**, 1460.
37. Frenken, J. W. M., van der Veen, J. F., and Allan, G. (1983) *Physical Review Letters* **51**, 1876.
38. van der Veen, J. F., Tromp, R. M., Smeenk, R. G., and Saris, F. W. (1979) *Surface Science* **82**, 468.

39. (1983) *Surface Science* **134**, 329.
40. Gauthier, Y., Baudoing, R., Joly, Y., and Gaubert, C. (1984) *Journal of Physics C* **17**, 4547.
41. Xu, M. L. and Tong, S. Y. (1985) *Physical Review B* **31**, 6332.
42. Adams, D. L., Peterson, L. E., and Sorenson, C. S. (1985) *Journal of Physics C* **18**, 1753.
43. Yalisove, S. M., Graham, W. R., Adams, E. D., Copel, M., and Gustafsson, T. (1986) *Surface Science* **171**, 400.
44. Narusawa, T., Gibson, W. M., and Törnquist, E. (1981) *Physical Review Letters* **47**, 417.
45. Adams, D. L., Moore, W. T., and Mitchell, K. A. R. (1985) *Surface Science* **149**, 407.
46. Clarke, L. J. (1980) *Surface Science* **91**, 131.
47. Morales, L., Garza, D. O., and Clarke, L. J. (1981) *Journal of Physics C* **14**, 5391.
48. Behm, R. J., Christmann, K., Ertl, G., and Van Hove, M. A. (1980) *Journal of Chemical Physics* **73**, 2984.
49. Barnes, C. J., Ding, M. Q., Lindroos, M., Diehl, R. D., and King, D. A. (1985) *Surface Science* **162**, 59.
50. Kuk, Y., Feldman, L. C., and Silverman, P. J. (1983) *Physical Review Letters* **50**, 511.
51. Ohtani, H., Van Hove, M. A., and Somorjai, G. A. (to be published)
52. Feder, R. (1977) *Surface Science* **68**, 229.
53. Davies, J. A., Jackman, T. E., Jackson, D. P., and Norton, P. R. (1981) *Surface Science* **109**, 20.
54. Adams, D. L., Nielsen, H. B., and Van Hove, M. A. (1979) *Physical Review B* **20**, 4789.
55. van der Veen, J. F., Smeenk, R. G., Tromp, R. M., and Saris, F. W. (1979) *Surface Science* **79**, 219.
56. Feder, R., Pleyer, H., Bauer, P., and Müller, N. (1981) *Surface Science* **109**, 419.
57. Hayek, K., Glassl, H., Gutmann, A., Leonhard, H., Prutton, M., Tear, S. P., and Welton-Cook, M. R. (1985) *Surface Science* **152**, 419.

58. Davis, H. L. and Zehner, D. M. (1980) *Journal of Vacuum Science and Technology* **17**, 190.
59. Hengrasmee, S., Mitchell, K. A. R., Watson, P. R., and White, S. J. (1980) *Canadian Journal of Physics* **58**, 200.
60. Van Hove, M. A. and Koestner, R. J. (1984) in "Surface Structure by LEED" (P. M. Marcus and F. Jona, ed.), Plenum, New York.
61. Michalk, G., Moritz, W., Pfnür, H., and Menzel, D. (1983) *Surface Science* **129**, 92.
62. Tougaard, S., Ignatiev, A., and Adams, D. L. (1982) *Surface Science* **115**, 270.
63. Titov, A. and Moritz, W. (1982) *Surface Science* **123**, L709.
64. Meyer, R. J., Salaneck, W.R., Duke, C. B., Paton, A., Griffiths, C. H., Kovnat, L., and Meyer, L. E. (1980) *Physical Review B* **21**, 4542.
65. Shih, H. D., Jona, F., Jepsen, D. W., and Marcus, P. M. (1976) *Journal of Physics C* **9**, 1405.
66. Jensen, V., Andersen, J.N., Nielsen, H. B., and Adams, D. L. (1982) *Surface Science* **116**, 66.
67. Adams, D. L. and Nielsen, H. B. (1981) *Surface Science* **107**, 305.
68. Adams, D. L. and Nielsen, H. B. (1982) *Surface Science* **116**, 598.
69. Debe, M. K. and King, D. A. (1982) *Journal of Physics C* **15**, 2257.
70. Van Hove, M. A. and Tong, S. Y. (1976) *Surface Science* **54**, 91.
71. Unertl, W. N. and Thapliyal, H. V. (1975) *Journal of Vacuum Science and Technology* **12**, 263.
72. Moore, W. T., Watson, P. R., Frost, D. C., and Mitchell, K. A. R. (1979) *Journal of Physics C* **12**, L887.

TABLE V. Alloys and Reconstructed Metals

Substrate and Unit Cell	Structure	Method
Au (110) (fcc) (2x1)	Missing-row reconstruction confirmed by x-ray diffraction. Lateral displacement of second layer rows toward missing row position by 0.12 ± 0.02 Å. Anti-phase domains due to monatomic steps observed. Evidence for top-layer expansion or contraction of ~ 0.25 Å.	X-Ray Diffraction/1/
Au (110) (fcc) (2x1)	Missing-row reconstruction. Every other top layer ($\bar{1}\bar{1}0$) row is missing. The second layer lateral displacements are ~ 0.07 Å, and the second row is buckled by -0.24 Å. The first layer spacing is -20.1% , and the second and third is -6.3% relative to the 1.44 Å bulk layer spacing.	LEED/2/
Au (110) (fcc) (2x1)	Missing-row reconstruction studied by channeling and blocking, top layer spacing contracted by 18% , second layer spacing expanded by 4% from bulk value of 1.44 Å. Third layer buckled by ± 0.10 Å or $\pm 7\%$, with atoms under missing row moving up, alternate rows down.	MEIS/3/
Au (110) (fcc) (2x1)	Missing-row reconstruction studied with top layer spacing contracted by 0.15 ± 0.10 Å (-11%) from bulk value of 1.44 Å.	LEIS/4/

(continued)

TABLE V (continued)

Substrate and Unit Cell	Structure	Method
α -CuAl (111) (fcc) $(\sqrt{3}\times\sqrt{3})R30^\circ$	Al substituted in 1/3 of top layer Cu sites, second layer pure Cu, no buckling in top layer, layer spacing is 2.05 ± 0.05 Å, the same as bulk copper. Alloy composition 16% Al atoms in Cu.	LEED/5/
Ir (100) (fcc) (5x1)	The top layer of the surface reconstructs to form a compact hexagonal surface, with 6/5 the density of unreconstructed surface. The layer spacing expands by $14.6\pm 5.2\%$ from the bulk value of 1.92 Å. Some top-layer atoms are buckled outward by up to an additional 0.2 ± 0.02 Å so the hexagonal layer can fit the square layer below. This is 1/2 to 2/3 of the buckling required to have top layer atoms in hard-sphere contact with all substrate atoms.	LEED/6/
Ir (100) (fcc) (5x1)	The top layer of the surface reconstructs to form a compact hexagonal surface, with 6/5 the density of unreconstructed surface. The layer spacing expands by $7.3\pm 2.6\%$ from the bulk value of 1.92 Å. Some top-layer atoms are buckled outward by up to an additional 0.48 ± 0.02 Å so the hexagonal layer can fit the square layer below. This puts the top layer atoms in hard-sphere contact with all substrate atoms.	LEED/7/

(continued)

TABLE V (continued)

Substrate and Unit Cell	Structure	Method
Ir (110) (fcc) (2x1)	Missing-row reconstruction similar to gold (110). One top layer row is missing, the second layer lateral displacements are ~ 0.04 Å, and the second row is buckled by -0.23 Å. The first layer spacing is -12.4% , and the second and third -5.8% relative to the 1.36 Å bulk layer spacing.	LEED/8/
NiAl (110) (CsCl) (1x1)	Top layer spacing 1.92 Å, contracted 6% from bulk value of 2.04 Å. Al atoms buckled out by 0.22 Å.	LEED/9/
Ni ₃ Al (Cu ₃ Au) (100)	Top layer is 50-50 nickel and aluminum, second layer nickel, etc. Top layer spacing is 1.73 ± 0.03 Å with Al atoms buckled outward by 0.02 ± 0.03 Å, second layer spacing is the bulk value of 1.78 Å within ± 0.03 Å.	LEED/10/
Pd (110) (fcc) (2x1)	Missing-row model with third layer assumed bulk-like. Second layer found to be bulk-like, first layer spacing -0.1% relative to 1.37 Å bulk spacing. Saw-tooth model almost as good.	LEED/11/
Pt (100) (fcc)	Top layer reconstruction, quasi-hexagonal surface given by $\begin{pmatrix} 1 & 4 & 1 \\ -1 & 5 & 0 \end{pmatrix}$, also called "1x5" or "4x20" reconstruction. Degree of top-layer buckling and top-layer registry proposed.	LEED/6/

(continued)

TABLE V (continued)

Substrate and Unit Cell	Structure	Method
Pt (110) (fcc) (2x1)	Missing-row model with the top layer expanded by 23% to 1.1 Å from bulk value of 1.387 Å. Lateral shift of second layer rows of 0.05 Å.	LEED/12/
Pt (110) (fcc) (2x1)	Missing-row model is better than buckled-row, paired-row or saw-tooth models. Terminated-bulk positions assumed for remaining atoms.	LEIS/13/
Pt _z Ni _{1-z} (110) (fcc)	LEED study of random substitutional alloy shows Pt enhancement in 1 st and 3 rd layers, along with a Pt depletion in the 2 nd layer.	LEED/14/
W (100) (bcc) (2x1)	Below room temperature the "zig-zag" reconstruction occurs on the W(100) surface. Alternate atoms move along the (011) and (0 $\bar{1}\bar{1}$) directions by $\pm 0.22 \pm 0.07$ Å, while the top layer spacing contracts by 0.05 ± 0.05 Å from the bulk value of 1.58 Å. There are two domains, since atoms may also move along the (0 $\bar{1}\bar{1}$) and (01 $\bar{1}$) directions.	LEED/15/
W (100) (bcc) ($\sqrt{2} \times \sqrt{2}$)R45°	Below room temperature the "zig-zag" reconstruction occurs on the W(100) surface. Alternate atoms move along the (011) and (0 $\bar{1}\bar{1}$) directions by ± 0.16 Å, while the top layer spacing contracts by 0.09 Å (6%) from the bulk value of 1.58 Å.	LEED/16/

REFERENCES

1. Robinson, I. K., Kuk, Y., and Feldman, L. C. (1984) *Physical Review* **B29**, 4762.
2. Moritz, W. and Wolf, D. (1985) *Surface Science* **163**, L655.
3. Copel, M. and Gustafsson, T. (1986) *Physical Review Letters* **57**, 723.
4. Möller, J., Niehaus, H., and Heiland, W. (1986) *Surface Science* **166**, L111.
5. Baird, R. J., Ogletree, D. F., Van Hove, M. A., and Somorjai, G. A. (1986) *Surface Science* **165**, 345.
6. Van Hove, M. A., Koestner, R. J., Stair, P. C., Bibérian, J. P., Kesmodel, L. L., Bartoš, I., and Somorjai, G. A. (1981) *Surface Science* **103**, 218.
7. Lang, E., Müller, K., Heinz, K., Van Hove, M. A., Koestner, R. J., and Somorjai, G. A. (1983) *Surface Science* **127**, 347.
8. Chan, C.-M. and Van Hove, M. A. (to be published) *Surface Science*
9. Davis, H. L. and Noonan, J. R. (1985) *Physical Review Letters* **54**, 566.
10. Sondericker, D., Jona, F., and Marcus, P. M. (1986) *Physical Review* **B 33**, 900.
11. Barnes, C. J., Ding, M. Q., Lindroos, M., Diehl, R. D., and King, D. A. (1985) *Surface Science* **162**, 59.
12. Adams, D. L., Nielsen, H. B., Van Hove, M. A., and Ignatiev, A. (1981) *Surface Science* **104**, 47.
13. Niehaus, H. and Comsa, G. (1984) *Surface Science* **140**, 18.
14. Gauthier, Y., Baudoing, R., Joly, Y., Rundgren, J., Bertolini, J. C., and Massardier, J. (1985) *Surface Science* **162**, 348.
15. Barker, R. A., Estrup, P. J., Jona, F., and Marcus, P. M. (1978) *Solid State Communications* **25**, 375.
16. Walker, J. A., Debe, M. K., and King, D. A. (1981) *Surface Science* **104**, 405.

TABLE VI. Chalcogen Chemisorption on Metals

(Where relaxation of the metal layer spacing has been investigated this is listed in the table after the adsorbate information.)

Substrate Face	Overlayer Unit Cell	Adsorption Site	Adsorbate Spacing	Bond Length	Method
OXYGEN					
Ag (110)	(2x1)	long bridge	0.20	2.05	SEXAFS/1/
Al (111)	(1x1)	3-fold fcc	0.70±0.12	1.79±0.05	LEED/2/
Al (111)	(1x1)	3-fold fcc	0.60±0.10	1.75±0.03	NEXAFS/3/
Al (111)	(1x1)	sub-surface tetrahedral	0.60±0.10	1.75±0.03	NEXAFS/3/
Al (111)	(1x1)	3-fold fcc	0.70	1.79	LEED/4/
Al (111)	undetermined	3-fold fcc	0.98±0.10	1.92±0.05	EXAFS/5/
Co (100)	c(2x2)	4-fold	0.80	1.94	LEED/6/
Cu (100)	c(2x2)	4-fold	1.40	2.28	LEED/7/
Cu (100)	c(2x2)	4-fold	0.70±0.01	1.94±0.01	SEXAFS/8/
Cu (100)	c(2x2)	4-fold	0.80	1.97	NPD/9/
Cu (110)	(2x1)				ALICISS/10/
		confirm surface missing-row model			
Cu (100)	c(2x2)			1.97	ALICISS/11/
		Bulk layer spacing 1.28 Å. First layer spacing expanded 25±1.0%, second and third layers contracted by 10±5.			
Cu (110)	disordered	long bridge	0.35		SEXAFS/12/
Cu (110)	(2x1)	long bridge			HEIS/13/
		top layer buckled, [001] rows alternate +0.27±0.05 Å and -0.02±0.03 Å second layer spacing expanded by 0.06±0.03 Å			
Cu (410)	(1x1)	quasi 4-fold	0.4±0.2	1.85±0.04	ARXPD/14/
		at step edge			

(continued)

TABLE VI (continued)

Substrate Face	Overlayer Unit Cell	Adsorption Site	Adsorbate Spacing	Bond Length	Method
Cu (410)	(1x1)	quasi 4-fold at step edge and 4-fold	0.4 ± 0.2	1.85 ± 0.04	ARXPD/14/
Fe (100)	(1x1)	4-fold top layer	0.48 ± 0.10 1.54 ± 0.10	2.08 ± 0.02 +7.7%	LEED/15/
Ir (110)	c(2x2)	short bridge top layer	1.37 ± 0.05 1.33 ± 0.07	1.93 ± 0.04 -2.2%	LEED/16/
Ir (111)	(2x2) or (2x1)	3-fold fcc	1.30 ± 0.05	2.04 ± 0.03	LEED/17/
Ni (100)	(2x2)	4-fold	0.86 ± 0.07	1.96 ± 0.03	EXAFS/18/
Ni (100)	c(2x2)	4-fold	0.86 ± 0.07	1.96 ± 0.03	EXAFS/18/
Ni (100)	(2x2)	4-fold	0.90 ± 0.10	1.98 ± 0.05	LEED/19/
Ni (100)	c(2x2)	4-fold	0.92 ± 0.05	1.99 ± 0.02	LEED/20/
Ni (100)	c(2x2)	4-fold	0.85 ± 0.05	1.96 ± 0.02	EXAFS/21/
Ni (100)	c(2x2)	4-fold	0.90 ± 0.04	1.98 ± 0.02	NPD/22/
Ni (100)	c(2x2)	4-fold	0.85 ± 0.04	1.96 ± 0.02	NPD/23/
Ni (100)	c(2x2)	4-fold top layer	0.86 ± 0.10 1.85 ± 0.10	1.96 ± 0.04 +5.1%	HEIS/24/
Ni (100)	c(2x2)	4-fold	0.90 ± 0.10	1.98 ± 0.05	XANES/25/
Ni (100)	c(2x2)	4-fold	0.90	1.98	HREELS/26,27/
Ni (100)	c(2x2)	4-fold	0.922		HREELS/28/
Ni (110)	(2x1)	missing row, long bridge	0.25		ALICISS/29/
Ni (111)	$(\sqrt{3}\times\sqrt{3})R30^\circ$	3-fold hcp	1.20	1.87	HEIS/30/
Ta (100)	(3x1)	sub-surface tetrahedral top layer	-0.43 1.55 ± 0.05	1.95 -6.1%	LEED/31/
W (100)	disordered	4-fold	0.55 ± 0.10	2.30 ± 0.02	LEED/32/

(continued)

TABLE VI (continued)

Substrate Face	Overlayer Unit Cell	Adsorption Site	Adsorbate Spacing	Bond Length	Method
W (110)	(2x1)	3-fold	1.25±0.01	2.09±0.01	LEED/33/
Zr (0001)	(2x2)	sub-surface octahedral	1.37	2.31	LEED/34/
SULFUR					
Co (100)	c(2x2)	4-fold	1.30	2.20	LEED/35/
Cu (100)	(2x2)	4-fold	1.39	2.28	ARXPS/36/
Fe (100)	c(2x2)	4-fold	1.09±0.05	2.30±0.02	LEED/37/
Fe (110)	(2x2)	4-fold	1.43	2.02	LEED/38/
reconstructed					
Ir (111)	($\sqrt{3}\times\sqrt{3}$)R30°	3-fold fcc	1.65±0.07	2.28±0.05	LEED/39/
Ni (100)	(2x2)	4-fold	1.30±0.10	2.19±0.06	LEED/19/
Ni (100)	c(2x2)	4-fold	1.28±0.05	2.18±0.03	LEED/20/
Ni (100)	c(2x2)	4-fold	1.30±0.05	2.19±0.03	LEED/40/
Ni (100)	c(2x2)	4-fold	1.30±0.04	2.19±0.02	NPD/22/
Ni (100)	c(2x2)	4-fold	1.39±0.04	2.24±0.02	SEXAFS/41/
Ni (100)	c(2x2)	4-fold	1.37±0.05	2.23±0.03	ARPEFS/42/
Ni (100)	c(2x2)	4-fold	1.35±0.10	2.22±0.06	ARXPS/43/
Ni (100)	c(2x2)	4-fold	1.35	2.22	ARXPS/36/
Ni (100)	disordered	4-fold	1.36±0.03	2.22±0.02	SEXAFS/44/
Ni (110)	c(2x2)	4-fold	0.9	2.34	ARXPS/45/
Ni (110)	c(2x2)	4-fold	0.84±0.03	2.31±0.01	LEED/46/
		top layer	1.372±0.02	+9.6%	
		next layer	1.201±0.02	-4.0%	
Ni (110)	c(2x2)	4-fold	0.87±0.03	2.32±0.01	MEIS/47/
		top layer	1.31±0.04	+4.8%	

(continued)

TABLE VI (continued)

Substrate Face	Overlayer Unit Cell	Adsorption Site	Adsorbate Spacing	Bond Length	Method
Mo (100)	c(2x2)	4-fold top layer	1.04 1.42	-10%	LEED/48/
Pd (100)	c(2x2)	4-fold	1.30±0.05	2.33±0.03	LEED/49/
Pd (111)	($\sqrt{3}\times\sqrt{3}$)R30°	3-fold fcc	1.53±0.05	2.20±0.03	LEED/50/
Pt (111)	($\sqrt{3}\times\sqrt{3}$)R30°	3-fold fcc	1.62±0.05	2.28±0.04	LEED/51/
Rh (100)	(2x2)	4-fold	1.29	2.30	LEED/52/
Rh (110)	c(2x2)	4-fold	0.77	2.45	LEED/53/
Rh (111)	($\sqrt{3}\times\sqrt{3}$)R30°	3-fold fcc	1.53	2.18	LEED/54/
SELENIUM					
Ag (100)	c(2x2)	4-fold	1.91±0.04	2.80±0.03	LEED/55/
Ni (100)	(2x2)	4-fold	1.55±0.10	2.35±0.07	LEED/19/
Ni (100)	c(2x2)	4-fold	1.45±0.10	2.28±0.06	NPD/56/
Ni (100)	c(2x2)	4-fold	1.55	2.35	NPD/57/
Ni (110)	c(2x2)	4-fold	1.10±0.04	2.42±0.02	NPD/58/
Ni (111)	(2x2)	3-fold fcc	1.80±0.04	2.30±0.03	NPD/58/
TELLURIUM					
Cu (100)	(2x2)	4-fold	1.70±0.15	2.48±0.10	LEED/59/
Cu (100)	(2x2)	4-fold	1.90±0.04	2.62±0.03	SEXAFS/60/
Ni (100)	(2x2)	4-fold	1.80±0.10	2.52±0.07	LEED/19/
Ni (100)	c(2x2)	4-fold	1.90±0.10	2.59±0.07	LEED/61/
Ni (100)	c(2x2)	4-fold	1.9		XPD/62/
Ni (100)	c(2x2)	4-fold	1.9		SPLEED/63/

REFERENCES

1. Puschmann, A. and Haase, J. (1984) *Surface Science* **144**, 559.
2. Martinez, V., Soria, F., Munoz, M. C., and Sacedon, J. L. (1983) *Surface Science* **128**, 424.
3. Norman, D., Brennan, S., Jaeger, R., and Stöhr, J. (1981) *Surface Science* **105**, L297.
4. Neve, J., Rundgren, J., and Westrin, P. (1982) *Journal of Physics C* **15**, 4391.
5. Bachrach, R. Z., Hansson, G. V., and Bauer, R. S. (1981) *Surface Science* **109**, L560.
6. Maglietta, M., Zanazzi, E., Bardi, U., and Jona, F. (1978) *Surface Science* **77**, 101.
7. Onuferko, J. and Woodruff, D. P. (1980) *Surface Science* **95**, 555.
8. Döbler, U., Baberschke, K., Stöhr, J., and Outka, D. A. (1985) *Physical Review B* **31**, 2532.
9. Tobin, J. G., Klebanoff, L. E., Rosenblatt, D. H., Davis, R. F., Umbach, E., Baca, A. G., Shirley, D. A., Huang, Y., Kang, W. M., and Tong, S. Y. (1982) *Physical Review B* **26**, 7076.
10. Niehaus, H. and Comsa, G. (1984) *Surface Science* **140**, 18.
11. Yarmoff, J. A. and Williams, R. S. (1985) *Journal of Vacuum Science and Technology A* **4**, 1274.
12. Döbler, U., Baberschke, K., Haase, J., and Puschmann, A. (1985) *Surface Science* **152/153**, 569.
13. (1983) *Surface Science* **128**, 281.
14. Thompson, K. A. and Fadley, C. S. (1984) *Surface Science* **146**, 281.
15. Legg, K. O., Jona, F., Jepsen, D. W., and Marcus, P. M. (1977) *Physical Review B* **16**, 5271.
16. Chan, C. M., Luke, K. L., Van Hove, M. A., Weinberg, W. H., and Withrow, S. P. (1978) *Surface Science* **78**, 386.
17. Chan, C.-M. and Weinberg, W. H. (1979) *Journal of Chemical Physics* **71**, 2788.

18. Stöhr, J., Jaeger, R., and Kendelewicz, T. (1982) *Physical Review Letters* **49**, 142.
19. Van Hove, M. A. and Tong, S. Y. (1975) *Journal of Vacuum Science and Technology* **12**, 230.
20. Marcus, P. C., Demuth, J. E., and Jepsen, D. W. (1975) *Surface Science* **53**, 501.
21. de Crescenzi, M., Antonangeli, F., Bellini, C., and Rosei, R. (1983) *Physical Review Letters* **50**, 1949.
22. Rosenblatt, D. H., Tobin, J. G., Mason, M. G., Davis, R. F., Kevan, S. D., Shirley, D. A., Li, C. H., and Tong, S. Y. (1981) *Physical Review B* **23**, 3828.
23. Tong, S. Y., Kang, W. M., Rosenblatt, D. H., Tobin, J. G., and Shirley, D. A. (1983) *Physical Review B* **27**, 4632.
24. Frenken, J. W. M., van der Veen, J. F., and Allan, G. (1983) *Physical Review Letters* **51**, 1876.
25. Norman, D., Stöhr, J., Jaeger, R., Durham, P. J., and Pendry, J. B. (1983) *Physical Review Letters* **51**, 2052.
26. Rahman, T. S., Black, J. E., and Mills, D. L. (1981) *Physical Review Letters* **46**, 1469.
27. Rahman, T. S., Mills, D. L., Black, J. E., Szeftel, J. M., Lehwald, S., and Ibach, H. (1984) *Physical Review B* **30**, 589.
28. Strong, R. L. and Erskine, J. L. (1985) *Physical Review Letters* **54**, 346.
29. Niehaus, H. and Comsa, G. (1985) *Surface Science* **151**, L171.
30. Narusawa, T. and Gibson, W. M. (1981) *Surface Science* **114**, 331.
31. Titov, A. V. and Jagodzinski, H. (1985) *Surface Science* **152/153**, 409.
32. Heinz, K., Saldin, D. K., and Pendry, J. B. (1985) *Physical Review Letters* **55**, 2312.
33. Van Hove, M. A. and Tong, S. Y. (1975) *Physical Review Letters* **35**, 1092.
34. Hui, K. C., Milne, R. H., Mitchell, K. A. R., Moore, W. T., and Zhou, M. Y. (1985) *Solid State Communications* **56**, 83.
35. Maglietta, M. (1982) *Solid State Communications* **43**, 395.
36. Bullock, E. L., Fadley, C. S., and Orders, P. J. (1983) *Physical Review B* **28**, 4867.

37. Legg, K. O., Jona, F., Jepsen, D. W., and Marcus, P. M. (1977) *Surface Science* **66**, 25.
38. Shih, F. E., Jona, F., Jepsen, D. W., and Marcus, P. M. (1981) *Physical Review Letters* **46**, 731.
39. Chan, C.-M. and Weinberg, W. H. (1979) *Journal of Chemical Physics* **71**, 3988.
40. Gauthier, Y., Aberdam, D., and Baudoing, R. (1978) *Surface Science* **78**, 339.
41. Stöhr, J., Jaeger, R., and Brennan, S. (1982) *Surface Science* **117**, 503.
42. Barton, J. J., Bahr, C. C., Hussain, Z., Robey, S. W., Klebanoff, L. E., and Shirley, D. A. (1984) *Journal of Vacuum Science and Technology A* **2**, 847.
43. Orders, P. J., Sinkovic, B., Fadley, C. S., Trehan, R., Hussain, Z., and Lecante, J. (1984) *Physical Review B* **30**, 1838.
44. Stöhr, J., Kollin, E. B., Fischer, D. A., Hastings, J. B., Zaera, F., and Sette, F. (1985) *Physical Review Letters* **55**, 1468.
45. Baudoing, R., Blanc, E., Gaubert, C., Gauthier, Y., and Gnuchev, N. (1983) *Surface Science* **128**, 22.
46. Gauthier, Y., Baudoing, R., Joly, Y., Rundgren, J., Bertolini, J. C., and Massardier, J. (1985) *Surface Science* **162**, 348.
47. van der Veen, J. F., Tromp, R. M., Smeenk, R. G., and Saris, F. W. (1979) *Surface Science* **82**, 468.
48. Clarke, L. J. (1981) *Surface Science* **102**, 331.
49. Berndt, W., Hora, R., and Scheffler, M. (1982) *Surface Science* **117**, 188.
50. Maca, F., Scheffler, M., and Berndt, W. (1985) *Surface Science* **160**, 467.
51. Hayek, K., Glassl, H., Gutmann, A., Leonhard, H., Prutton, M., Tear, S. P., and Welton-Cook, M. R. (1985) *Surface Science* **152**, 419.
52. Hengrasmee, S., Watson, P. R., Frost, D. C., and Mitchell, K. A. R. (1979) *Surface Science* **87**, L249.
53. Hengrasmee, S., Watson, P. R., Frost, D. C., and Mitchell, K. A. R. (1980) *Surface Science* **92**, 71.
54. Wong, P. C., Zhou, M. Y., Hui, K. C., and Mitchell, K. A. R. (1985) *Surface Science* **163**, 172.
55. Ignatiev, A., Jona, F., Jepsen, D. W., and Marcus, P. M. (1973) *Surface Science* **40**, 439.

56. Demuth, J. E., Jepsen, D. W., and Marcus, P. M. (1973) *Physical Review Letters* **31**, 540.
57. Rosenblatt, D. H., Kevan, S. D., Tobin, J. G., Davis, R. F., Mason, M. G., Shirley, D. A., Tang, J. C., and Tong, S. Y. (1982) *Physical Review B* **26**, 3181.
58. Rosenblatt, D. H., Kevan, S. D., Tobin, J. G., Davis, R. F., Mason, M. G., Denley, D. R., Shirley, D. A., Huang, Y., and Tong, S. Y. (1982) *Physical Review B* **26**, 1812.
59. Salwén, A. and Rundgren, J. (1975) *Surface Science* **53**, 523.
60. Comin, F., Citrin, P. H., Eisenberger, P., and Rowe, J. E. (1982) *Physical Review B* **26**, 7060.
61. Demuth, J. E., Jepsen, D. W., and Marcus, P. M. (1973) *Journal of Physics C* **6**, L307.
62. Smith, N. V., Farrell, H. H., Traum, M. M., Woodruff, D. P., Norman, D., Woolfson, M. S., and Holland, B. W. (1980) *Physical Review B* **21**, 3119.
63. Lang, J. K., Jamison, K. D., Dunning, F. B., Walters, G. K., Passier, M. A., Ignatiev, A., Tamura, E., and Feder, R. (1982) *Surface Science* **123**, 247.

TABLE VII. Other Atomic Adsorbates on Metal Surfaces

(Where relaxation of the metal layer spacing has been investigated this is listed in the table after the adsorbate information.)

Adsorption system	Overlayer Unit Cell	Adsorption Site	Adsorbate Spacing	Method
Ag (100)-Cl	c(2x2)	4-fold	1.62	LEED/1/
Ag (111)-Au	(1x1)	3-fold fcc	2.35±0.10	HEIS/2/
Ag (111)-I	($\sqrt{3}\times\sqrt{3}$)R30°	3-fold fcc and hcp	2.29±0.06	LEED/3/
	top layer	0.0%	2.36±0.06	
Ag (111)-I	($\sqrt{3}\times\sqrt{3}$)R30°	3-fold	2.34±0.02	SEXAFS/4/
Ag (111)-Xe	hexagonal (1x1)	incommensurate	3.55±0.10	LEED/5/
randomly oriented hexagonal Xe lattice, Xe-Xe spacing 1.51 Å				
Al (100)-Na	c(2x2)	4-fold	2.08±0.12	LEED/6/
Al (100)-Na	c(2x2)	4-fold	2.05±0.10	LEED/7/
Au (111)-Ag	(1x1)	3-fold fcc	2.35±0.10	HEIS/2/
Cu (100)-Cl	c(2x2)	4-fold	1.60±0.03	LEED/8/
	top layer	+3%	1.85±0.03	
Cu (111)-Cs	(2x2)	top	3.01±0.05	LEED/9/
Cu (100)-I	(2x2)	4-fold	1.98±0.02	SEXAFS/10/
Cu (111)-I	($\sqrt{3}\times\sqrt{3}$)R30°	3-fold hcp	2.21±0.02	SEXAFS/10/
Cu (111)-Ni	(1x1)	3-fold fcc	2.04±0.02	LEED/11/
Cu (100)-Pb	c(2x2)	4-fold	2.05±0.05	LEED/12/
Cu (100)-3Pb	c(5 $\sqrt{2}\times\sqrt{2}$)R45°	4-fold	2.4±0.05	LEED/12/
overlayer relaxed with anti-phase domain walls and off-center atoms				
Fe (100)-C+O	c(2x2)	4-fold	0.48	LEED/13/
CO decomposes on Fe(100), C and O occupy random sites in (2x2) lattice				
Fe (110)-H	(2x1)	quasi 3-fold	0.90±0.10	LEED/14/
Fe (110)-2H	(3x1)	quasi 3-fold	1.00±0.10	LEED/14/
Fe (100)-N	c(2x2)	4-fold	0.25±0.05	LEED/15/
	top layer	+8%	1.54±0.05	

(continued)

TABLE VII (continued)

Adsorption system	Overlayer Unit Cell	Adsorption Site	Adsorbate Spacing	Method
Ir (110)-S	(2x2)			LEED/16/
Sulfur is adsorbed in 3-fold sites on the (111) facets left by the clean-surface missing-row reconstruction. The first Ir-Ir spacing is contracted by 3.3%, the second expanded by 1.3%. Ir-S is 2.39 Å for first-layer Ir atoms and 2.26 Å for second-layer Ir atoms.				
Mo (100)-N	c(2x2)	4-fold	1.02	LEED/17/
Mo (100)-Si	(1x1)	4-fold	1.16±0.10	LEED/18/
Ni (100)-Br	c(2x2)	4-fold	1.51±0.03	EXAFS/19/
Ni (100)-C+O	c(2x2)	4-fold	0.93±0.10	LEED/20/
CO decomposes on Ni(100), C and O occupy random sites in (2x2) lattice				
Ni (100)-2C	(2x2)	4-fold	0.10±0.10	LEED/21/
	top layer	+22%	1.96±0.05	
	reconstructed	lateral motions -	0.25±0.35 Å	
Ni (100)-Cu	(1x1)	4-fold	1.80±0.03	LEED/22/
Ni (100)-Na	c(2x2)	4-fold	2.2±0.10	LEED/23/
Ni (100)-Na	c(2x2)	4-fold	2.23±0.10	LEED/24/
Ni (100)-Na	c(2x2)	4-fold	1.9	XPD/25/
Ni (110)-C				SEELFS/26/
Graphitic layer on Ni(110), 3 carbon sites: A - off top, Ni-C = 1.95 Å				
B - 4-fold, Ni-C = 2.49 Å, C - off bridge, Ni-C = 1.95, Ca-Cb = 1.49 Å				
Ni (111)-2C	(1x1)	3-fold hcp and fcc	2.80±0.08	SEELFS/27/
Ni (111)-2H	(2x2)	3-fold hcp and fcc	1.15±0.10	LEED/28/
Pd (111)-Au	(1x1)	3-fold fcc	2.25±0.19	HEIS/29/
Ti (0001)-Cd	(1x1)	3-fold fcc	2.57	LEED/30/
Ti (0001)-Cd	(1x1)	3-fold fcc	2.63	LEED/31/
Two Cd layers, Cd-Cd distance 2.81 Å, Cd-Ti 2.63 Å				

(continued)

TABLE VII (continued)

Adsorption system	Overlayer Unit Cell	Adsorption Site	Adsorbate Spacing	Method
Ti (0001)-N	(1x1)	sub-surface tetrahedral	-1.22±0.05	LEED/32/
W (100)-H	c(2x2)	4-fold	1.32	LEED/33/
W (100)-2H	(1x1)	short bridge		HREELS/34/
W (100)-2H	(1x1)	short bridge	1.74	HREELS/35/
W (100)-2H	(1x1)	2-fold	1.17±0.04	LEED/36/
	top layer	-1.3%	1.56±0.02	
W (100)-N	c(2x2)	4-fold	0.49±0.06	LEED/37/
	top layer	+1.3%	1.60±0.06	

REFERENCES

1. Jona, F. and Marcus, P. M. (1983) *Physical Review Letters* **50**, 1823.
2. Culbertson, R. J., Feldman, L. C., Silverman, P. J., and Boehm, H. (1981) *Physical Review Letters* **47**, 657.
3. Maglietta, M., Zanazzi, E., Bardi, U., Sondericker, D., Jona, F., and Marcus, P. M. (1982) *Surface Science* **123**, 141.
4. Citrin, P. H., Eisenberger, P., and Hewitt, R. C. (1979) *Surface Science* **89**, 28.
5. Stoner, N., Van Hove, M. A., Tong, S. Y., and Webb, M. B. (1978) *Physical Review Letters* **40**, 243.
6. Van Hove, M. A., Tong, S. Y., and Stoner, N. (1976) *Surface Science* **54**, 259.
7. Hutchins, B. A., Rhodin, T. N., and Demuth, J. E. (1976) *Surface Science* **54**, 419.

8. Jona, F., Westphal, D., Goldman, A., and Marcus, P. M. (1983) *Journal of Physics C* **16**, 3001.
9. Lindgren, S. A., Walldén, L., Rundgren, J., Westrin, P., and Neve, J. (1983) *Physical Review B* **28**, 6707.
10. Citrin, P. H., Eisenberger, P., and Hewitt, R. C. (1980) *Physical Review Letters* **45**, 1948.
11. Tear, S. P. and Roell, K. (1982) *Journal of Physics C* **15**, 5521.
12. Hoesler, W. and Moritz, W. (1982) *Surface Science* **117**, 196.
13. Legg, K. O., Jona, F., Jepsen, D. W., and Marcus, P. M. (1977) *Physical Review B* **16**, 5271.
14. Moritz, W., Imbihl, R., Behm, R. J., Ertl, G., and Matsushima, T. (1985) *Journal of Chemical Physics* **83**, 1959.
15. Imbihl, R., Behm, R. J., Ertl, G., and Moritz, W. (1982) *Surface Science* **123**, 129.
16. Chan, C.-M. and Van Hove, M. A. (1987) *Surface Science* **183**, 303.
17. Ignatiev, A., Jona, F., Jepsen, D. W., and Marcus, P. M. (1975) *Surface Science* **49**, 189.
18. Ignatiev, A., Jona, F., Jepsen, D. W., and Marcus, P. M. (1975) *Physical Review B* **11**, 4780.
19. Lairson, B., Rhodin, T. N., and Ho, W. (1985) *Solid State Communications* **55**, 925.
20. Passler, M. A., Lin, T. H., and Ignatiev, A. (1981) *Journal of Vacuum Science and Technology* **18**, 481.
21. Onuferko, J. H., Woodruff, D. P., and Holland, B. W. (1979) *Surface Science* **87**, 357.
22. Abu-Joudeh, M., Vaishnav, P. P., and Montano, P. A. (1984) *Journal of Physics C* **17**, 6899.
23. Andersson, S. and Pendry, J. B. (1975) *Solid State Communications* **16**, 563.
24. Demuth, J. E., Jepsen, D. W., and Marcus, P. M. (1975) *Journal of Physics C* **8**, L25.
25. Smith, N. V., Farrell, H. H., Traum, M. M., Woodruff, D. P., Norman, D., Woolfson, M. S., and Holland, B. W. (1980) *Physical Review B* **21**, 3119.
26. Papagno, L. and Caputi, L. S. (1984) *Physical Review B* **29**, 1483.

27. Rosei, R., de Crescenzi, M., Sette, F., Quaresima, C., Savoia, A., and Perfetti, P. (1983) *Physical Review B* **28**, 1161.
28. Christmann, K., Behm, R. J., Ertl, G., Van Hove, M. A., and Weinberg, W. H. (1979) *Journal of Chemical Physics* **70**, 4168.
29. Kuk, Y., Feldman, L. C., and Silverman, P. J. (1983) *Physical Review Letters* **50**, 511.
30. Shih, H. D., Jona, F., Jepsen, D. W., and Marcus, P. M. (1977) *Physical Review B* **15**, 5550.
31. Shih, H. D., Jona, F., Jepsen, D. W., and Marcus, P. M. (1977) *Physical Review B* **15**, 5561.
32. Shih, H. D., Jona, F., Jepsen, D. W., and Marcus, P. M. (1976) *Surface Science* **60**, 445.
33. Willis, R. F. (1979) *Surface Science* **89**, 457.
34. Ho, W., Willis, R. F., and Plummer, E. W. (1980) *Physical Review B* **21**, 4202.
35. Woods, J. P. and Erskine, J. L. (1985) *Physical Review Letters* **55**, 2595.
36. Passler, M. A., Lee, B. W., and Ignatiev, A. (1985) *Surface Science* **150**, 263.
37. Griffiths, K., King, D. A., Aers, G. C., and Pendry, J. B. (1982) *Journal of Physics C* **15**, 4921.

TABLE VIII. Semiconductor Surface Structures

Substrate	Unit Cell	Structure	Method
AlP (110) (zincblende)	(1x1)	Surface reconstructed with 25° bond angle rotation preserving bond lengths. Top layer buckled with P +0.06 Å, Al -0.57 Å and layer spacing contracted to 1.33 Å (bulk 1.927 Å). Second layer buckled P -0.035 Å, Al +0.035 Å, layer expanded to 1.92 Å. First layer in-plane displacements of ~ 0.25 Å to preserve bond lengths.	LEED/1/
CdTe (110) (zincblende)	(1x1)	Te is buckled out from the top layer by 0.82±0.05 Å. Top layer Cd atoms contract by ~ 0.5 Å, and there are lateral motions of ~ 0.4 Å to conserve bond lengths.	LEED/2/
GaAs (110) (zincblende)	(1x1)	As is buckled out from the top layer by 0.70 Å. Top layer Ga atoms contract by ~ 0.5 Å, and there are lateral motions of ~ 0.4 Å to conserve bond lengths. The lateral motions may be reduced by ~ 3/4 to give a better agreement with MEIS results without significantly worsening the LEED fit.	LEED/3/
GaAs (110) (zincblende)	(1x1)	As is buckled out from the top layer by 0.69 Å. Top layer Ga atoms contract by ~ 0.5 Å, and there are lateral motions of ~ 0.3 Å to conserve bond lengths.	LEED/4/

(continued)

TABLE VIII (continued)

Substrate	Unit Cell	Structure	Method.
GaAs (110) (zincblende)	(1x1)	As is buckled out from the top layer by 0.40 ± 0.30 Å. Top layer Ga atoms contract by $\sim 0.20 \pm 0.30$ Å, with no lateral motions.	HEIS/5/
GaAs (111) (zincblende) (Ga terminated)	(2x2)	One quarter of the top layer Ga atoms are missing, and the remaining atoms are almost co-planar with the first As layer, within 0.20 Å. Ga bonding is sp^2 rehybridized, instead of the normal sp^3 configuration. There are first bi-layer lateral motions of ~ 0.2 Å, and some buckling in the third layer to maintain optimum bond-lengths and angles.	LEED/6/
GaP (110) (zincblende)	(1x1)	Surface reconstructed with 27.5° bond angle rotation preserving bond lengths. Top layer buckled with Ga $+0.09$ Å, As -0.54 Å and layer spacing contracted to 1.39 Å. Second layer spacing expanded to 1.93 Å.	LEED/7/

(continued)

TABLE VIII (continued)

Substrate	Unit Cell	Structure	Method
GaP (111) (zincblende) (Ga terminated)	(2x2)	One quarter of the top layer Ga atoms are missing, and the remaining atoms are almost co-planar with the first P layer. Ga bonding is sp^2 rehybridized, instead of the normal sp^3 configuration. There are lateral motions up to $\sim 2 \text{ \AA}$, and some buckling in the third layer to maintain optimum bond-lengths and angles.	LEED/6/
GaSb (110) (zincblende)	(1x1)	Sb is buckled out from the top layer by $0.77 \pm 0.05 \text{ \AA}$. Top layer Ga atoms contract by $\sim 0.5 \text{ \AA}$, and there are lateral motions of $\sim 0.4 \text{ \AA}$ to conserve bond lengths.	LEED/8,9/
GaSb (110) (zincblende)	(1x1)	Consistent with LEED results (above) for layer displacements and lateral motions.	MEIS/10/
GaSb (110) (zincblende)	(1x1)	Bond-length conserving rotations of $28.5 \pm 2.6^\circ$ bring Sb atoms up, Ga atoms down.	MEIS/11/
Ge (100) (diamond)	(2x1)	The top layer buckles, with one Ge atom moving out by $0.62 \pm 0.04 \text{ \AA}$ and the other moving in by $0.66 \pm 0.04 \text{ \AA}$. There are lateral displacements of $\sim 0.9 \text{ \AA}$ in the first layer and $\sim 0.1 \text{ \AA}$ in the second layer.	XRD/12/

(continued)

TABLE VIII (continued)

Substrate	Unit Cell	Structure	Method
InAs (110) (zinblende)	(1x1)	The top layer has As buckled outward by $\sim 0.8 \text{ \AA}$ with lateral motions of $\sim 0.6 \text{ \AA}$ in the first three layers to conserve bond lengths.	LEED/13/
InAs (110) (zinblende)	(1x1)	Bond-length conserving rotations of $30.0 \pm 2.4^\circ$ bring As atoms up, In atoms down.	MEIS/11/
InSb (111) (zinblende)	(2x2)	One quarter of the top-layer In atoms are missing in the "vacancy buckling" model. Top layer is not buckled, in plane Sb atoms expand radially by $0.45 \pm 0.04 \text{ \AA}$ from their normal positions and In atoms contract radially by $0.23 \pm 0.05 a_g$ from their normal positions. No data on layer spacing changes.	X-Ray Diffraction/14/
InP (110) (zinblende)	(1x1)	Preliminary results show layer buckling with the P atom buckled out, and lateral and vertical shifts in the top layer $\sim 0.4 \text{ \AA}$. Second and deeper layer shifts were not investigated.	LEED/15/
InP (110) (zinblende)	(1x1)	Top layer buckling with the P atom buckled out by $0.69 \pm 0.10 \text{ \AA}$, and lateral and vertical shifts in the top layer $\sim 0.4 \text{ \AA}$. The second layer spacing is contracted by $0.41 \pm 0.10 \text{ \AA}$ with a slight buckling of $0.07 \pm 0.10 \text{ \AA}$. Only first layer lateral displacements were investigated.	LEED/16/

(continued)

TABLE VIII (continued)

Substrate	Unit Cell	Structure	Method
Si (100) (diamond)	(2x1)	Buckled dimer model is best fit to data. Surface atoms dimerize to take up dangling bonds, surface buckles for best bond angles. There are lateral and vertical ion-core motions for at least 4 layers into the bulk crystal. Authors conclude that (2x1), (2x2) and c(4x2) buckled dimer domains may exist on the surface.	MEIS/17/
Si (100) (diamond)	(2x1)	LEED analysis considering vertical and lateral displacements in the top three atomic layers supports a buckled dimer model.	LEED/18/
Si (111) (diamond)	(1x1) laser annealed	The first two layers are almost coplanar, instead of the normal 0.78 Å separation. The first layer spacing is 0.08 ± 0.02 , a contraction of 90%, and the second layer spacing is 2.95 ± 0.20 Å, a 25.5% expansion from 2.35 Å.	LEED/19/
Si (111) (diamond)	(2x1)	The top layer is buckled by 0.30 ± 0.05 Å, the second layer spacing is 0.70 ± 0.05 , a change of +2.9%, and the third layer spacing is contracted by 3.4% to 2.27 ± 0.02 from 2.35 Å. There are second-layer lateral shifts of ~ 0.12 Å. (More recent results favor the "π-bonded chain" model, see below.)	LEED/20/

(continued)

TABLE VIII (continued)

Substrate	Unit Cell	Structure	Method
Si (111) (diamond)	(2x1)	Analysis of LEED data supports a " π -bonded chain" model for the (2x1) reconstruction. Trial geometries based on strain-minimization calculations for the model, involving vertical motions four layers deep with lateral motions along the long side of the unit cell.	LEED/21/
Si (111) (diamond)	(2x1)	Best fit to " π -bonded chain" model. This model involves buckling in layers 2 to 6 of up to 0.27 Å and small lateral shifts in the first six layers.	MEIS/22/
GaP (110) (zincblende)	(1x1)	Surface reconstructed with 28.0° bond angle rotation preserving bond lengths. Top layer buckled with Zn +0.08 Å, S -0.51 Å and layer spacing contracted to 1.40 Å. Second layer spacing expanded to 1.91 Å.	LEED/7/
ZnSe (110) (zincblende)	(1x1)	Two different models were consistent with LEED data. First; Se is buckled outward by ~ 0.70 Å and the second layer spacing is contracted by ~ 0.60 Å, with lateral motions of ~ 0.7 Å. Second; Se buckled out by 0.10 Å and the second layer spacing contracted by 0.09 Å, with lateral motions of ~ 0.07 Å.	LEED/23/

(continued)

TABLE VIII (continued)

Substrate	Unit Cell	Structure	Method
ZnTe (110) (zincblende)	(1x1)	Te is buckled out from the top layer by 0.71 ± 0.05 Å. Top layer Zn atoms contract by ~ 0.5 Å, and there are lateral motions of ~ 0.4 Å to conserve bond lengths.	LEED/9/

REFERENCES

1. Duke, C. B., Paton, A., and Bonpace, C. R. (1983) *Physical Review* **B28**, 852.
2. Duke, C. B., Paton, A., Ford, W. K., Kahn, A., and Scott, G. (1982) *Journal of Vacuum Science and Technology* **20**, 778.
3. Duke, C. B. and Paton, A. (1984) *Journal of Vacuum Science and Technology B* **2**, 327.
4. Tong, S. Y., Mei, W. M., and G. Xu, (1984) *Journal of Vacuum Science and Technology B* **2**, 393.
5. Grossman, H. J. and Gibson, W.M. (1984) *Journal of Vacuum Science and Technology B* **2**, 343.
6. Xu, G., Hu, W. Y., Puga, M. W., Tong, S. Y., Yeh, J. L., Wang, S. R., and Lee, B. W. (1985) *Physical Review B* **32**, 8473.
7. Duke, C. B., Paton, A., and Kahn, A. (1984) *Journal of Vacuum Science and Technology* **A2**, 515.
8. Duke, C. B., Paton, A., and Kahn, A. (1983) *Physical Review B* **27**, 3436.
9. Duke, C. B., Paton, A., and Kahn, A. (1983) *Journal of Vacuum Science and Technology A* **1**, 672.

10. Smit, L., Tromp, R. M., and van der Veen, J. F. (1984) *Physical Review B* **29**, 4814.
11. Smit, L. and van der Veen, J. F. (1986) *Surface Science* **166**, 183.
12. Eisenberger, P. and Marra, W. C. (1981) *Physical Review Letters* **46**, 1081.
13. Duke, C. B., Paton, A., Kahn, A., and Bonapace, C. B. (1983) *Physical Review B* **27**, 6189.
14. (1985) *Physical Review Letters* **54**, 1275.
15. Tear, S. P., Welton-Cook, M. R., Prutton, M., and Walker, J. A. (1980) *Surface Science* **99**, 598.
16. Meyer, R. J., Duke, C. B., Paton, A., Tsang, J. C., Yeh, J. L., Kahn, A., and Mark, P. (1980) *Physical Review B* **22**, 6171.
17. Tromp, R. M., Smeenk, R. G., Saris, F. W., and Chadi, D. J. (1983) *Surface Science* **133**, 137.
18. Holland, B. W., Duke, C. D., and Paton, A. (1984) *Surface Science* **140**, L269.
19. Jones, G. J. R. and Holland, B. W. (1985) *Solid State Communications* **53**, 45.
20. Feder, R., Mönch, W., and Auer, P. P. (1979) *Journal of Physics C* **12**, L179.
21. Himpsel, F. J., Marcus, P. M., Tromp, R., Batra, I. P., Cook, M. R., Jona, F., and Liu, H. (1984) *Physical Review B* **30**, 2257.
22. Smit, L., Tromp, R. M., and van der Veen, J. F. (1985) *Surface Science* **163**, 315.
23. Duke, C. B., Paton, A., Kahn, A., and Tu, D. W. (1984) *Journal of Vacuum Science and Technology B* **2**, 366.

TABLE XI. Carbon Monoxide, Di-Nitrogen and Nitric Oxide Chemisorption on Metals

(In all the listed structures the CO or NO molecule is believed to adsorb perpendicular to the surface with the oxygen end away from the surface. For CO structures with multiple non-equivalent adsorption sites these are listed on consecutive lines. If the metal layer spacing has been investigated this is listed after the adsorbate information.)

Substrate Face	Overlayer Unit Cell	Adsorption Site	C-Metal \perp Spacing	C-O Bond Length	Method
Cu (100)	c(2x2)-CO	top	1.90±0.10	1.13±0.10	LEED/1/
Cu (100)	c(2x2)-CO	top	1.92±0.05		NEXAFS/2/
Ni (100)	c(2x2)-CO	top	1.72	1.15	LEED/3/
Ni (100)	c(2x2)-CO	top	1.80±0.10	1.15±0.05	ARXPS/4/
Ni (100)	c(2x2)-CO	top	1.80±0.10	1.15±0.05	LEED/5/
Ni (100)	c(2x2)-CO	top	1.70±0.10	1.13±0.10	LEED/6/
Ni (100)	c(2x2)-CO	top	1.71±0.10	1.15±0.10	LEED/7/
Ni (100)	c(2x2)-CO	top	1.80±0.04	1.13	NPD/8/
Ni (111)	($\sqrt{3}\times\sqrt{3}$)R30°-CO	bridge	1.27±0.05	1.13±0.05	NPD/8/
Ni (100)	disordered-CO	top			NEXAFS/9/ molecular axis \perp to surface $\pm 10^\circ$
Ni (100)	disordered-NO	top			NEXAFS/9/ molecular axis \perp to surface $\pm 10^\circ$
Ni (100)	disordered-N ₂	top			NEXAFS/9/ molecular axis \perp to surface $\pm 10^\circ$
Pd (100)	($2\sqrt{2}\times\sqrt{2}$)R45°-2CO	bridge	1.36±0.10	1.15±0.10	LEED/10/
		top layer	1.945±0.10	+0.4%	
Pd (111)	($\sqrt{3}\times\sqrt{3}$)R30°-2CO	3-fold fcc	1.29±0.05	1.15±0.05	LEED/11/
Pd (111)	(3x3)-2CO*	3-fold fcc	1.30±0.05	1.17±0.05	LEED/12/
Pt (111)	c(4x2)-2CO	top	1.85±0.05	1.15±0.10	LEED/13/
		bridge	1.55±0.05	1.15±0.10	

(continued)

TABLE XI (continued)

Substrate Face	Overlayer Unit Cell	Adsorption Site	C-Metal \perp Spacing	C-O Bond Length	Method
		top layer	2.26 ± 0.025	0.0%	
Pt (111)	$(2\sqrt{3} \times 4)$ rect-4CO*	bridge	1.45	1.15	LEED/14/
Rh (111)	(3×3) -2CO*	3-fold hcp	1.30	1.17	LEED/15/
Rh (111)	$c(2\sqrt{3} \times 4)$ rect-CO*	3-fold fcc	1.50 ± 0.05	1.21 ± 0.10	LEED/16/
Rh (111)	$c(4 \times 2)$ -CO*	3-fold hcp	1.30 ± 0.05	1.17 ± 0.05	LEED/17/
Rh (111)	$c(4 \times 2)$ -NO*	3-fold fcc	1.30 ± 0.05	1.17 ± 0.05	LEED/17/
Rh (111)	(2×2) -3CO	quasi-top	1.87 ± 0.10	1.15 ± 0.10	LEED/18/
		quasi-top	1.87 ± 0.10	1.15 ± 0.10	
		bridge	1.52 ± 0.10	1.15 ± 0.10	
Rh (111)	$(\sqrt{3} \times \sqrt{3})R30^\circ$ -CO	top	1.95 ± 0.10	1.07 ± 0.10	LEED/19/
		top layer	2.19 ± 0.10	0.0%	
Ru (0001)	$(\sqrt{3} \times \sqrt{3})R30^\circ$ -CO	top	2.00 ± 0.10	1.09 ± 0.10	LEED/20/

* These structures involve carbon monoxide co-adsorbed with other molecules. See table XII for more details.

REFERENCES

1. Andersson, S. and Pendry, J. B. (1980) *Journal of Physics C* **13**, 2547.
2. McConville, C. F., Woodruff, D. P., Prince, K. C., Paolucci, G., Chab, V., Surman, M., and Bradshaw, A. M. (1986) *Surface Science* **166**, 221.
3. Passler, M., Ignatiev, A., Jona, F., Jepsen, D. W., and Marcus, P. M. (1979) *Physical Review Letters* **43**, 360.
4. Petersson, L. G., Kono, S., Hall, N. F. T., Fadley, C. S., and Pendry, J. B. (1979) *Physical Review Letters* **42**, 1545.
5. Heinz, K., Lang, E., and Müller, K. (1979) *Surface Science* **87**, 595.

6. Tong, S. Y., Maldonado, A., Li, C. H., and Van Hove, M. A. (1980) *Surface Science* **94**, 73.
7. Andersson, S. and Pendry, J. B. (1980) *Journal of Physics C* **13**, 3547.
8. Kevan, S. D., Davis, R. F., Rosenblatt, D. H., Tobin, J. G., Mason, M. G., Shirley, D. A., Li, C. H., and Tong, S. Y. (1981) *Physical Review Letters* **46**, 1629.
9. Stöhr, J. and Jaeger, R. (1982) *Physical Review B* **26**, 4111.
10. Behm, R. J., Christmann, K., Ertl, G., and Van Hove, M. A. (1980) *Journal of Chemical Physics* **73**, 2984.
11. Ohtani, H., Van Hove, M. A., and Somorjai, G. A. (to be published)
12. Ohtani, H., Van Hove, M. A., and Somorjai, G. A. (to be published)
13. Ogletree, D. F., Van Hove, M. A., and Somorjai, G. A. (1986) *Surface Science* **173**, 351.
14. Ogletree, D. F., Van Hove, M. A., and Somorjai, G. A. (1987) *Surface Science* **187**, 1.
15. Van Hove, M. A., Lin, R. F., Blackman, G. A., and Somorjai, G. A. (to be published) *Acta Crystallographica*
16. Van Hove, M. A., Lin, R. F., and Somorjai, G. A. (1986) *Journal of the American Chemical Society* **108**, 2532.
17. Bent, B. E., Mate, C. M., Koestner, R. J., Blackman, G. S., Kao, C. T., Hove, M. A. Van, and Somorjai, G. A. (to be published)
18. Van Hove, M. A., Koestner, R. J., Frost, J. C., and Somorjai, G. A. (1983) *Surface Science* **129**, 482.
19. Koestner, R. J., Van Hove, M. A., and Somorjai, G. A. (1981) *Surface Science* **107**, 439.
20. Michalk, G., Moritz, W., Pfnür, H., and Menzel, D. (1983) *Surface Science* **129**, 92.

TABLE X. Insulator and other Compound Surface Structures

Substrate	Unit Cell	Structure	Method
C (111) (diamond)	(1x1)	Terminated bulk diamond, no relaxation in layer spacing.	LEED/1/
C (111)-H (diamond)	(1x1)	Hydrogen terminated diamond, surface layer spacing relaxed by -0.05 ± 0.05 Å.	MEIS/2/
C (111)-H (diamond)	(1x1)	Hydrogen in (1x1) arrangement. Determined to be in top site, assumed 1.09 Å H-C bond length.	Helium diffraction/3/
C (111) (diamond)	(2x2)	Evidence for "π-bonded chain reconstruction.	MEIS/2/
C (0001) (graphite)	(1x1)	Normal graphite layer stacking, first layer contracted 1.4% to 3.30 Å from bulk spacing of 3.35 Å.	LEED/4/
C (0001)-K (graphite)	intercalated	When K is adsorbed on C(0001) it is intercalated between layers, changing the carbon stacking sequence from ABAB... to AAAA... and increasing the layer spacing to 5.35 Å from 3.35 Å.	LEED/5/
C (0001)-Ar (graphite)	incommensurate	Ar forms an incommensurate hexagonal overlayer on graphite 3.2 ± 0.10 Å above the graphite surface.	LEED/6/

(continued)

TABLE X (continued)

Substrate	Unit Cell	Structure	Method
C (0001)-Kr (graphite)	$(\sqrt{3} \times \sqrt{3})R30^\circ$	Kr adsorbs in 6-fold hollow sites on the graphite basal plane 3.35 ± 0.01 Å above the graphite surface. No nearest neighbor sites are occupied. At higher coverages next-nearest neighbor sites are occupied.	LEED/7/
CaO (100) (rocksalt)	(1x1)	Top layer contracts by 1.2% to 2.38 Å from 2.41 Å. No top-layer buckling.	LEED/8/
CoO (111) (rocksalt)	(1x1)	Oxygen termination with fcc stacking, top layer contraction of 17% to 1.06 Å from bulk 1.27 Å.	LEED/9/
CoO (100) (rocksalt)	(1x1)	Terminated bulk structure, top layer spacing is 2.85 ± 0.08 Å.	LEED/10/
MgO (100) (rocksalt)	(1x1)	Top-layer oxygen buckled out by 0.04 ± 0.05 , and top layer contracted by 0.02 ± 0.07 Å. Bulk layer spacing 2.10 Å.	LEED/11/
MgO (100) (rocksalt)	(1x1)	Terminated bulk structure, no change from bulk layer spacing of 2.10 Å.	LEED/12/
MoS ₂ (0001) (layer compound)	(1x1)	Normal stacking, S-Mo-S termination, top layer contraction by 5% to 1.51 Å from bulk 1.59 Å. No second layer contraction.	LEED/13/
Na ₂ O (111) (fluorite)	(1x1)	Oxidation of epitaxial Na(110) on Ni(100) substrate. Determine fluorite lattice with Na-O-Na termination.	LEED/14/

(continued)

TABLE X (continued)

Substrate	Unit Cell	Structure	Method
NbSe ₂ (0001) (layer compound)	(1x1)	Normal layer stacking with Se-Nb-Se termination, no evidence for relaxation of first two layer spacings.	LEED/13/
NiI ₂ (0001)	(1x1)	Bulk NiI ₂ is a layer compound with hexagonal metal layers and octohedral coordination in a cubic unit cell. At the surface the bulk Ni-I bond length of 2.78 Å decreases by 0.036±0.010 Å and the I-I separation of 3.89 Å decreases by -0.48±0.010.	SEXAFS/15/
NiO (100) (rocksalt)	(1x1)	Top layer unbuckled, contracted 2% to 2.04 Å from bulk value of 2.08 Å.	LEED/16/
Sb ₂ Te ₂ Se (0001) (layer com- pound)	(1x1)	This is an elemental layer compound with Te-Sb-Se-Sb-Te stacking. The Te-Te interfaces are cleavage planes. At the surface the bulk Te-Sb layer spacing of 1.733 Å is contracted by ~ 3% to 1.683±0.05 Å.	ARUPS/17/
TiS ₂ (0001) (layer com- pound)	(1x1)	This is an elemental layer compound with Ti-S-Ti stacking. The Ti-Ti interfaces are cleavage planes. At the surface the bulk Ti-S layer spacing is contracted by ~ 5% and the first Van der Waal spacing (Ti-S-Ti Ti-S-Ti) is also contracted by 5%.	LEED/18/

(continued)

TABLE X (continued)

Substrate	Unit Cell	Structure	Method
TiSe ₂ (0001) (layer compound)	(1x1)	This is an elemental layer compound with Ti-Se-Ti stacking. The Ti-Ti interfaces are cleavage planes. At the surface the bulk Ti-Se layer spacing is expanded by ~ 5% and the first Van der Waal spacing (Ti-Se-Ti Ti-Se-Ti) is contracted by 5%.	LEED/18/
ZnO (0001) (wurtzite)	(1x1)	Zn termination, top layer spacing 0.60±0.10 Å, a 25% contraction from the bulk value of 0.80 Å.	LEED/19/
ZnO (10 $\bar{1}$ 0) (wurtzite)	(1x1)	Oxygen buckled outward by ~ 0.8 Å and Zn contracted by 1.2 Å in the first layer. Bulk layer spacing 1.88 Å.	LEED/20/
ZnO (11 $\bar{2}$ 0) (wurtzite)	(1x1)	Terminated bulk structure, no evidence for reconstruction or relaxation in layer spacings.	LEED/20/

REFERENCES

1. Yang, W. S., Sokolov, J., Jona, F., and Marcus, P. M. (1982) *Solid State Communications* **41**, 191.
2. Derry, T. E., Smit, L., and van der Veen, J. F. (1986) *Surface Science* **167**, 502.

3. Vidali, G., Cole, M. W., Weinberg, W. H., and Steele, W. A. (1983) *Physical Review Letters* **51**, 118.
4. Wu, N. J. and Ignatiev, A. (1982) *Physical Review B* **25**, 2983.
5. Wu, N. J. and Ignatiev, A. (1983) *Physical Review B* **28**, 7288.
6. Shaw, C. G., Fain, S. C. Jr., Chinn, M. D., and Toney, M. F. (1980) *Surface Science* **97**, 128.
7. Bouldin, C. and Stern, E. A. (1982) *Physical Review B* **25**, 3462.
8. Prutton, M., Ramsey, J. A., Walker, J. A., and Welton-Cook, M. R. (1979) *Journal of Physics C* **12**, 5271.
9. Ignatiev, A., Lee, B. W., and Van Hove, M. A. (1977) in "Proceedings of the 7th International Vacuum Congress and 3rd International Conference on Solid Surfaces", Vienna.
10. Felton, R. C., Prutton, M., P. Tear, S., and Welton-Cook, M. R. (1979) *Surface Science* **88**, 474.
11. Welton-Cook, M. R. and Berndt, W. (1982) *Journal of Physics C* **15**, 569.
12. Urano, T., Kanaji, T., and Kaburagi, M. (1983) *Surface Science* **134**, 109.
13. Mrstik, B. J., Kaplan, R., Reinecke, T. L., Van Hove, M. A., and Tong, S. Y. (1977) *Physical Review B* **15**, 897.
14. Andersson, S., Pendry, J. B., and Echenique, P. M. (1977) *Surface Science* **65**, 539.
15. Jones, R. G., Ainsworth, S., Crapper, M. D., Somerton, C., Woodruff, D. P., Brooks, R. S., Campuzano, J. C., King, D. A., and Lambe, G. M. (1985) *Surface Science* **152/153**, 443.
16. Welton-Cook, M. R. and Prutton, M. (1980) *Journal of Physics C* **13**, 3993.
17. Benbow, R. L., Thuler, M. R., Hurych, Z., Lau, K. H., and Tong, S. Y. (1983) *Physical Review B* **28**, 4161.
18. Lau, B., Mrstik, B. J., Tong, S. Y., and Van Hove, M. A. (to be published)
19. Lubinsky, A. R., Duke, C. B., Chang, S. C., Lee, B. W., and Mark, P. (1976) *Journal of Vacuum Science and Technology* **13**, 189.
20. Duke, C. B., Lubinsky, A. R., Lee, B. W., and Mark, P. (1976) *Journal of Vacuum Science and Technology* **13**, 761.

TABLE IX. Atomic Adsorption on Semiconductor Surfaces

(Where substrate relaxations or reconstructions have been investigated this information is listed in the table after the adsorbate information.)

Adsorption System	Overlayer Cell	Adsorbate Site	Layer Spacing	Method
GaAs (110)-Sb	(1x1)	2-fold	note 1	LEED/1/
GaAs (110)-Al	(1x1)	sub surface	note 2	LEED/2/
Ge (111)-Cl	(2x8)	top	2.07 ± 0.03	SEXAFS/3/
Ge (111)-I	(1x1)	top	2.50 ± 0.04	SEXAFS/4/
Ge (111)-Br	undetermined	top	2.10 ± 0.04	X-ray resonance/5/
Ge (111)-Te	(2x2)	hcp hollow		SEXAFS/4/
Si (111)-Au	($\sqrt{3} \times \sqrt{3}$)	note 3	0.30	ALICISS/6/
Si (111)-Br	undetermined	top	2.18 ± 0.06	X-ray resonance/7,8/
Si (111)-Ag	(7x7)	top	0.70 ± 0.04	SEXAFS/9/
Si (111)-Ag	($2\sqrt{3} \times 2\sqrt{3}$)	subsurface	-0.68 ± 0.15	SEXAFS/9/
	layer 1-2		1.36 ± 0.30	
	layer 2-3		-0.30	
Si (111)-Cl	($\sqrt{19} \times \sqrt{19}$)	top	1.98 ± 0.04	SEXAFS/3/
Si (111)-Cl	(7x7)	top	2.03 ± 0.03	SEXAFS/3/
Si (111)-I	(7x7)	top	2.44 ± 0.03	SEXAFS/4/
	top layer	+15%	0.90 ± 0.05	
Si (111)-NiSi ₂	(1x1)	tetrahedral	note 4	LEED/10/
Si (111)-NiSi ₂	(1x1)	tetrahedral	note 5	MEIS/11/
Si (111)-Se	undetermined	4-fold	1.68	X-ray resonance/12/
Si (111)-Te	(7x7)	2-fold	1.51	SEXAFS/4/

Note 1 -- Sb atoms fill As and Ga type sites in a slightly buckled (0.10 Å) first layer spaced 2.3 Å above the GaAs surface, with lateral distortions to form a sp^3 bonded chain.

Note 2 -- Aluminum substitutes for sub-surface Ga atoms. For 0.5 monolayers second layer Ga atoms are replaced, for 1.0 monolayers second and third layer Ga atoms are replaced. Above 1.5 monolayers all near surface Ga atoms are replaced by Al, forming an epitaxial AlAs(110) surface. In all cases the first interlayer spacing contracts by ~ 0.10 Å.

Note 3 -- Modified triplet cluster model - Au triplets substituted for Si atoms with a 2.9 Å Au-Au bond length between the triplet Au atoms.

Note 4 -- Structure of $NiSi_2$, grown on Si(111) substrate. Forms fluorite structure layer compound Si-Ni-Si with nickel in tetrahedral sites. Silicon layer terminates crystal, with a first-layer contraction of $\sim 25\%$.

Note 5 -- Ion scattering investigation of $NiSi_2$ - bulk Si interface. Determine Si-Ni-Si layer is 3.06 ± 0.08 Å above the next non-collinear Si atom (the bulk value is $0.77 + 2.35 = 3.12$). Of the two possible terminations this most closely matches the bulk silicon structure.

REFERENCES

1. Duke, C. B., Paton, A., Ford, W. K., Kahn, A., and Carelli, J. (1982) *Physical Review B* **26**, 803.
2. Kahn, A., Carelli, J., Kanani, D., Duke, C. B., Paton, A., and Brillson, L. (1981) *Journal of Vacuum Science and Technology* **19**, 331.
3. Citrin, P. H., Rowe, J. E., and Eisenberger, P. (1983) *Physical Review B* **28**, 2299.
4. Citrin, P. H., Eisenberger, P., and Rowe, J. E. (1982) *Physical Review Letters* **48**, 802.
5. Bedzyk, M. and Materlik, G. (1985) *Surface Science* **152/153**, 10.
6. Oura, K., Katayama, M., Shoji, F., and Hanawa, T. (1895) *Physical Review Letters* **55**, 1486.

7. Golovchenko, J. A., Patel, J. R., Kaplan, D. R., Cowan, P. L., and Bedzyk, M. J. (1982) *Physical Review Letters* **49**, 1560.
8. Materlik, G., Frohm, A., and Bedzyk, M. J. (1984) *Physical Review Letters* **52**, 441.
9. Stöhr, J., Jaeger, R., Rossi, G., Kendelewicz, T., and Lindau, I. (1983) *Surface Science* **134**, 813.
10. Yang, W. S., Jona, F., and Marcus, P. M. (1983) *Physical Review B* **28**, 7377.
11. van Loenen, E. J., Frenken, J. W. M., van der Veen, J. F., and Valeri, S. (1985) *Physical Review Letters* **54**, 827.
12. Dev, B. N., Thundat, T., and Gibson, W. M. (1985) *Journal of Vacuum Science and Technology A* **3**, 946.

TABLE XII. Other Molecular Adsorption Structures

System	Structure	Method
Cu (100) HCO ₂ disordered	The formate radical is in a plane \perp to the surface with the two oxygens closest to the surface, and a formate O-C-O bond angle of 125° is assumed. The O atoms are slightly off-center above two adjacent 4-fold hollow sites. The O atoms are 1.54 Å above the Cu surface and separated by 2.17 Å. The C atom is 2.11 Å above the surface.	NEXAFS/1/
Cu (110) HCO ₂ disordered	The formate radical is in a plane \perp to the surface along the [001] direction. The oxygen atoms are closest to the surface, slightly off-center from two adjacent bridge sites, 1.51 Å above the surface and 2.29 Å apart. The O atom is 2.04 Å above the Cu atom.	NEXAFS/2/
Ni (111) C ₂ H ₂ (2x2)	The acetylene molecules are adsorbed with the C-C bond parallel to the surface and the center of the C-C bond is over a bridge site. The C-C bond is perpendicular to the Ni-Ni bridge. The C-C bond length is 1.50 Å and the carbon atoms are 2.1±0.10 Å above the surface.	LEED/3/
Pd (111) C ₆ H ₆ +2CO (3x3)	One benzene and two CO's per unit cell. CO is \perp to the surface, adsorbed 1.30 Å above 3-fold fcc sites. Benzene is parallel to the surface, centered 2.25 Å over a 3-fold hcp site.	LEED/4/
Pt (111) C ₂ H ₂ disordered	Acetylene bonded parallel to surface with C-C bond length 1.45±0.03 Å.	NEXAFS/5/

(continued)

TABLE XII (continued)

System	Structure	Method
Pt (111) C ₂ H ₃ disordered	Ethylidyne (CCH ₃) bonded \perp to surface with C-C bond 1.47 ± 0.03 Å.	NEXAFS/6/
Pt (111) C ₂ H ₃ disordered	Ethylidyne (CCH ₃) bonded \perp to surface with C-C bond 1.49 ± 0.02 Å.	NMR/7/
Pt (111) C ₂ H ₃ (2x2)	Ethylidyne (CCH ₃) bonded \perp to surface in 3-fold fcc sites, C-C bond 1.50 ± 0.05 Å and C-surface \perp distance 1.20 ± 0.05 Å.	LEED/8/
Pt (111) C ₂ H ₄ disordered	Ethylene bonded parallel to surface with C-C bond length 1.49 ± 0.03 Å.	NEXAFS/5/
Pt (111) 2C ₆ H ₆ disordered	Benzene ring parallel to surface, C-C bond length 1.40 ± 0.02 Å.	NEXAFS/9/
Pt (111) 2C ₆ H ₆ +4CO (2 $\sqrt{3}$ x4) rect	Benzene ring parallel to surface over bridge sites, 2.10 Å above surface, with two benzenes and four CO's per unit cell. CO also over bridge sites, 1.45 Å above the metal surface. Benzene ring is expanded with small in-plane distortions consistent with local symmetry.	LEED/10/
Rh (111) C ₂ H ₃ (2x2)	Ethylidyne (CCH ₃) is adsorbed with the C-C axis \perp to the surface with a 1.45 ± 0.10 Å bond length. The terminal carbon atom is 1.31 ± 0.10 Å above a 3-fold hcp hollow site.	LEED/11/

(continued)

TABLE XII (continued)

System	Structure	Method
Rh (111) C ₂ H ₃ +CO c(4x2)	Ethylidyne (CCH ₃) is adsorbed in 3-fold fcc sites with a 1.30±0.05 Å metal-terminal carbon distance. The C-C axis is ⊥ to the surface with a 1.45±0.05 Å bond length. CO molecules are adsorbed ⊥ to the surface in 3-fold hcp sites, carbon atom down, with a carbon-metal bond length of 1.30±0.05 Å and a C-O bond length of 1.17±0.05 Å.	LEED/12/
Rh (111) C ₂ H ₃ +NO c(4x2)	Ethylidyne (CCH ₃) is adsorbed in 3-fold hcp sites with a 1.30±0.05 Å metal-terminal carbon distance. The C-C axis is ⊥ to the surface with a 1.45±0.05 Å bond length. NO molecules are adsorbed ⊥ to the surface in 3-fold hcp sites, nitrogen atom down, with a nitrogen-metal bond length of 1.30±0.05 Å and a N-O bond length of 1.17±0.05 Å.	LEED/12/
Rh (111) C ₆ H ₆ +2CO (3x3)	One benzene and two CO's per unit cell. CO is ⊥ to the surface, adsorbed 1.30 Å above 3-fold hcp sites. Benzene is parallel to the surface, centered 2.20 Å over a 3-fold hcp site. Slight in-plane Kekulé distortion of the benzene molecule.	LEED/13/

(continued)

TABLE XII (continued)

System	Structure	Method
Rh (111) C ₆ H ₆ +CO c(2√3x4) rect	Benzene is coadsorbed with CO, each with one molecule per unit cell, both centered over 3-fold hcp sites; benzene is parallel to and 2.25±0.05 Å above the surface. CO is ⊥ to the surface and the metal-carbon spacing is 1.50±0.05 Å. The benzene molecule has an in-plane Kekulé distortion, with alternating long and short bonds.	LEED/14/

REFERENCES

1. Outka, D. A., Madix, R. J., and Stöhr, J. (1985) *Surface Science* **164**, 235.
2. Puschman, A., Haase, J., Crapper, M. D., Riley, C. E., and Woodruff, D. P. (1985) *Physical Review Letters* **54**, 2250.
3. Casalone, G., Cattania, M. G., Merati, F., and Simonetta, M. (1982) *Surface Science* **120**, 171.
4. Ohtani, H., Van Hove, M. A., and Somorjai, G. A. (to be published)
5. Stöhr, J., Sette, F., and Johnson, A. L. (1984) *Physical Review Letters* **53**, 1684.
6. Horsley, J. A., Stöhr, J., and Koestner, R. J. (1985) *Journal of Chemical Physics* **83**, 3146.
7. Wang, P.-K., Slichter, C. P., and Sinfelt, J. J. (1985) *Journal of Physical Chemistry* **89**, 3606.
8. Kesmodel, L. L., Dubois, L. H., and Somorjai, G. A. (1979) *Journal of Chemical Physics* **70**, 2180.

9. Horsley, J. A., Stöhr, J., Hitchcock, A. P., Newbury, D. C., Johnson, A. L., and Sette, F. (1985) *Journal of Chemical Physics* **83**, 6099.
10. Ogletree, D. F., Van Hove, M. A., and Somorjai, G. A. (1987) *Surface Science* **187**, 1.
11. Koestner, R. J., Van Hove, M. A., and Somorjai, G. A. (1982) *Surface Science* **121**, 321.
12. Bent, B. E., Mate, C. M., Koestner, R. J., Blackman, G. S., Kao, C. T., Hove, M. A. Van, and Somorjai, G. A. (to be published)
13. Van Hove, M. A., Lin, R. F., Blackman, G. A., and Somorjai, G. A. (to be published) *Acta Crystallographica*
14. Van Hove, M. A., Lin, R. F., and Somorjai, G. A. (1986) *Journal of the American Chemical Society* **108**, 2532.

6. FUTURE NEEDS AND DIRECTIONS OF SURFACE STUDIES

It is our hope that this review conveys the rapid developments in surface structural chemistry during the past decade. We have attempted to describe the various techniques that are employed and the types of structural information that has been obtained from experiment.

The theories of surface structure and bonding have been reviewed. It should be clear to the reader that surface structural chemistry is indeed a frontier area for both theorists and experimental researchers. From an experimentalists viewpoint the data base of atomic and molecular surface structures is very small at present. Most investigations have been carried out on flat, low Miller index surfaces of monatomic solids, either clean or with atomic or small molecules as adsorbates.

The structure of clean surfaces of polyatomic solids (alloys, halides, oxides, sulfides, etc.) should be explored along with molecular solid surfaces (organic systems). More open, rough surfaces with high Miller indices should be investigated, including the structure of atoms and molecules bonded to steps and kinks on surfaces. Such sites are known to be key for some important surface chemical processes, but little is known of their structure.

Molecular adsorbates of increasing size should be a fertile area of research. Such research could lead to the study of biological surfaces. The surface structure at solid-gas, solid-liquid, and solid-solid interfaces should be explored and compared with the results for the solid-vacuum interface. Structural properties of thin films, electrodes, and composite materials can be obtained in this way.

Time resolved surface structure analysis can be employed for studies of order-order and order-disorder surface phase transitions, growth, and evaporation. Surface structures and their alterations could then be explored under extreme conditions of high temperature and irradiation by photons or particles.

Once bond distances and angles become available for a large number of systems with diverse chemistry, correlation should lead to a deeper understanding of the nature of the surface chemical bond.

REFERENCES

1. Ogletree, D. F., Van Hove, M. A., and Somorjai, G. A. (1987) *Surface Science* **187**, 1.
2. Moritz, W. and Wolf, D. (1985) *Surface Science* **163**, L655.
3. Heilmann, P., Lang, E., Heinz, K., and Müller, K. (1984) in "Determination of Surface Structure by LEED" (P. M. Marcus and F. Jona, ed.), Plenum Press, New York.
4. Ogletree, D. F., Somorjai, G. A., and Katz, J. E. (1986) *Review of Scientific Instruments* **57**, 3012.
5. Stair, P. C. (1980) *Review of Scientific Instruments* **51**, 132.
6. McRae, E. G., Malic, R. A., and Kapilow, D. A. (1985) *Review of Scientific Instruments* **56**, 2077.
7. Ogletree, D. F. (1986) *PhD Thesis*, Physics Department, University of California at Berkeley.
8. Weiss, A. H., Rosenberg, I. J., Canter, K. F., Duke, C. B., and Paton, A. (1983) *Physical Review B* **27**, 867.
9. Pierce, D. T. and Coletta, R. J. (1981) in "Advances in Electronic and Electron Physics" **56** (C. Marton, ed.), Academic Press, New York.
10. Masud, N., Kinniburgh, C. G., and Pendry, J. B. (1977) *Journal of Physics C* **10**, 1.
11. Barton, J. J. and Van Hove, M. A. (to be published)
12. Saldin, D. K., Pendry, J. B., Van Hove, M. A., and Somorjai, G. A. (1985) *Physical Review B* **31**, 1216.
13. Rous, P. R., Pendry, J. B., Saldin, D. K., Heinz, K., Müller, K., and Bickel, N. (1986) *Physical Review Letters* **57**, 2951.
14. Orders, P. J., Sinkovic, B., Fadley, C. S., Trehan, R., Hussain, Z., and Lecante, J. (1984) *Physical Review B* **30**, 1838.
15. Barton, J. J., Robey, S. W., and Shirley, D. A. (1986) *Physical Review B* **34**, 778.
16. Norman, D., Stöhr, J., Jaeger, R., Durham, P. J., and Pendry, J. B. (1983) *Physical Review Letters* **51**, 2052.

17. Sette, F., Stöhr, J., Kollin, E. B., Dwyer, D. J., Gland, J. L., Robbins, J. L., and Johnson, A. L. (1985) *Physical Review Letters* **54**, 935.
18. Müller, E. W. (1951) *Zeitschrift Physik* **136**, 131.
19. Ehrlich, G. (1985) in "*The Structure of Surfaces*" (M. A. Van Hove and S. Y. Tong, ed.), Springer Verlag, Berlin.
20. Batra, I. P., Barker, J. A., and Auerbach, D. J. (1983) *Journal of Vacuum Science and Technology A* **2**, 943.
21. Binnig, G., Rohrer, H., Gerber, C., and Weibel, E. (1982) *Applied Physics Letters* **40**, 178.
22. Binnig, G., Rohrer, H., Gerber, C., and Weibel, E. (1983) *Surface Science* **131**, L379.
23. Copel, M. and Gustafsson, T. (1986) *Physical Review Letters* **57**, 723.
24. Ibach, H. and Mills, D. L. (1982) "*Electron Energy Loss Spectroscopy and Surface Vibrations*", Academic Press, New York.
25. Shen, Y. R. (1985) in "*The Structure of Surfaces*" (M. A. Van Hove and S. Y. Tong, ed.), p. 77, Springer Verlag, Berlin.
26. Madey, T. E. (1985) in "*The Structure of Surfaces*" (M. A. Van Hove and S. Y. Tong, ed.), p. 264, Springer Verlag, Berlin.
27. Pendry, J. B. (1974) "*Low Energy Electron Diffraction*", Academic Press, London.
28. Van Hove, M. A. and Tong, S. Y. (1979) "*Surface Crystallography by LEED*", Springer Verlag, Berlin.
29. Clarke, L. J. (1985) "*Surface Crystallography; An Introduction to Low Energy Electron Diffraction*", Wiley-Interscience, Chichester.
30. Li, C. H., Tong, S. Y., and Mills, D. L. (1980) *Physical Review B* **21**, 3057.
31. Einstein, T. L. (1982) *Applications of Surface Science* **11/12**, 42.
32. Rosei, R., de Crescenzi, M., Sette, F., Quaresima, C., Savoia, A., and Perfetti, P. (1983) *Physical Review B* **28**, 1161.
33. Polizzi, S., Antonangeli, F., Chiarello, G., and de Crescenzi, M. (1984) *Surface Science* **136**, 555.
34. Kincaid, B. M., Meixner, A. E., and Platzman, P. M. (1978) *Physical Review Letters* **40**, 1296.

35. Csillag, S., Johnson, D. E., and Stern, E. A. (1981) in "EXAFS Spectroscopy Techniques and Applications" (B. K. Teo and D. C. Joy, ed.), Plenum, New York.
36. Rosenblatt, D. H., Tobin, J. G., Mason, M. G., Davis, R. F., Kevan, S. D., Shirley, D. A., Li, C. H., and Tong, S. Y. (1981) *Physical Review B* **23**, 3828.
37. Kevan, S. D., Davis, R. F., Rosenblatt, D. H., Tobin, J. G., Mason, M. G., Shirley, D. A., Li, C. H., and Tong, S. Y. (1981) *Physical Review Letters* **46**, 1629.
38. Barton, J. J., Bahr, C. C., Hussain, Z., Robey, S. W., Tobin, J. G., Klebanoff, L. E., and Shirley, D. A. (1983) *Physical Review Letters* **51**, 272.
39. Teo, B. K. and Joy, D. C. eds. (1981) "EXAFS Spectroscopy Techniques and Applications", Plenum, New York.
40. Bouldin, C. and Stern, E. A. (1982) *Physical Review B* **25**, 3462.
41. Lee, P. A. (1976) *Physical Review B* **13**, S261.
42. Lee, P. A., Citrin, P. H., Eisenberger, P., and Kincaid, B. M. (1981) *Reviews of Modern Physics* **53**, 769.
43. Stöhr, J., Jaeger, R., and Brennan, S. (1982) *Surface Science* **117**, 503.
44. Rothberg, G. M., Choudhary, K. M., den Boer, M. L., Williams, G. P., Hecht, M. H., and Lindau, I. (1984) *Physical Review Letters* **53**, 1183.
45. Stöhr, J. and Jaeger, R. (1982) *Physical Review B* **20**, 4111.
46. Norman, D., Stöhr, J., Jaeger, R., Durham, P. J., and Pendry, J. B. (1983) *Physical Review Letters* **51**, 2052.
47. Bunker, G. and Stern, E. A. (1984) *Physical Review Letters* **52**, 1990.
48. Stöhr, J. (1985) in "The Structure of Surfaces" (M. A. Van Hove and S. Y. Tong, ed.), Springer Verlag, Berlin.
49. Pendry, J. B. (1976) *Surface Science* **57**, 679.
50. Plummer, E. W. and Eberhardt, W. (1982) "Advances in Chemical Physics", Wiley, New York.
51. Fadley, C. S. (1983) in "Progress in Surface Science" (S. G. Davidson, ed.), Pergamon, New York.
52. Einstein, T. L. *private communication*.

53. Masud, N., Kinniburgh, C. G., and Pendry, J. B. (1977) *Journal of Physics C* **10**, 1.
54. Masud, N. (1980) *Journal of Physics C* **13**, 6359.
55. Maksym, P. A. and Beeby, J. L. (1984) *Surface Science* **140**, 77.
56. Maksym, P. A. and Beeby, J. L. (1981) *Surface Science* **110**, 423.
57. Hirsch, P. B., Howie, A., Nicholson, R. B., Pashley, D. W., and Whelan, M. J. (1965) "*Electron Microscopy of Thin Crystals*", Butterworth, London.
58. Goodman, P. ed. (1981) "*Fifty Years of Electron Diffraction*", D. Reidel, Dordrecht.
59. Duke, C. B. and Laramore, G. E. (1970) *Physical Review B* **2**, 4765.
60. Duke, C. B. and Laramore, G. E. (1970) *Physical Review B* **2**, 4783.
61. Ibach, H. and Mills, D. L. (1982) "*Electron Energy Loss Spectroscopy and Surface Vibrations*", Academic Press, New York.
62. Crowell, J. E., Koestner, R. J., Dubois, L. H., Van Hove, M. A., and Somorjai, G. A. (1982) in "*Recent Advances in Analytical Spectroscopy*" (K. Fuwa, ed.), p. 211, Pergamon Press, New York.
63. Tong, S. Y., Li, C. H., and Mills, D. L. (1981) *Physical Review B* **24**, 806.
64. Ertl, G. and Küppers, J. (1974) "*Low Energy Electrons and Surface Chemistry*", Verlag Chemie, Weinheim.
65. Avouris, P., DiNardo, N. J., and Demuth, J. E. (1984) *Journal of Chemical Physics* **80**, 491.
66. Taft, T. and Zhu, J. (1982) *Ultramicroscopy* **9**, 349.
67. Aberdam, D., Baudoing, R., Blanc, E., and Gaubert, C. (1978) *Surface Science* **71**, 279.
68. Baudoing, R., Blanc, E., Gaubert, C., Gautheir, Y., and Gnuchev, N. (1983) *Surface Science* **128**, 22.
69. Asaad, W. N. (1963) *Nuclear Physics* **44**, 415.
70. McGuire, E. J. (1971) *Sandia Laboratories Report* **SC-RR-710075**.
71. Umbach, E. and Hussain, Z. (1984) *Physical Review Letters* **52**, 457.
72. Truhlar, D. G., Abdallah, J. Jr., and Smith, R. L. (1974) *Advances in Chemical Physics* **25**, 211.
73. Beeby, J. L. (1968) *Journal of Physics C* **1**, 1982.
74. Andersson, S. and Pendry, J. B. (1980) *Journal of Physics C* **13**, 2547.
75. Andersson, S. and Pendry, J. B. (1980) *Journal of Physics C* **13**, 3547.

76. Pendry, J. B. (1975) *Journal of Physics C* **8**, 2413.
77. Zimmer, R. S. and Holland, B. W. (1975) *Journal of Physics C* **8**, 2395.
78. Saldin, D. K., Vvedensky, D. D., and Pendry, J. B. (1985) in "*The Structure of Surfaces*" (M. A. Van Hove and S. Y. Tong, ed.), p. 131, Springer Verlag, Berlin.
79. Saldin, D. K., Pendry, J. B., Van Hove, M. A., and Somorjai, G. A. (1985) *Physical Review B* **31**, 1216.
80. Van Hove, M. A., Lin, R. F., and Somorjai, G. A. (1983) *Physical Review Letters* **51**, 778.
81. Levinson, H. J., Plummer, E. W., and Feibelman, P. J. (1979) *Physical Review Letters* **43**, 952.
82. Li, C. H., Lubinsky, A. R., and Tong, S. Y. (1978) *Physical Review B* **17**, 3128.
83. Tong, S. Y. *private communication*.
84. Gadzuk, J. W. (1976) *Surface Science* **60**, 76.
85. Mehl, M. J. and Einstein, T. L. (to be published)
86. Van Hove, M. A. and Somorjai, G. A. (1982) *Surface Science* **114**, 171.
87. Batra, I. P. (1982) in "*Topics in Current Physics*" **29** (W. H. Marlow, ed.), p. 55, Springer Verlag, Heidelberg.
88. Louie, S. G. and Cohen, M. L. (1984) *Annual Review of Physical Chemistry* **35**, 537.
89. Louie, S. G. (1985) in "*Electronic Structure, Dynamics, and Quantum Structural Properties of Condensed Matter*" (J. T. Devreese and P. Van Camp, ed.), p. 335, Plenum, New York and London.
90. Ohnishi, S., Freeman, A. J., and Wimmer, E. (1984) *Physical Review B* **29**, 5267.
91. Smith, J. R. (Ed.) (1980) "*Theory of Chemisorption*", Springer Verlag, Berlin.
92. Fu, C. L., Ohnishi, S., Wimmer, E., and Freeman, A. J. (1984) *Physical Review Letters* **53**, 675.
93. Mattheiss, L. F. and Hamann, D. R. (1984) *Physical Review B* **29**, 5372.
94. Inglesfield, J. E. (to be published)
95. Hoffmann, R. (1963) *Journal of Chemical Physics* **39**, 137.
96. Lohr, L. L. Jr. and Pyykkö, P. (1979) *Chemical Physics Letters* **62**, 333.

97. Messmer, R. P. (1985) *Surface Science* **158**, 40.
98. Wolfsberg, M. and Helmholtz, L. (1952) *Journal of Chemical Physics* **20**, 837.
99. Bennett, A. J., McCarroll, B., and Messmer, R. P. (1971) *Surface Science* **24**, 191.
100. Bennett, A. J., McCarroll, B., and Messmer, R. P. (1971) *Physical Review B* **3**, 1397.
101. Pople, J. A. and Segal, G. A. (1966) *Journal of Chemical Physics* **44**, 3289.
102. Anderson, A. B. and Hoffmann, R. (1974) *Journal of Chemical Physics* **60**, 4271.
103. Anderson, A. B. (1975) *Journal of Chemical Physics* **62**, 1187.
104. Simonetta, M. and Gavezzotti, A. (1980) *Advances in Quantum Chemistry* **12**, 103.
105. Baetzold, R. C. and Hamilton, J. F. (1983) *Progress in Solid State Chemistry* **15**, 1.
106. Ray, N. K. and Anderson, A. B. (1983) *Surface Science* **125**, 803.
107. Froitzheim, H., Hopster, H., Ibach, H., and Lehwald, S. (1977) *Applied Physics* **13**, 147.
108. Ogletree, D. F., Van Hove, M. A., and Somorjai, G. A. (1986) *Surface Science* **173**, 351.
109. Krebs, H. I. and Lüth, H. (1977) *Applied Physics* **14**, 337.
110. Norton, P. R., Goodale, J. W., and Selkirk, E. B. (1979) *Surface Science* **83**, 189.
111. Campbell, C. T., Ertl, G., Kuipers, H., and Segner, J. (1980) *Journal of Chemical Physics* **73**, 5862.
112. Gavezzotti, A., Ortoleva, E., and Simonetta, M. (1982) *Journal of the Chemical Society, Faraday Transactions 1* **78**, 425.
113. Gavezzotti, A. and Simonetta, M. (1980) *Surface Science* **99**, 453.
114. Anderson, A. B. and Hubbard, T. (1980) *Surface Science* **99**, 384.
115. Ibach, H. and Lehwald, S. (1978) *Journal of Vacuum Science and Technology* **15**, 407.
116. Johnson, K. H. (1966) *Journal of Chemical Physics* **45**, 3085.
117. Korringa, J. (1947) *Physica (Utrecht)* **13**, 392.

118. Kohn, W. and Rostoker, N. (1954) *Physical Review* **94**, 1111.
119. Yang, C. Y., Johnson, K. H., Salahub, D. R., Kaspar, J., and Messmer, R. P. (1981) *Physical Review B* **24**, 5673.
120. Yang, C. Y. and Rabii, S. (1975) *Physical Review A* **12**, 362.
121. Kohn, W. and Sham, L. J. (1965) *Physical Review A* **140**, 1133.
122. Slater, J. C. (1951) *Physical Review* **81**, 385.
123. Schwarz, K. (1972) *Physical Review B* **5**, 2466.
124. Batra, I. P. and Brundle, C. R. (1976) *Surface Science* **57**, 12.
125. Danese, J. B. and Connolly, J. W. D. (1974) *Journal of Chemical Physics* **61**, 3063.
126. Danese, J. B. (1974) *Journal of Chemical Physics* **61**, 3071.
127. Johnson, K. H. (1971) *International Journal of Quantum Chemistry* **S4**, 153.
128. Kasowski, R. V. (1947) *Physical Review Letters* **33**, 1147.
129. Slater, J. C. and Johnson, K. H. (1972) *Physical Review B* **5**, 844.
130. Yu, H. L. (1977) *Physical Review B* **15**, 3609.
131. Demuth, J. E. and Eastman, D. E. (1976) *Solid State Communications* **18**, 1497.
132. Messmer, R. P. and Lamson, S. H. (1979) *Chemical Physics Letters* **65**, 465.
133. Norton, P. R., Tapping, R. L., and Goodale, J. W. (1978) *Surface Science* **72**, 33.
134. Messmer, R. P., Lamson, S. H., and Salahub, D. R. (1982) *Physical Review B* **25**, 3576.
135. Demuth, J. E. and Eastman, D. E. (1974) *Physical Review Letters* **32**, 1123.
136. Rösch, N. and Rhodin, T. N. (1974) *Physical Review Letters* **32**, 1189.
137. Howard, I. A. and Dresselhaus, G. (1984) *Surface Science* **136**, 229.
138. Yang, C. Y., Yu, H. L., and Case, D. A. (1981) *Chemical Physics Letters* **81**, 170.
139. Baerends, E. J., Ellis, D. E., and Ros, P. (1973) *Chemical Physics* **2**, 41.
140. Rosén, A., Ellis, D. E., Adachi, H., and Averill, F. W. (1976) *Journal of Chemical Physics* **65**, 3629.
141. Mulliken, R. S. (1955) *Journal of Chemical Physics* **23**, 1833.

142. Mulliken, R. S. (1955) *Journal of Chemical Physics* **23**, 1841.
143. Eastman, D. E. and Cashion, J. K. (1971) *Physical Review Letters* **27**, 1520.
144. Hagstrum, H. D. and Becker, G. E. (1971) *Journal of Chemical Physics* **54**, 1015.
145. Andersson, S. (1977) *Solid State Communications* **21**, 75.
146. Andersson, S. (1977) in "Proceedings of the 7th International Vacuum Congress and 3rd International Conference on Solid Surfaces", p. 815, Vienna.
147. Rosén, A., Baerends, E. J., and Ellis, D. E. (1979) *Surface Science* **82**, 139.
148. Ellis, D. E., Baerends, E. J., Adachi, H., and Averill, F. W. (1977) *Surface Science* **64**, 649.
149. Baerends, E. J. and Ros, P. (1975) *Molecular Physics* **30**, 1735.
150. Allyn, C. L., Gustafsson, T., and Plummer, E. W. (1977) *Chemical Physics Letters* **47**, 127.
151. Davenport, J. (1976) *Physical Review Letters* **36**, 945.
152. Cao, Pei-Lin, Ellis, D. E., and Freeman, A. T. (1982) *Physical Review B* **25**, 2124.
153. Ziegler, A. and Rank, A. (1977) *Theoretica Chimica Acta* **46**, 1.
154. Bagus, P. S. and Hermann, K. (1981) *Journal of Vacuum Science and Technology* **18**, 435.
155. Bagus, P. S. (1981) *Physical Review B* **23**, 2065.
156. Bagus, P. S. (1981) *Physical Review B* **23**, 5464.
157. Bagus, P. S., Brundle, C. R., Hermann, K., and Menzel, D. (1980) *Journal of Electron Spectroscopy and Related Phenomena* **20**, 253.
158. Seeland, M. and Bagus, P. S. (1983) *Physical Review B* **28**, 2023.
159. Bauschlicher, C. W. Jr., Walch, S. P., Bagus, P. S., and Brundle, C. R. (1983) *Physical Review Letters* **50**, 864.
160. Bauschlicher, C. W. Jr., Bagus, P. S., and Yarkony, D. R. (1981) *Proceedings of the Workshop on Recent Developments and Applications of the MC-HF method*, 67. , Lawrence Berkeley Laboratory
161. Brundle, C. R., Bagus, P. S., Menzel, D., and Hermann, K. (1981) *Physical Review B* **24**, 7041.

162. Bagus, P. S. and Roos, B. O. (1981) *Journal of Chemical Physics* **12**, 5961.
163. Bagus, P. S., Nelin, C. J., and Bauschlicher, C. W. Jr. (1983) *Physical Review B* **28**, 5423.
164. Bauschlicher, C. W. Jr. and Bagus, P. S. (1984) *Physical Review Letters* **52**, 200.
165. Melius, C. F., Bisson, C. L., and Wilson, W. D. (1978) *Physical Review B* **18**, 1647.
166. Lehwald, S. and Ibach, H. (1982) in "Vibrations at Surfaces" (R. Caudano, J.-M. Gilles, and A. A. Lucas, ed.), p. 137, Plenum, New York.
167. Stöhr, J., Jaeger, R., and Kendelewicz, T. (1982) *Physical Review Letters* **49**, 142.
168. Van Hove, M. A. and Tong, S. Y. (1975) *Journal of Vacuum Science and Technology* **12**, 230.
169. Marcus, P. C., Demuth, J. E., and Jepsen, D. W. (1975) *Surface Science* **53**, 501.
170. Upton, T. H. and Goddard, W. A. III (1981) *Physical Review Letters* **46**, 1635.
171. Upton, T. H. and Goddard, W. A. III (1981) *Critical Reviews of Solid State and Material Science* **10**, 261.
172. Batra, I. P., Bagus, P. S., and Hermann, K. (1984) *Physical Review Letters* **52**, 384.
173. Goddard, W. A. III, Redondo, A., and McGill, T. C. (1976) *Solid State Communications* **18**, 981.
174. Redondo, A., Goddard, W. A. III, Swarts, C. A., and McGill, T. C. (1981) *Journal of Vacuum Science and Technology* **19**, 498.
175. Ibach, H., Bruchmann, H. D., and Wagner, H. (1982) *Applied Physics A* **29**, 113.
176. Whitten, J. L. (1973) *Journal of Chemical Physics* **58**, 4496.
177. Whitten, J. L. and Pakkanen, T. A. (1980) *Physical Review B* **21**, 4357.
178. Cremaschi, P. and Whitten, J. L. (1981) *Surface Science* **112**, 343.
179. Madhavan, P. and Whitten, J. L. (1982) *Journal of Chemical Physics* **77**, 2673.

180. Hunt, W. J., Hay, P. J., and Goddard, W. A. III (1972) *Journal of Chemical Physics* **57**, 738.
181. Upton, T. H. and Goddard, W. A. III (1982) in "Chemistry and Physics of Solid Surfaces" **3** (R. Vanselow and W. England, ed.), p. 127, CRC Press, Boca Raton.
182. Bobrowicz, F. W. and Goddard, W. A. III (1977) in "Modern Theoretical Chemistry; Methods of Electronic Structure Theory" **3** (H. F. Schaefer, III, ed.), p. 738, Plenum Press, New York.
183. Allison, J. N. and Goddard, W. A. III (1982) *Surface Science* **115**, 553.
184. Melius, C. F., Olafson, B. D., and Goddard, W. A. III (1974) *Chemical Physics Letters* **28**, 457.
185. Meutner, J. S. (1975) *Journal of Molecular Spectroscopy* **55**, 490.
186. Tracy, J. C. (1972) *Journal of Chemical Physics* **56**, 2736.
187. Barton, J. J., Swarts, C. A., Goddard, W. A. III, and McGill, T. C. (1980) *Journal of Vacuum Science and Technology* **17**, 164.
188. Goddard, W. A. III, Barton, J. J., Redondo, A., and McGill, T. C. (1978) *Journal of Vacuum Science and Technology* **15**, 1274.
189. Tong, S. Y., Lubinsky, A. R., Mrstik, B. J., and Van Hove, M. A. (1978) *Physical Review B* **17**, 3303.
190. Kahn, A., So, E., Mark, P., Duke, C. B., and Meyer, R. J. (1978) *Journal of Vacuum Science and Technology* **15**, 1223.
191. Miller, D. J. and Haneman, D. (1978) *Journal of Vacuum Science and Technology* **15**, 1267.
192. Meyer, R. J., Duke, C. B., Patton, A., Kahn, A., So, E., Yeh, J. L., and Mark, P. (1979) *Physical Review B* **19**, 5194.
193. Stöhr, J., Bauer, R. S., McMnamin, J. C., Johansson, L. I., and Brennan, S. (1979) *Journal of Vacuum Science and Technology* **16**, 1195.
194. Wilkins, C. W., Hagen, K., Hedberg, L., Shen, O., and Hedberg, K. (1975) *Journal of the American Chemical Society* **97**, 6352.
195. Rojhantalab, H. (1976) *Spectrochimica Acta A* **32**, 947.
196. Carlson, R. and Meek, D. W. (1974) *Inorganic Chemistry* **13**, 1741.
197. Brundle, C. R. and Seybold, D. (1979) *Journal of Vacuum Science and Technology* **16**, 1186.

198. Pianetta, P., Lindau, I., Garner, C., and Spicer, W. E. (1975) *Physical Review Letters* **35**, 1356.
199. Spicer, W. E., Pianetta, P., Lindau, I., and Chye, P. W. (1977) *Journal of Vacuum Science and Technology* **14**, 885.
200. Chye, P. W., Pianetta, P., Lindau, I., and Spicer, W. E. (1977) *Journal of Vacuum Science and Technology* **14**, 917.
201. Pauling, L. (1960) "*The Nature of the Chemical Bond*", Cornell University Press, Ithaca, New York.
202. Ohtani, H., Kao, C.-T., Van Hove, M. A., and Somorjai, G. A. (1986) *Progress In Surface Science* **23**, 155.

LAWRENCE BERKELEY LABORATORY
CENTER FOR ADVANCED MATERIALS
1 CYCLOTRON ROAD
BERKELEY, CALIFORNIA 94720

ACE308



LBL Libraries